Targeted editing of DNA methylation

Downregulation of MGMT expression by targeted editing of DNA methylation enhances temozolomide sensitivity in glioblastoma

Doctoral thesis

to obtain a doctorate (MD/PhD)

from the Faculty of Medicine

of the University of Bonn

Xinyu Han

From Shandong (Jinan)/(PR) China

2024

Written with authorization of

the Faculty of Medicine of the University of Bonn

First reviewer: Prof. Dr. Ullrich Wüllner

Second reviewer: Prof. Dr. Wolfram S. Kunz

Day of oral examination: 30.08.2024

From department of Parkinson, sleep, and movement disorders of
the University Hospital Bonn

Director: Prof. Dr. Ullrich Wüllner

Table of Contents

List of abbreviations

Abbreviation	Full name
5-ALA	5-aminolevulinic acid
5mC	5-methylcytosine
ADC	Apparent diffusion coefficient
APNG	Alkylpurine-DNA-N-glycosylase
BCA	Bicinchoninic Acid
BER	Base excision repair
BSA	Bovine Serum Albumin
Cas9	Nuclease 9
CBV	Cerebral blood volume
CDK4	Cyclin-dependent kinase 4
CDKN2A/B	Cyclin-dependent kinase inhibitor 2A/B
CGIs	CpG islands
CNS	Central Nervous System
CpG	Cytosine-guanine dinucleotides
CRISPR	clustered regularly interspaced short palindromic repeats
CRISPRa	CRISPR activation
CRISPRi	CRISPR interference
crRNA	CRISPR RNA
Ct	cycle threshold
dCas9	Catalytically inactive Cas9
DGE	Differential gene expression
DMEM	Dulbecco’s Modified Eagle’s medium
DMSO	Dimethyl sulfoxide
DNMTs	DNA methyltransferases
DSBs	DNA double-strand breaks

DSC	Dynamic susceptibility contrast
EGFR	Epidermal growth factor receptor
EgRNA	Empty sgRNA
EM	Epigenetic modifiers
FBS	Fetal bovine serum
G-CIMP	CpG island methylator phenotype
GTR	Gross total resection
HDR	Homology-directed repair
HPRT1	Hypoxanthine phosphoribosyl-transferase 1
HRP	Horseradish peroxidase
HUWE1	HECT domain-containing E3 ubiquitin ligase
IC50	50 % growth-inhibitory concentrations
IDH-wt	Isocitrate dehydrogenase-wildtype
KLF4	Krüppel-like factor 4
KRAB	Krüppel-associated box
MeCP2	Methyl CpG binding protein 2
MGMT	O^6-methylguanine DNA methyltransferase
MMR	Mismatch repair
MRI	Magnetic resonance imaging
NF1	Neurofibromatosis type 1
NHEJ	Non-homologous end-joining
O_6-BG	O_6-benzylguanine
OXPHOS	Oxidative phosphorylation
PAM	protospacer adjacent motif
PCA	Principal component analysis
PDGFRα	Platelet derived growth factor alpha
PI	Propidium iodide
PKM2	Pyruvate kinase M2

qRT-PCR	quantitative reverse transcription polymerase chain reaction
RNP	Ribonucleoprotein
SAM	S-adenosyl methionine
scRNAseq	Single cell RNA sequencing
SD	Standard deviation
sgRNA	Single guide RNA
siRNAs	Small interfering RNAs
SpCas9	Streptococcus pyogenes
SSC-A	Side scatter area
STAT3	Signal transducer and activator of transcription 3
TALENs	Transcription activator-like effector nuclease
TBE	Tris-borate-EDTA
TERT	Telomerase reverse transcriptase
TFs	Transcription factors
TM	Transcriptional modifiers
TMZ	Temozolomide
tracrRNA	Trans-activating CRISPR RNA
TSS	Transcription start site
UBC	Ubiquitin C
VP16	virus protein 16
VST	Variance stabilizing transformation
WHO	World Health Organization
WT	Wild type
ZFNs	Zinc finger nucleases

1. Introduction

1.1 Glioblastoma

1.1.1 Definition

Globally, the age-standardized prevalence rates of tumors in the central nervous system (CNS) exhibited a notable increase of around 17.3 % from 1990 to 2016 (Patel et al., 2019). In 2016, the prevalence of brain and other CNS tumors was approximately 0.33 million cases, resulting in approximately 0.227 million deaths (Patel et al., 2019). Gliomas, considered to arise from glial cells, are the most predominant malignant brain tumors in adults, with an incidence rate of 4.67 to 7.73 per 100, 000 people (Canoll and Goldman, 2008; Delgado‐Martín and Medina, 2020).

According to the World Health Organization (WHO) grading system, glioblastoma is a WHO grade IV adult–type glioma and is considered as the most common and aggressive primary brain tumor, accounting for almost 57 % of all gliomas and 48 % of all primary malignant tumors in CNS (Dewdney et al., 2023; Ostrom et al., 2018). The pathologic characteristics of glioblastoma encompass those of a diffusely infiltrative neoplasm with an astroglial appearance, accompanied by microvascular proliferation and/or pseudopalisading necrosis (Wen et al., 2020). Although recent advances in the molecular pathogenesis, biology, and multimodal therapy of glioblastoma, it's still incurable. A five year of survival after the initial diagnosis is achieved only in less than 5 % of patients with glioblastoma, and this rate has not improved in the past century (Brodbelt et al., 2015; Dobes et al., 2011; Stupp et al., 2009; Topkan et al., 2018). Recurring tumorigenesis and chemoresistance are the two main roadblocks to improve the prognosis of glioblastoma patients (Wen et al., 2020).

1.1.2 Epidemiology

The incidence of glioblastoma ranges from 0.59 to 5 per 100,000 people in the world (highest in North America, Australia, Northern and Western Europe), and some studies

have reported an increase in the incidence, as shown in **Figure 1** (Grech et al., 2020; Leece et al., 2017). Additionally, this incidence varies by age and sex. The median age at glioblastoma diagnosis is 65 years, with peak incidence occurring between 75 and 84 years, and is higher among white men (Tan et al., 2020).

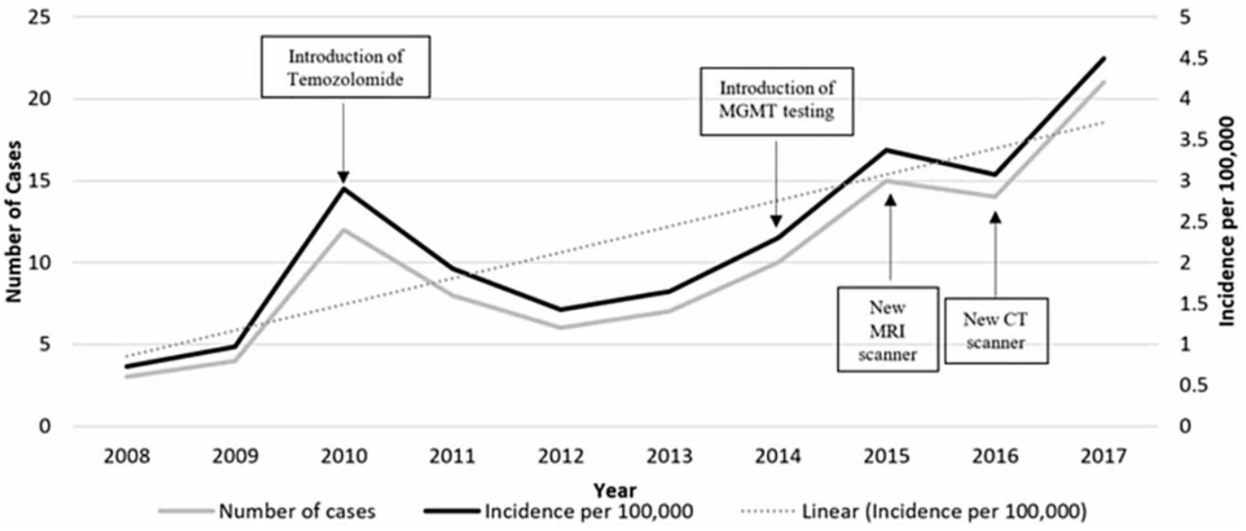

Figure 1: Annual cases and incidence of glioblastoma, along with potential causal factors. The figure is taken from (Grech et al., 2020).

Glioblastoma arises supposedly from DNA mutations, resulting in uncontrolled cellular proliferation. Unfortunately, only a few risk factors for glioblastoma have been validated. Exposure to ionizing radiation of the head and neck is the only known risk factor; conversely, a history of allergies, asthma, and other atopic diseases have been validated as a protective factor (Amirian et al., 2016; Fisher et al., 2007; Linos et al., 2007). The overwhelming majority of patients with glioblastoma has no family history of cancer, and only about 5 % of all glioma patients manifest genetic syndromes such as Lynch and Li-Fraumeni syndrome (Ranger et al., 2014; Scheurer et al., 2010).

1.1.3 Classification and characteristics

Traditionally, glioblastoma has been categorized into primary and secondary forms. The primary glioblastomas account for approximately 90 %, which are Isocitrate

dehydrogenase-wildtype (IDH-wt) and predominate in elderly patients without any identifiable precursor lesion, resulting in the worst prognosis (Delgado‐Martín and Medina, 2020; Ohgaki and Kleihues, 2013). In contrast, secondary glioblastomas typically emerge from lower-grade gliomas (diffuse or anaplastic astrocytoma), which harbor the IDH mutation and appear in younger patients with a more favorable prognosis (Delgado‐Martín and Medina, 2020; Tan et al., 2020). Notably, according to the updates for WHO classification of CNS tumors in 2021, the term IDH mutant “glioblastoma” has been dropped and replaced with the term IDH-mutant “astrocytoma or oligodendroglioma” to distinguish them from IDH-wt glioblastoma, as shown in **Figure 2** (Torp et al., 2022).

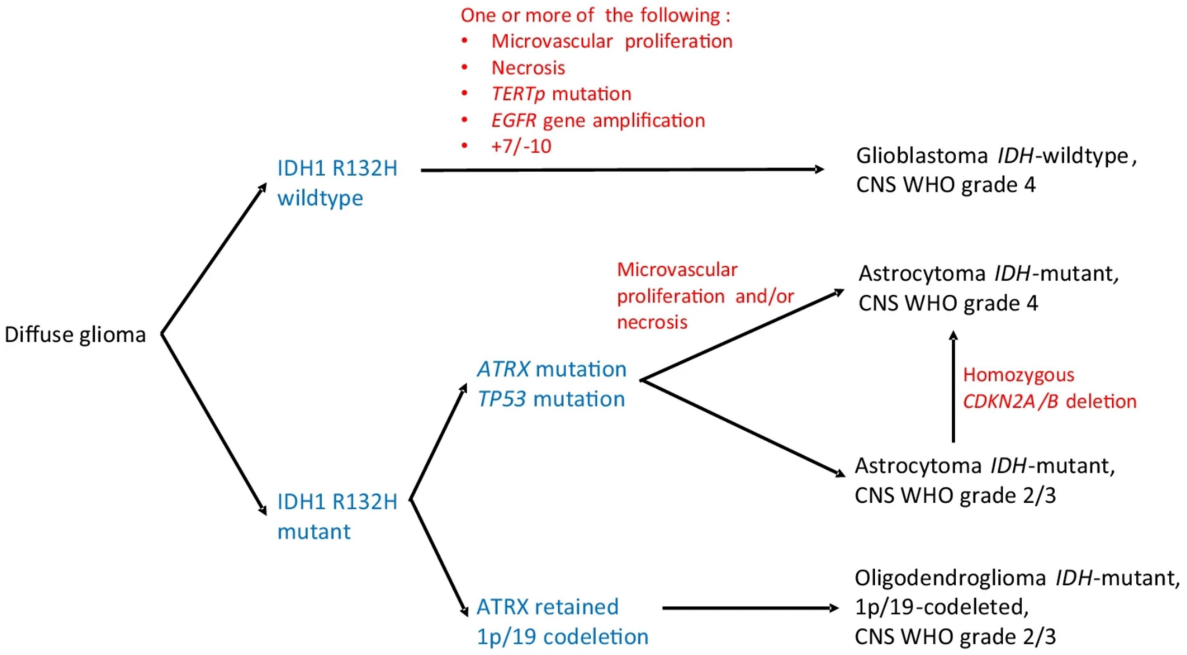

Figure 2: Streamlined classification and diagnostic algorithm of diffuse glioma based on the 2021 WHO classification of CNS tumor. The figure is taken from (Torp et al., 2022).

In recent years, a deeper understanding of glioblastoma pathology has been facilitated by continued advances in genetic sequencing capabilities. Therefore, glioblastomas can also be separated into three subgroups based on their genomic profiling, which include classical, mesenchymal, and proneural, each containing specific somatic alterations. For example, the classical subgroup is enriched for the tumors with a high frequency of

epidermal growth factor receptor (EGFR) amplifications, and loss of cyclin-dependent kinase inhibitor 2A/B (CDKN2A/B). The mesenchymal subgroup is marked by deletion of neurofibromatosis type 1 (NF1), and heightened tumor infiltration by macrophages. The proneural subgroup is characterized by amplifications of cyclin-dependent kinase 4 (CDK4) and platelet-derived growth factor alpha (PDGFRα) (Wen et al., 2020). These 3 subgroups, along with mixed entities between them, collectively encompass the majority of glioblastomas, and all linked to human telomerase reverse transcriptase (TERT) promoter mutations (Brennan et al., 2013; Ceccarelli et al., 2016; Sturm et al., 2012; Wang et al., 2017). In addition, the development of single-cell RNA sequencing (scRNAseq) analysis is also helpful in redefining the classification and characteristics of glioblastoma. Some scRNAseq studies revealed that tumor composition varies not only across patients but also exhibits significant heterogeneity within a single tumor in glioblastoma (Brennan et al., 2013; Couturier et al., 2020; Neftel et al., 2019).

1.1.4 Clinical presentation and diagnosis

The clinical presentation of glioblastoma is typically associated with the location and size of the tumor at diagnosis (Gilard et al., 2021). The headache is the most prevalent initial symptom in 30-50 % of glioblastoma patients, followed by motor deficits, weight loss, diminished overall condition, confusion, and visual or speech impairments (Gilard et al., 2021; Yuile et al., 2006). Furthermore, seizures appear in 20-40 % of patients with glioblastoma, effectively managed with anticonvulsants throughout the disease course (Chaichana et al., 2009). Occasionally, symptoms may escalate rapidly, potentially leading to misdiagnosis as a stroke (Omuro and DeAngelis, 2013).

Magnetic resonance imaging (MRI) scans have evolved as the gold standard imaging technique in the diagnosis of glioblastoma. The imaging characteristics of glioblastoma typically encompass an infiltrative, heterogeneous, ring-enhancing lesion exhibiting central necrosis and surrounded by peritumoral edema, and involvement of the corpus callosum is frequently observed in butterfly glioblastoma (Alexander and Cloughesy,

2017). Moreover, advancements in MRI technology also contributed to diagnosing glioblastoma more accurately by assessing the specific physiological or metabolic features. For example, Dynamic Susceptibility Contrast (DSC) MRI can employ the spatial distribution of a contrast agent to evaluate the size of blood vessels (Kalpathy-Cramer et al., 2014). Perfusion-weighted imaging, derived from the DSC technique, involves serial imaging capturing the initial passage of the contrast agent to generate maps of parameters, like cerebral blood volume (CBV) (Kalpathy-Cramer et al., 2014). Given that microvascular proliferation induced by tumor-induced angiogenesis is a characteristic of glioblastoma, CBV measurement may help to differentiate glioblastoma from other tumor types and grades (Kickingereder et al., 2014; Law et al., 2004; Lee et al., 2018; Suh et al., 2019; Wesseling et al., 1994). The apparent diffusion coefficient (ADC) based on diffusion-weighted MRI is inversely proportional to the density of the cell; which can be used as a tool to identify glioblastoma from lower-grade glioma and lymphoma (Guo et al., 2002; Hayashida et al., 2006; Higano et al., 2006; Lu et al., 2019; Sugahara et al., 1999).

1.1.5 Treatment and prognosis

So far, no curative treatment is available, and the protocol of standard treatment has remained unchanged for nearly 20 years (Wen et al., 2020). The current standard therapy consists of surgical resection followed by temozolomide (TMZ) chemotherapy, and concomitant ionizing radiotherapy; nevertheless, the prognosis of glioblastoma patients remains poor with a median overall survival of almost 15-18 months (Wen et al., 2020; Yang et al., 2022).

The gross total resection (GTR) is typically recommended when it is feasible. Some studies have revealed that GTR may enhance survival outcomes, even in old patients with glioblastoma; simultaneously, the improved survival by maximal resection is irrespective of molecular status (Brown et al., 2016; Chaichana et al., 2014; Molinaro et al., 2020; Noorbakhsh et al., 2014). A randomized trial also indicated that the utilization of

5-aminolevulinic acid (5-ALA), an optical imaging agent, facilitates the visualization of malignant tissue during surgery, leading to enhanced rates of gross total resection and improved 6-month progression-free survival (Stummer et al., 2006).

Even with GTR, infiltrating tumor cells will remain after surgical resection, in part because of the balance between resection and preservation of neurological function during surgery (Kelly et al., 1987; Lacroix and Toms, 2014; Wen et al., 2020; Yamahara et al., 2010). Therefore, patients with glioblastoma need to receive adjuvant therapy. Typically, patients undergo a 6-week course of radiation therapy (60 gray, delivered in 30 fractions of 2 gray) along with concurrent administration of TMZ (Schaff and Mellinghoff, 2023; Stupp et al., 2009; Stupp et al., 2005). TMZ, one of the first-line chemotherapeutic agents, is commonly used to treat glioblastoma because of its limited side effects. TMZ is a DNA alkylating agent known to induce cell cycle arrest at G2/M leading to apoptosis. The cytotoxicity of TMZ is mainly mediated by the addition of methyl groups at multiple sites; especially, O^6 sites on guanines in genomic DNA as shown in **Figure 3** (Della Monica et al., 2022). This leads to the insertion of a thymine instead of a cytosine opposite the methylguanine during subsequent DNA replication and can induce cell death through the DNA mismatch repair (MMR) pathway (Della Monica et al., 2022). Notably, the incorporation of TMZ has demonstrated an improvement in survival by several months and an enhancement in long-term survival when compared with radiotherapy alone (Stupp et al., 2005). However, patients with glioblastoma frequently develop TMZ resistance, largely due to O^6-methylguanine DNA methyltransferase (MGMT) expression which is determined by DNA methylation in MGMT promoter (Hegi et al., 2005; Wang et al., 2022a). We will further explain the relationship between the TMZ effect and MGMT expression in the following sections.

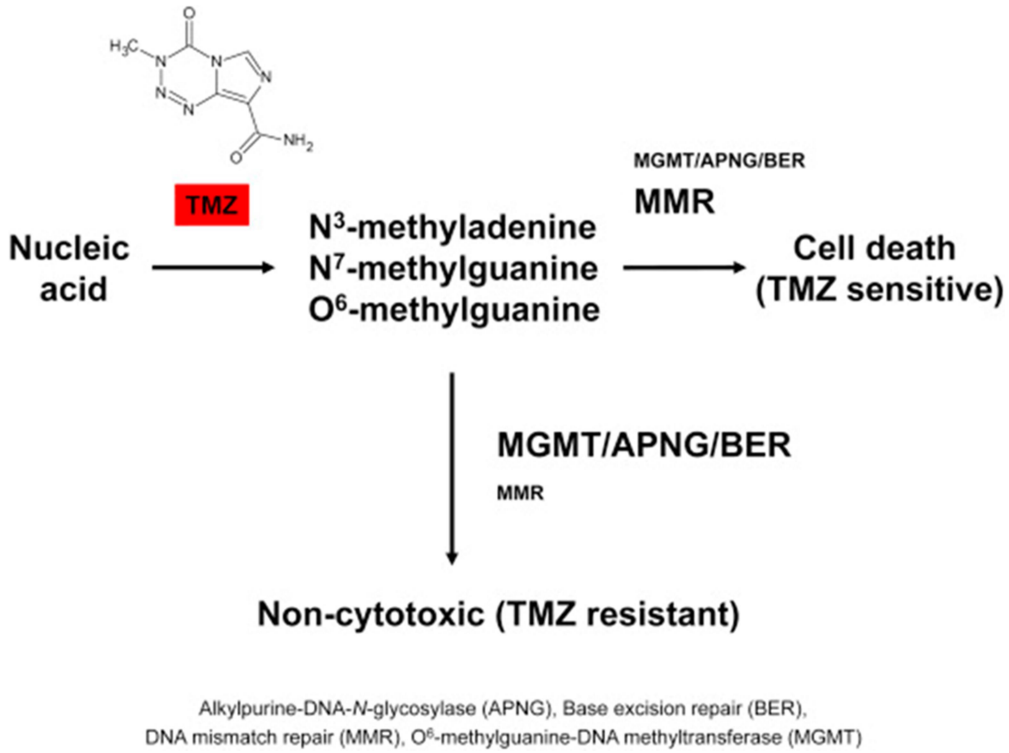

Alkylpurine-DNA-*N*-glycosylase (APNG), Base excision repair (BER), DNA mismatch repair (MMR), O^6-methylguanine-DNA methyltransferase (MGMT)

Figure 3: Mechanism of temozolomide and temozolomide resistance. TMZ adds methyl groups at different positions on nucleic acid (N^7 and O^6 sites on guanine, N^3 sites on adenine), and the mutation can be retained. On one hand, the damaged DNA is fixed through the activated MMR pathway, resulting in glioblastoma cells being sensitive to TMZ. On the other hand, the methylated positions can also be removed through different pathways, such as MGMT, APNG, and BER; subsequently, the glioblastoma cells are TMZ-resistant. TMZ, temozolomide; MMR, DNA mismatch repair; MGMT, O^6-methylguanine methyltransferase; APNG, alkylpurine-DNA-N-glycosylase; BER, base excision repair. The figure is taken from (Lee, 2016).

The recurrence of glioblastoma is inevitable, and the median progression-free survival is around 7 months for the patients (Stupp et al., 2005; Stupp et al., 2017). Once recur, the estimated median overall survival ranges from 24 to 44 weeks, and no standardized systemic treatment is currently established for patients with glioblastoma (Clarke et al., 2011; Lamborn et al., 2008; Wu et al., 2010). Therefore, there is an urgent demand for the improvement of glioblastoma therapeutic strategies, some novel approaches have emerged in recent years such as precision therapy, immunotherapy, and viral therapy. However, these efforts have not translated into substantial outcomes due to the unique biological factors of glioblastoma, like significant inter- and intratumoral heterogeneity, the blood-brain barrier, and the special tumor microenvironment (Wen et al., 2020).

1.2 The role of DNA methylation and MGMT in glioblastoma

1.2.1 DNA methylation definition

Epigenetics encompasses the inherited changes in gene expression during mitosis, which is caused by structural and chemical alterations in DNA and its associated regulatory proteins, excluding changes in nucleotide sequences (Felsenfeld, 2014; Holliday, 2006). Epigenetic modifications include DNA methylation, histone modification, non-coding RNA-induced modification, and chromatin remodeling (Dawson and Kouzarides, 2012; Johnson et al., 2015).

DNA methylation is the most widely studied epigenetic modification. It is characterized by the addition of methyl group at various positions, including the C-5 site of cytosine, N-4 site of cytosine, N-7 site of guanine, and N-6 site of adenine (Jones, 2012; Lövkvist et al., 2016). Among these, DNA methylation at the C-5 site of cytosine within the context of cytosine-guanine dinucleotides (CpG) is the most common in mammalian cells, as shown in **Figure 4A** (Uddin et al., 2022). Furthermore, DNA methylation plays a crucial role in cell physiology, encompassing the regulation of gene expression, silencing of retroelements, maintenance of centromere stability and chromosome segregation during mitosis, as well as governing X chromosome inactivation and the monoallelic silencing of imprinted genes (Bird, 1986; Gartler and Riggs, 1983; Mohandas et al., 1981).

The reaction of DNA methylation is induced by DNA methyltransferases (DNMTs). The identified members of the DNMT family include DNMT1, DNMT2, DNMT3a, DNMT3b, and DNMT3L (Berger, 2007). These enzymes transfer a methyl group from a common methyl donor, S-adenosyl methionine (SAM), to different positions on DNA (Bird, 2002; Dong and Cui, 2019). DNMT1 is mainly responsible for maintaining this epigenetic modification (Kulis and Esteller, 2010). DNMT3a and DNMT3b are de novo DNA methyltransferases, simultaneously responsible for the correction during the methylation process (House, 2013). Although DNMT2 and DNMT3L do not have the function of promoting DNA methylation, research suggests that DNMT3L can enhance the

methyltransferase activity of DNMT3a and inhibit gene transcription through interaction with histone deacetylase 1 (Chedin et al., 2002; Deplus et al., 2002).

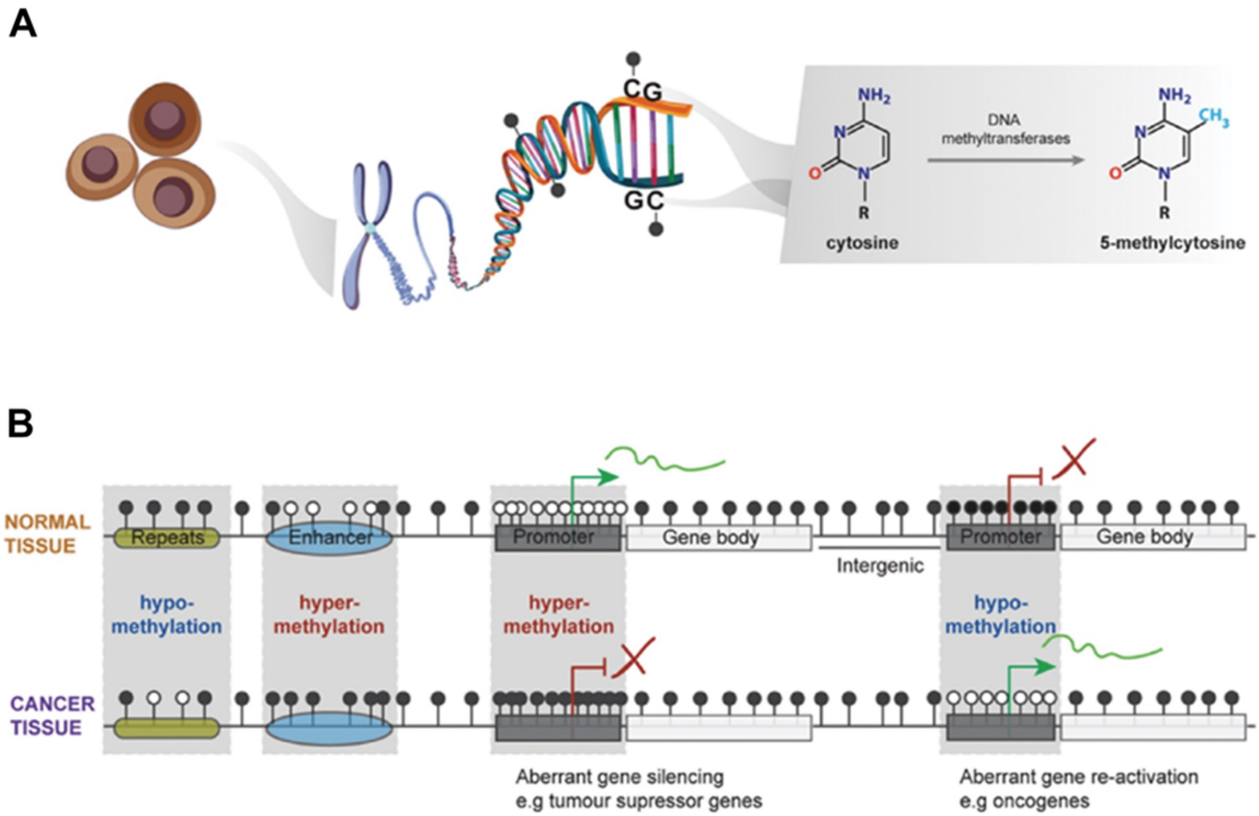

Figure 4: The differential profiling of DNA methylation in normal and cancer genomes. (A) The DNA DNMT enzymes transfer a methyl group to the C-5 site of cytosine within the context of CpG dinucleotide. **(B)** The widespread distinct pattern of DNA methylation between normal (upper) and cancer (down) tissues across the whole genome, including all of the gene regulatory elements. One of the hallmarks of cancer tissue is the overall loss of 5mC compared with normal tissue, accompanied by aberrant DNA methylation across enhancers and promoters. This feature leads to the activation of oncogenes and repression of tumor suppressor genes. White circle, unmethylated CpG; black circle, methylated CpG. DNMT, DNA methyltransferase; CpG, cytosine-guanine dinucleotides; 5mC, 5-methylcytosine. The figure is taken from (Skvortsova et al., 2019).

There are approximately 28 million CpG sites in the human genome, 70 % of which are methylated (Skvortsova et al., 2019). However, CpG sites are not as evenly distributed as imagined; instead, they are concentrated in certain regions called CpG islands (CGIs) (Gardiner-Garden and Frommer, 1987). The CGIs are generally about 500-1000 bases in length and are widely distributed in the promoter or the first exon of genes, and

housekeeping genes (Gardiner-Garden and Frommer, 1987; Takai and Jones, 2002). Studies have shown that CGIs exist in 60 % of gene promoter regions (Saxonov et al., 2006). In normal somatic cells, in contrast to scattered CpG sites, CpG sites within CGIs are typically unmethylated, as shown in **Figure 4B**. In addition, the distribution density of the CpG site itself does not affect the expression of genes, but is regulated by the methylation level of CGIs in the promoter region. Unmethylated or hypomethylated CGIs can maintain the open structure of chromatin and provide a binding platform for transcription factors to activate gene transcription (Tost, 2009). However, when CGIs are hypermethylated, they will prevent the transcription of transcription factors, resulting in the inhibition of gene expression (Maxwell et al., 2009).

1.2.2 The role of DNA methylation in the regulation of MGMT expression

Although TMZ is widely used as a chemotherapy agent for postoperative treatment in glioblastoma patients, chemoresistance is in high prevalence. This is because the DNA adducts generated by TMZ can be rapidly reversed by an intracellular suicide DNA repair enzyme called MGMT, resulting in reduced effectiveness of TMZ in patients, as shown in **Figure 3** (Mansouri et al., 2019). MGMT is ubiquitously expressed in normal human tissues, it can transfer the methyl group at the O^6 position of guanine to its own cysteine residue, restoring the nucleotide to its natural state and facilitating the repair of DNA (Gerson et al., 1986; Hegi et al., 2008; Yu et al., 2019).

The MGMT encoding gene is located on chromosome 10, with a total length of 300,437 bp (Kent, 2002; Pruitt et al., 2005). It is well known that *MGMT* gene expression is controlled by DNA methylation of the promoter region and hypermethylation results in decreased transcription and expression of the MGMT protein (Christmann et al., 2010). The state of CGI hypermethylation can cause heterochromatinization, accompanied by rearrangement and random positioning of nucleosomes; which may cover the transcription start site (TSS) and prevent transcription factors (TFs) from binding (Costello et al., 1994; Watts et al., 1997). *MGMT* promoter hypermethylation has been

observed in a variety of tumors, which is consistent with epigenetics serving as a common mechanism for tumor suppressor gene silencing during malignant tumor progression (Esteller et al., 2001; Esteller et al., 1999; Ting et al., 2006).

In glioblastoma, the effectiveness of TMZ is closely related to the methylation status of the *MGMT* promoter region. Several clinical studies demonstrated that glioblastoma patients with hypermethylation of the *MGMT* promoter benefit most from treatment with TMZ and have significantly improved overall survival compared with patients with hypomethylation of the *MGMT* promoter (Hegi et al., 2005; Hegi et al., 2008; Stupp et al., 2009). Patients with a hypermethylated *MGMT* promoter experienced recurrence after a more extended time interval under the combined treatment of radiotherapy and TMZ, in contrast to patients with an unmethylated *MGMT* promoter (Brandes et al., 2009). Therefore, the methylation status of the *MGMT* promoter is not only a valid biomarker for predicting tumor sensitivity to TMZ but also for the prognosis of glioblastoma patients (Mansouri et al., 2019; Perry et al., 2017). On the other hand, this finding makes MGMT a potential target for modulating TMZ resistance in tumors with MGMT expression. Some MGMT inhibitors, such as O_6-benzylguanine (O_6-BG) is a synthetic derivative of guanine, have been tested in combination with TMZ treatment; unfortunately, the systemic toxicity of O_6-BG reduced TMZ therapeutic window instead of a better clinical benefit compared with TMZ alone (Quinn et al., 2009; Warren et al., 2012).

1.2.3 DNA methylation in other cancer-related research

More and more studies revealed aberrant epigenetic changes as a hallmark in human cancers, including glioblastoma (Kelly and Issa, 2017; Lu et al., 2020; Topper et al., 2020). Many studies also indicated that the methylation patterns in glioma cells differ from those in normal cells (de Souza et al., 2018; Liao et al., 2018). Thus, the initiation and progression of tumorigenesis involve the disruption of normal epigenetic processes, which is mainly featured by genome-wide hypomethylation accompanied by hypermethylation of GGI in certain gene promoter regions, as shown in **Figure 4B**

(Baylin and Jones, 2011; Jones and Baylin, 2002; Jones and Baylin, 2007).

Genome-wide hypomethylation contributes to heightened genomic instability and aneuploidy, which are common features across various cancer genomes (Ehrlich and Lacey, 2012). Simultaneously, the loss of DNA methylation can result in abnormal expression of oncogenes, transposable elements, and repetitive sequences (Ehrlich and Lacey, 2012; Jones and Baylin, 2007). Interestingly, some CpG-deficient enhancer regions that are unmethylated in normal tissues, are often methylated in tumor tissues (Akhtar-Zaidi et al., 2012; Aran et al., 2013; Taberlay et al., 2016).

Hypermethylation of GGI in gene promoter regions is typically related to the silencing of some tumor suppressor genes, as well as genes regulating cell growth and downstream signaling pathways (Skvortsova et al., 2019). The CpG island methylator phenotype (G-CIMP) that is related to other predictive biomarkers of glioblastoma, such as the methylation statues of *MGMT* and *IDH-1* mutation, is thought to be a predictor of prognosis in patients with glioma (Mack et al., 2014; Malta et al., 2018). The G-CIMP in the majority of glioblastoma patients is negative (Kloosterhof et al., 2013).

DNA methylation also plays an important role in glioblastoma metabolism, such as glycolysis, mitochondria function, and oxidative phosphorylation (OXPHOS) (Dong and Cui, 2019). For instance, pyruvate kinase M2 (PKM2), an enzyme governing the destiny of pyruvate during glycolysis, exhibits a high expression that is closely associated with the hypomethylation of intron 1 in its coding genes in a variety of tumors, including glioblastoma (Desai et al., 2014). Conversely, other genes related to glycolysis are hypermethylated in IDH1-mutant glioblastoma, such as GLAM, GAPDH, LDHA, and ENO1 (Chen et al., 2017). Another study showed that Krüppel-like factor 4 (KLF4), as a zinc finger transcription factor, stimulates mitochondrial fusion and augments spare respiratory capacity by methylation-dependent KLF4 binding activity in glioblastoma (Wang et al., 2018).

1.3 Genome editing and the CRISPR/Cas9 system

1.3.1 The development of genome editing

DNA, carrying the genetic code, serves as the blueprint for the synthesis of proteins, which are essential macromolecules with diverse functions in cells. This relationship is governed by the processes of transcription and translation. Mutations at specific DNA loci can lead to abnormal protein expression, and more than 3,000 mutations have already been confirmed to be associated with disease phenotypes. In classic genetics, radiation and chemical mutagens were utilized to mediate the non-specific DNA mutations in lower organisms to reveal important processes in development and human disease, but it's infeasible for higher organisms such as mice due to the generation of a large number of mutations (Bier, 2005; Capecchi, 2001; Nüsslein-Volhard and Wieschaus, 1980). On the contrary, reverse genetics is a molecular genetics method to elucidate the function of a gene by analyzing the phenotypic effects resulting from specific engineered gene sequences (Khalil, 2020). Advances in genetic promoted the development of therapeutic genome editing techniques.

Programmable nucleases-mediated genome editing technologies have been shown effective genome editing in various model organisms and mammalian cells. Ongoing endeavors in both industry and academia aim to further develop these tools into potential therapeutics (Genovese et al., 2014; Li et al., 2011; Tebas et al., 2014; Yin et al., 2014). These nucleases mainly include four main types: meganucleases, zinc finger nucleases (ZFNs), transcription activator-like effector nuclease (TALENs), and clustered regularly interspaced short palindromic repeats (CRISPR)-associated nuclease 9 (Cas9) (CRISPR/Cas-9) (Khalil, 2020). All the nucleases achieve specific DNA binding through protein-DNA interactions, except Cas9 which is targeted to specific DNA positions under the guidance of a short RNA molecule that base-pairs directly with the target sequence and through protein-DNA interactions (Cox et al., 2015).

The mechanism of programmable nucleases-mediated genome editing is based on the induction of DNA double-strand breaks (DSBs) at specific genomic positions, and followed by the recruitment of endogenous repair machinery. There are two different ways to repair the DSB: The first one is homology-directed repair (HDR), which requires precise DNA repair through homologous recombination based on exogenous DNA templates. In contrast to this, the second one is non-homologous end-joining (NHEJ), which could repair the DNA by directly rejoining the two ends of DSB without a template. While this process is effective in DNA repair, it is also susceptible to introducing errors and mutations (Jasin and Rothstein, 2013; Rouet et al., 1994).

1.3.2 The origin, composition, and function of CRISPR/Cas9 system

The CRISPR/Cas system, a 21-47 bp repetitive DNA cluster, was originally discovered in bacteria and archaea as a naturally occurring protective immunity (Godde and Bickerton, 2006; Horvath et al., 2008; Hsu et al., 2014; Marraffini and Sontheimer, 2010). It protects prokaryotic cells from infection by phages and viruses, as well as any other harmful events, such as foreign genetic elements, invading pathogens, and plasmids (Chekani-Azar et al., 2020; Xu and Li, 2020). The CRISPR/Cas system is mainly composed of two components: a repeat spacer array capable of generating CRISPR RNA (crRNA) and trans-activating CRISPR RNA (tracrRNA), along with Cas proteins exhibiting endonuclease activity (Xu and Li, 2020). Typically, upon the initial invasion of a foreign genetic element, it will be broken down into short fragments by the Cas proteins and integrated into the CRISPR array to form a new spacer (naidu gopal Hariprabu et al., 2021). Therefore, when the same invader invades again, prokaryotic cells can quickly recognize foreign DNA under the guidance of crRNA, and then Cas proteins cleave it to protect the host (Chekani-Azar et al., 2020; Xu and Li, 2020).

CRISPR/Cas9 system, class1-typeII CRISPR/Cas system, derived from Streptococcus pyogenes (SpCas9) (naidu gopal Hariprabu et al., 2021; Zhan et al., 2019). Since it relies on a single Cas protein to cleave foreign DNA, it has become the fastest-developing and

widely used genome editing tool (Jinek et al., 2012). The CRISPR/Cas9 system consists of two main parts: single guide RNA (sgRNA) and Cas9 protein (Cong et al., 2013; Mali et al., 2013). sgRNA is a synthetic complex formed by the hybridization of crRNA and tracrRNA: crRNA contains a 20bp nucleotide sequence that is complementary to the target DNA, which determines the specificity of the Cas9 protein cleavage; the main function of tracrRNA is to bind and activate Cas9 protein (Nishimasu et al., 2014; Sander and Joung, 2014). Cas9 primarily comprises two nuclease domains, HNH and RuvC, working collaboratively to generate ribonucleoprotein (RNP) (naidu gopal Hariprabu et al., 2021). The HNH domain is responsible for cleaving the DNA strand complementary to the spacer sequence, whereas the non-complementary strand is cleaved by the RuvC domain (Redman et al., 2016; Uddin et al., 2020; Xu and Li, 2020). Generally, the sgRNA initially binds to a complementary sequence at the specific DNA position, subsequently activating the Cas9 endonuclease enzyme to conduct gene editing on the target DNA loci, resulting in DNA DSBs as shown in **Fig 5**. Moreover, sgRNA can be readily designed using some specialized web-based tools, such as CHOPCHOP and CRISPROR. A crucial requirement in the design process is the presence of the protospacer adjacent motif (PAM) sequence, positioned immediately downstream of the sgRNA target sequence in the genome (Ansari et al., 2022). The PAM sequence plays a crucial role in sgRNA target recognition and varies based on the Cas9 protein source. For example, it is 5'-NGG-3’ in SpCas9 (Xu et al., 2020).

The CRISPR-Cas9 system has been widely applied in research areas such as gene knockout, knock-in, and high-throughput screening and modeling of the genome. Gene knockout mainly relies on the subsequent NHEJ repair method after the formation of DNA DSBs, NHEJ mediates the insertion and deletion of some base pairs, ultimately leading to gene inactivation and gene knockout; as for gene knock-in, it is mainly realized through the HDR method that relies on donor templates as shown in **Fig 5** (Cai et al., 2023). In recent years, the CRISPR system has emerged as the predominant tool for gene knock-out in both cellular and animal studies (Wang et al., 2022b; Zhu, 2022). In addition,

whether in vivo or in vitro experiments, CRISPR-Cas9 genome high-throughput screening can unveil novel biomarkers, oncogenic drivers, chemotherapy resistance mechanisms, and genes that enhance tumor cell sensitivity to standardized or coordinated treatments (Al-Sammarraie and Ray, 2021).

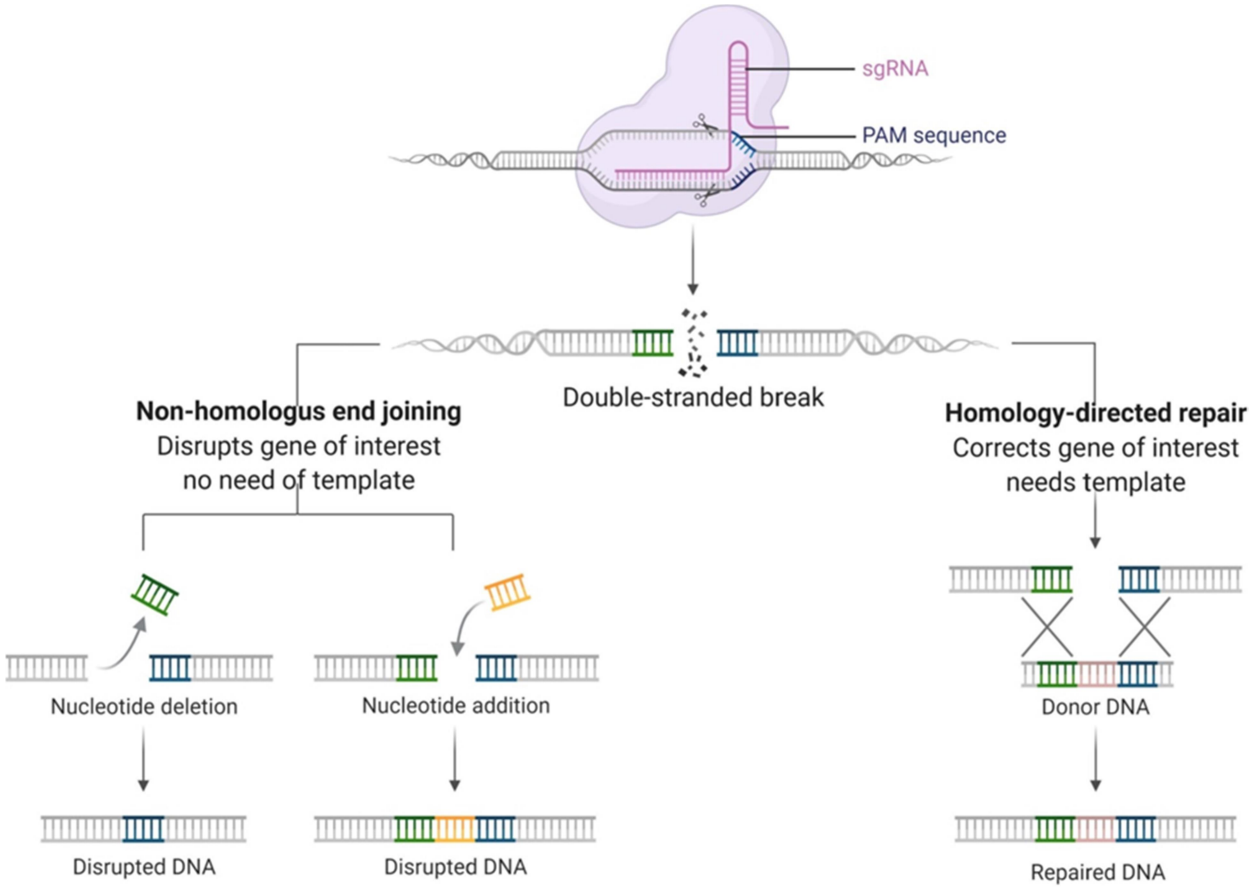

Figure 5: The mechanism of CRISPR/Cas9 genome editing system. The DSB generated through the sgRNA-mediated cleavage of Cas9 protein is closed to the region of the PAM sequence. Subsequent DNA repair occurs via the NHEJ or HDR pathways. The NHEJ-mediated error-prone repair is commonly used for gene knock-out, while the HDR pathway based on a donor DNA template is used for gene knock-in. The figure is taken from (naidu gopal Hariprabu et al., 2021).

1.3.3 dCas9-mediated epigenetic editing and CRISPRoff system

While CRISPR enables precise DNA editing, the stability of the genome structure may be compromised by structural changes resulting from the insertion or deletion of extensive DNA sequences (Cullot et al., 2019; Egli et al., 2018). With the ongoing advancement of

CRISPR gene editing technology, a novel system that regulates gene expression at the gene transcription or post-transcriptional level without damaging the genome sequence has been invented, called the CRISPR/ catalytically inactive Cas9 (dCas9) system. This modified CRISPR system is attained by introducing point mutations into the nuclease domain of the Cas9 protein (point mutations of D10A in the RuvC domain and H840A in the HNH domain) (Ansari et al., 2022; Jinek et al., 2012). These point mutations render the Cas9 protein devoid of endonuclease activity, but it does not impact the sgRNA-mediated binding efficiency to the target genome (Gilbert et al., 2013; Jinek et al., 2012).

The binding of the dCas9 protein itself at the target site disrupts transcriptional activity by impeding transcription elongation, RNA polymerase binding, or transcription factor binding (Gilbert et al., 2013). However, while this editing technology is highly effective in prokaryotic cells like bacteria and fungi, the efficiency of inhibiting gene expression in mammalian cells is very low (Gilbert et al., 2013). Notably, the dCas9 protein can be further fused to a variety of effector domains to mediate different types of gene editing at specific DNA targets. These effector domains are mainly divided into transcriptional modifiers (TM) and epigenetic modifiers (EM) (Brocken et al., 2018). The gene editing system fused with TM is called CRISPR interference (CRISPRi), which mainly relies on the fusion of dCas9 and the KRAB repressor domain to suppress gene transcription; and CRISPR activation (CRISPRa), which activates gene transcription through the fusion of dCas9 and the activator domain (Ansari et al., 2022; Gilbert et al., 2013; Kampmann, 2018). Common examples include the herpes simplex virus protein 16 (VP16) and its various copies such as VP48, VP64, VP120, along with the nuclear factor kappa B transactivation domain (p65) (Ansari et al., 2022).

In addition to the above-mentioned TMs, various EMs are fused to the dCas9 protein. Guided by sgRNA, these fusion effectors conduct precise epigenetic modification at specific DNA target locations. For instance, CRISPR systems incorporating

dCas9-DNMT3A or DNMT3A-DNMT3L fusion proteins can suppress gene transcription by inducing DNA methylation at CpG sites within specific DNA target regions (McDonald et al., 2016; Stepper et al., 2016; Vojta et al., 2016). Conversely, the dCas9-TET1 fusion protein selectively decreases DNA methylation levels (Xu et al., 2016). Furthermore, the dCas9 conjugated with p300 exhibits programmable histone acetyltransferase properties, enabling direct modification of the chromatin state and enhancing the accessibility of genomic regions (Hilton et al., 2015).

CRISPRoff is a CRISPR/dCas9 gene editing system (DNMT3A-DNMT3L-dCas9-KRAB) invented by Nunez et al., which contains multiple fusion effector domains (Nunez et al., 2021). It can induce hypermethylation at specific CpG sites in DNA through transient expression in cells. Compared with previously reported similar CRISPR systems, it has the following advantages: 1. It can not only induce DNA methylation within the CGI region but also increase the methylation level of scattered CpG sites, enabling the inhibition of the expression of a majority of genes. 2. It can precisely mediate methylation within a targeted window, typically spanning approximately 1000 base pairs; 3. The mediated gene inhibition effect is heritable and remains stable through cell division and stem cell differentiation (Nunez et al., 2021).

1.4 Aim of the study

In summary, glioblastoma is the most common malignant and incurable tumor in the CNS. Despite the limited benefit of TMZ-mediated chemotherapy and the frequent occurrence of chemoresistance, it remains an important part of current standard therapy. Hence, it's urgent to solve the problem of TMZ resistance. According to the current studies, the intracellular expression of MGMT plays a crucial role in TMZ resistance, whose expression is negatively correlated with the DNA methylation level of its promoter region. In this study, we used the CRISPRoff epigenetic editing system to address the following questions:

(1) Test whether we could downregulate the MGMT expression through targeted DNA methylation using CRISPRoff in different stable transfection human glioblastoma cell lines.

(2) Investigate whether successful downregulation of MGMT expression can reverse the TMZ resistance in human glioblastoma cell lines.

(3) Characterize the changes of DNA methylation level at CpG sites within the *MGMT* promoter region, and evaluate potential off-target effects of the CRISPRoff epigenetic editing system.

2. Materials and Methods

2.1 Materials

2.1.1 Chemicals and reagents

Table 1: Chemicals and reagents

Item	Manufacturer
10X NEB buffer	New England Biolabs, Frankfurt, Germany
10X Oligo annealing buffer	Invitrogen, Carlsbad, USA
2-Propanol	AppliChem GmbH, Darmstadt, Germany
30 % Hydrogen peroxide	Merck, Darmstadt, Germany
6X DNA loading buffer	Biotium, Fremont, CA, USA
Agar-Agar, Kobe I	Carl Roth, Karlsruhe, Germany
Agarose	Sigma-Aldrich, Steinheim, Germany
AlamarBlue cell viability reagent	Invitrogen, Carlsbad, USA
Ammonium persulfate	Sigma-Aldrich, Steinheim, Germany
Ampicillin sodium salt	Carl Roth, Karlsruhe, Germany
Ampuwa rinsing solution	Fresenius Kabi, Bad Homburg, Germany
Benzonase	Merck, Darmstadt, Germany
Boric acid	Sigma-Aldrich, Steinheim, Germany
Bromophenol blue sodium salt	Sigma-Aldrich, Steinheim, Germany
BsaI-HF®v2 restriction enzyme	New England Biolabs, Frankfurt, Germany
DNA-exitusPlus IF	AppliChem GmbH, Darmstadt, Germany
Ethanol	Merck, Darmstadt, Germany
Ethanol 70 %	Fischar, Saarbrücken, Germany
Ethylene diamine tetra-acetic acid disodium salt (EDTA)	Sigma-Aldrich, Steinheim, Germany
GelRed® Nucleic Acid Gel Stain	Biotium, Fremont, CA, USA

Glucose	Carl Roth, Karlsruhe, Germany
Glycerol	Carl Roth, Karlsruhe, Germany
Glycine	Carl Roth, Karlsruhe, Germany
Halt Protease Inhibitor-Cocktail	Thermo Fisher Scientific, Waltham, USA
Hydrochloric acid 37 %	Carl Roth, Karlsruhe, Germany
LB Broth	Carl Roth, Karlsruhe, Germany
Methanol	Sigma-Aldrich, Steinheim, Germany
PageRuler™ Plus Prestained Protein Ladder, 10 to 250 kDa	Thermo Fisher Scientific, Waltham, USA
Phosphate buffered saline tablet	Sigma-Aldrich, Steinheim, Germany
Pierce ECL Western Blotting Substrate	Thermo Fisher Scientific, Waltham, USA
Potassium hydroxide (KOH)	Sigma-Aldrich, Steinheim, Germany
Powdered milk	Carl Roth, Karlsruhe, Germany
Propidium iodide (PI)	Merck, Darmstadt, Germany
Proteinase K solution	Carl Roth, Karlsruhe, Germany
Puromycin dihydrochloride	Carl Roth, Karlsruhe, Germany
PyroMark annealing solution	Qiagen, Dusseldorf, Germany
PyroMark binding solution	Qiagen, Dusseldorf, Germany
PyroMark denaturation solution	Qiagen, Dusseldorf, Germany
PyroMark Gold Q96 Reagents	Qiagen, Dusseldorf, Germany
PyroMark washing buffer, 10X	Qiagen, Dusseldorf, Germany
Ready-to-Use 1 kb DNA Ladder	Biotium, Fremont, CA, USA
Ready-to-Use 100bp DNA Ladder	Biotium, Fremont, CA, USA
ROTI ® Fect PLUS	Carl Roth, Karlsruhe, Germany
ROTIPHORESE®Gel 30 (37.5:1)	Carl Roth, Karlsruhe, Germany
SDS solution (20 %)	Bio-Rad Laboratories, Munich, Germany
Silicone paste KORASILON	Carl Roth, Karlsruhe, Germany

Sodium chloride (NaCl)	Carl Roth, Karlsruhe, Germany
Sodium citrate dihydrate	Merck, Darmstadt, Germany
Sodium hydroxide (NaOH)	Carl Roth, Karlsruhe, Germany
Streptavidin Sepharose High Performance	Cytiva, Marlborough, United States
T4 DNA ligase	Thermo Fisher Scientific, Waltham, USA
T4 DNA Ligase Buffer (10X)	Thermo Fisher Scientific, Waltham, USA
TEMED	Carl Roth, Karlsruhe, Germany
Temozolomide (TMZ)	Sigma-Aldrich, Steinheim, Germany
Triton X-100	Sigma-Aldrich, Steinheim, Germany
Trizma base	Sigma-Aldrich, Steinheim, Germany
Tween 20	Carl Roth, Karlsruhe, Germany
Water, HPLC Gradient Grade	JT Baker, New Jersey, United States
β-mercaptoethanol	Sigma-Aldrich, Steinheim, Germany

2.1.2 Equipment

Table 2: Equipment

Device	Manufacturer
AccuBlock Digital Dry Baths	Labnet, Edison, NJ, USA
Automatic cell counter	Nanoentek, Seoul, Korea
Biometra TAdvanced cycler	Analytik Jena, Jena, Germany
BP211D Balance	Sartorius, Goettingen, Germany
Cell culture CO_2 incubator	Heraeus, Hanau, Germany
Centrifuge 5415 R	Eppendorf, Hamburg, Germany
Centrifuge 5810 R	Eppendorf, Hamburg, Germany
ChemoCam imager system	Intas, Göttingen, Germany
Conical flask	Technische Glaswerke Ilmenau, Minden, Germany

E1-ClipTip Electronic pipette	Thermo Fisher Scientific, Waltham, USA
Electrophoresis power supply (E831)	Consort, Turnhout, Belgium
Electrophoresis power supply (PowerPac 300)	Bio-Rad Laboratories, Munich, Germany
FACSCanto II Flow Cytometry System	BD Bioscience, Heidelberg, Germany
Flake ice maker AF 103	Scotsman, Vernon Hills, IL, USA
Grant Y22 Thermostatic water bath	Grant, Royston, UK
Heraeus MULTIFUGE X3 centrifuge	Heraeus, Hanau, Germany
Innova™ 40/40R Benchtop Incubator Shaker	New Brunswick Scientific, Edison, NJ, USA
Intas Gel iX Imager system	Intas, Göttingen, Germany
Leica DMIL LED Fluo Microscopes	Leica, Wetzlar, Germany
Magnetic stirrer (MR 3001)	Heidolph, Schwabach, Germany
Memmert BE500 Incubator	Memmert, Schwabach, Germany
Micro diaphragm vacuum pump LABOPORT® N 86 KT.18	KNF Neuberger, Freiburg, Germany
Microwave	AEG, Frankfurt, Germany
Mikro plate Mixer (RS-MM10)	Phoenix Instrument, Garbsen, Germany
Mini Protean glass plates	Bio-Rad Laboratories, Munich, Germany
Mini Protean short plates	Bio-Rad Laboratories, Munich, Germany
Mini-Centrifuge (SU1550)	Sunlab, Aschaffenburg, Germany
Mini-Protean Tetra Vertical Electrophoresis Cell	Bio-Rad Laboratories, Munich, Germany
Mini-PROTEAN® Casting Frame	Bio-Rad Laboratories, Munich, Germany
Multipette Xstream	Eppendorf, Hamburg, Germany
Nanodrop one	Thermo Fisher Scientific, Waltham, USA
Pipette controller, PIPETBOY 2	Integra Biosciences, Zizers, Switzerland

Portable Balance (SKX 222)	Ohaus, Parsippany, NJ, USA
PyroMark Q24 Cartridge (0015)	Qiagen, Dusseldorf, Germany
PyroMark Q24 system	Qiagen, Dusseldorf, Germany
PyroMark Q24 working station	Qiagen, Dusseldorf, Germany
Rotating shaker, Roto-Shake Genie	Scientific Industries, Bohemia, NY, USA
S20 SevenEasy™ pH meter	METTLER TOLEDO, Giessen, Germany
Safety Cabinet	Heraeus, Hanau, Germany
SPECTRAMAX GEMINI Microplate Reader/Spectrofluorometer	Molecular Devices, Munich, Germany
SPECTROstar Nano Reader	BMG Labtech, Ortenberg, Germany
Steam sterilizer high-pressure climate chamber	HP Laboratory Technology, Oberschleissheim, Germany
StepOnePlus™ Real-time PCR system	Thermo Fisher Scientific, Waltham, USA
Sub-Cell Model 96 Agarose Gel Electrophoresis Systems	Bio-Rad Laboratories, Munich, Germany
Table top autoclaves 25 T – 195 T	HP Laboratory Technology, Oberschleissheim, Germany
ThermoMixer comfort	Eppendorf, Hamburg, Germany
ThermoMixer F1.5	Eppendorf, Hamburg, Germany
Thermostatic circulator, MultiTemp III	Pharmacia Biotech, Potsdam, Germany
Tube Roller (SU1400)	Sunlab, Aschaffenburg, Germany
Vacuum pump system BVC 21	Vacuubrand, Wertheim, Germany
Vortex mixer, VORTEX Genius 3	IKA-Werke, Staufen, Germany
Wet/Tank Blotting Systems	Bio-Rad Laboratories, Munich, Germany

2.1.3 Consumables

Table 3: Consumables

Item	Manufacturer
0.45 µm Nitrocellulose membrane	GE Healthcare, Solingen, Germany
10 cm petri dish	Sarstedt, Nümbrecht, Germany
10 cm tissue culture dish	Sarstedt, Nümbrecht, Germany
adhesive seals (PCR plates)	Thermo Fisher Scientific, Waltham, USA
Bacteria culture tubes, 13 ml	Sarstedt, Nümbrecht, Germany
Cell counting slide	Nanoentek, Seoul, Korea
Cell culture flasks (T25, T75)	Sarstedt, Nümbrecht, Germany
Cell culture plates (12, 24, 48, 96 well)	Sarstedt, Nümbrecht, Germany
ClipTip sterile, 300 µl	Thermo Fisher Scientific, Waltham, USA
Combitips advanced	Eppendorf, Hamburg, Germany
CryoPure tube, 1.6ml, sterile	Sarstedt, Nümbrecht, Germany
Disposable scalpel	B/Braun, Tuttligen, Germany
Falcon tubes (15, 50 ml)	Greiner Bio-One, Frickenhausen, Germany
Filter Paper Qualitative 24.0 cm	GE Healthcare, Solingen, Germany
Filtered pipette tips (10, 20, 100, 200 1000 µl)	Nerbe plus, Winsen, Germany
Flow cytometry Tube, 5 ml	Sarstedt, Nümbrecht, Germany
Glass beads 4 mm	Carl Roth, Karlsruhe, Germany
Kim wipes	Kimtech Science, Koblenz, Germany
MicroAmp Fast Optical 96-Well Reaction Plate	Thermo Fisher Scientific, Waltham, USA
Microcentrifuge tubes (1.5, 2, 5 ml)	Sarstedt, Nümbrecht, Germany
Nalgene filtration product	Thermo Fisher Scientific, Waltham, USA
Parafilm	Bemis, Neenah, USA

Pasteur pipettes, glass	Brand, Wertheim, Germany
PCR tube，200 µl	Eppendorf, Hamburg, Germany
Peha-soft nitrile gloves, powder-free	Hartmann, Heidenheim, Germany
Pipettes (5, 10, 25 ml)	Greiner Bio-One, Frickenhausen, Germany
Pipettes tips (10, 20, 100, 1000 µl)	Nerbe plus, Winsen, Germany
Screw cap tubes graduated and sterile	Greiner Bio-One, Frickenhausen, Germany
Syringe filters, 0.22 µm pore size	GE Healthcare, Solingen, Germany
Syringes	BD Bioscience, Heidelberg, Germany

2.1.4 Cell culture reagents

Table 4: Cell culture reagents

Reagent	Manufacturer
1 % Trypsin-EDTA (1X)	Gibco, Grand Island, NY, USA
Dimethyl sulfoxide (DMSO)	Carl Roth, Karlsruhe, Germany
DMEM (1X) + GlutaMAX medium	Gibco, Grand Island, NY, USA
DPBS	PAN-Biotech, Aidenbach, Germany
FBS superior	Sigma-Aldrich, Steinheim, Germany
Ham's F-10	Gibco, Grand Island, NY, USA
Opti-MEM I (1X)	Gibco, Grand Island, NY, USA
Penicillin/Streptomycin	Gibco, Grand Island, NY, USA
Trypan blue stain 0.4 %	Nanoentek, Seoul, Korea

2.1.5 Kits

Table 5: Kits

Kit	Manufacturer
DNA Clean & Concentrator kit	Zymo Research, Freiburg, Germany
EZ DNA Methylation-Gold™ kit	Zymo Research, Freiburg, Germany
HotStarTaq Plus Master Mix kit	Qiagen, Dusseldorf, Germany

MethylFlash Global DNA methylation (5-mC) ELISA kit	Epigentek, Farmingdale, USA
NucleoBond Xtra Maxi kit	Macherey-Nagel, Dueren, Germany
Pierce™ BCA Protein Assay kit	Thermo Fisher Scientific, Waltham, USA
PyroMark PCR kit	Qiagen, Dusseldorf, Germany
QuantiTect SYBR Green RT-PCR kit	Qiagen, Dusseldorf, Germany
QuantSeq FWD 3' -mRNA-Seq Kit	Lexogen, Vienna, Austria
Quick-RNA MiniPrep kit	Zymo Research, Freiburg, Germany
ZR Plasmid Miniprep-Classic kit	Zymo Research, Freiburg, Germany
Zymoclean™ Gel DNA Recovery kit	Zymo Research, Freiburg, Germany

2.1.6 Cell lines

Table 6: Cell lines

Cell line	Origin	Source
LN18	Human glioblastoma	Institute for Neuropathology at UKB
T98G	Human glioblastoma	Institute for Neuropathology at UKB
U138MG	Human glioblastoma	Leibniz Institute DSMZ, Braunschweig, Germany

2.1.7 Antibodies

Table 7: Antibodies

Antibody	Catalog No. /Clone	Dilution	Dilution Company
MGMT Monoclonal Antibody	MA5-13506/ MT 3.1	1:1000	Thermo Fisher Scientific, Waltham, USA
Monoclonal Anti-β-Actin, antibody	A5441/AC-15	1:10000	Sigma-Aldrich, Steinheim, Germany
Polyclonal Goat Anti-mouse Immunoglobulins/HRP	P0447	1:5000	Agilent Technologies, Santa Clara, CA, USA

2.1.8 Primers

Table 8: Primers used in plasmid construction

item	Sequence (5’-3’)
hU6-F	GAGGGCCTATTTCCCATGATT
MGMT-gRNA2 U6 top	CCGGGGACCGGGATTCTCACTAAG (CGG)
MGMT-gRNA2 U6 bottom	AAACCTTAGTGAGAATCCCGGTCC
MGMT-gRNA4 U6 top	CCGGCCCGGCTTGTACCGGCCGAA (GGG)
MGMT-gRNA4 U6 bottom	AAACTTCGGCCGGTACAAGCCGGG
MGMT-gRNA10 U6 top	CCGGCACACCCGACGGCGAAGTGA (GGG)
MGMT-gRNA10 U6 bottom	AAACTCACTTCGCCGTCGGGTGTG

Note: U6 top strand is the sgRNA sequence, PAM sequence is in brackets.

Table 9: Primers used in qRT-PCR

Gene	Sequence (5’-3’)	Amplicon size (bp)	Annealing temperature (°C)
MGMT	F: CCTGGCTGAATGCCTATTTC	132	60
	R: ATTTCACAACCTTCAGCAGC		
UBC	F: ATTTGGGTCGCGGTTCTTG	133	60
	R: TGCCTTGACATTCTCGATGGT		
HPRT1	F: TGACACTGGCAAAACAATGCA	94	60
	R: GGTCCTTTTCACCAGCAAGCT		

Table 10: Primers used in pyrosequencing

Pyro assay	ID	Sequence (5’-3’)	Application	CpG sites covered
PCR1	DMR1 FW	ATTATTTTTGTGATAGGAAAAG GTA	Amplification	
	DMR1 RV	biotin-AAAACCTAAAAAAAACAA AAAAAC	Amplification	
	DMR1 seq-1 FW	TTGGTAAATTAAGGTATAGA	Sequencing	CpG 25-29

	DMR1 seq-2 FW	GGGTTAGGAGTATAGGGTAG	Sequencing	CpG 30-42
PCR2	DMR2 FW	biotin-GGATATGTTGGGATAGTT	Amplification	
	DMR2 RV	AAACTAAACAACACCTAAA	Amplification	
	DMR2 seq RV	CCCAAACACTCACCAAA	Sequencing	CpG 76-83
PCR3	DMR2 FW	GGATATGTTGGGATAGTT	Amplification	
	DMR2 RV	biotin-AAACTAAACAACACCTAAA	Amplification	
	DMR2 seq FW	TTTGGTGAGTGTTTGGG	Sequencing	CpG 84-90

2.1.9 Solutions and buffers

Table 11: 0.5 M EDTA (pH 8.0)

component	Volume or amount
disodium EDTA•2H2O	9186.1 g
ddH_2O	Up to 1000 ml
Adjust pH to 8.0 using NaOH solution	

Table 12: 1 M Tris-HCl buffer with different pH values

component	Volume or amount
Tris base	6.05 g
ddH_2O	Up to 50 ml
Adjust to the desired pH (6.8, 7.5, 8.0, 8.5) using 37 % HCl solution	

Table 13: Freezing media

component	Volume (ml)
fetal bovine serum (FBS)	25
Dimethyl sulfoxide (DMSO)	20
10x oligo annealing buffer	5
Total volume	50

Table 14: RIPA lysis buffer

component	Volume (ml)
1M Tris-HCl (PH 8.0)	2.5
1M NaCl	7.5
20 % Triton X	1.25
1M $MgCl_2$	0.5
ddH_2O	Up to 50

Table 15: 5X TBE buffer

component	Volume and amount
Tris base	108 g
boric acid	55 g
0.5M EDTA (pH 8.0)	40 ml
ddH_2O	Up to 2 l
Dilute 5X TBE buffer at a ratio of 1: 10 using ddH_2O for agarose gel preparation and electrophoresis	

Table 16: DNA lysis buffer

component	Volume (ml)
1 M Tris-HCl (pH 8.0)	5
0.5 M EDTA (pH 8.0)	20
5 M NaCl	2
20 % SDS	5
ddH_2O	Up to 100

Table 17: TE buffer

component	Volume (ml)
0.5M EDTA (pH 8.0)	0.2
1 M Tris-HCl (pH 8.0)	1
ddH_2O	Up to 100

Table 18: 10X T buffer

component	Volume and amount
Tris base	30.3 g
Glycine	143 g
ddH_2O	Up to 1000 ml

Table 19: SDS-PAGE gel buffer

Separating gel buffer		Stacking gel buffer	
component	Volume and amount	component	Volume and amount
Tris base	90.8 g	Tris base	15.1 g
20 % SDS	10 ml	20 % SDS	10 ml
Adjust pH to 8.8 using 37 % HCl solution, add ddH_2O to 500 ml		Adjust pH to 6.8 using 37 % HCl solution, add ddH_2O to 500 ml	

Table 20: WB electrophoresis running and blotting buffer

electrophoresis running buffer		blotting buffer	
component	Volume (ml)	component	Volume (ml)
10X T buffer	200	10X T buffer	200
20 % SDS	10	Methanol	400
Add ddH_2O to 2 l			

Table 21: 10X TBS buffer

component	Volume and amount
NaCl	80 g
KCl	2 g
Tris base	30 g
Adjust pH to 8.8 using 37 % HCl solution, and add ddH_2O to 1 l	

Table 22: TBST washing buffer

component	Volume (ml)
10X TBS buffer	80 g
Tween 20	2 g
ddH_2O	Up to 1 l

Table 23: Blocking buffer

component	Volume and amount
Powdered milk	2.5 g
TBST buffer	50 ml
Store in 4 °C for a week	

Table 24: ECL solutions

component	ECL-1 solution Volume	ECL-2 solution Volume
1 M Tris-HCl (pH 8.5)	0.5 ml	0.5ml
Peroxide Solution	22 µl	--
Luminol Enhancer Solution	50 µl	--
30 % Hydrogen peroxide	--	3 µl
ddH_2O	4.5 ml	4.5ml

Table 25: 100 mg/mL Ampicillin and 1 mg/mL puromycin stock

	Ampicillin	puromycin
component	Volume and amount	Volume and amount
antibiotics	1 g	10 mg
ddH_2O	Up to 10ml	Up to 10ml
The antibiotics solution is filtered by a 0.22 μm sterile filter, and store at -20 °C		

Table 26: LB agar plate with Ampicillin

component	Volume and amount
Agar-Agar	3.75 g
LB Broth	6.25 g
ddH2O	250 ml
autoclave, cool it down to 50 °C and add 250 μl 100 mg/mL Ampicillin stock, pour 25 ml into each 10 cm dish, and store at 4 °C	

Table 27: 4X Laemmli sample buffer

component	Volume
1 M Tris-HCl (pH 6.8)	10 ml
20 % SDS	20 ml
Glycerol	17 ml
β-Mercaptoethanol	3 ml
Bromophenol blue	0.1 g

Table 28: PI staining buffer

component	Volume
0.1 % trisodium citrate dihydrate solution	95 ml
PI stock (1 mg/ml)	5 ml
Triton X	100 μl

2.1.10 Softwares

Table 29: Software

software	Manufacturer
Adobe Illustrator	Adobe, San Jose, USA
ApE	M. Wayne Davis
FlowJo V10	FlowJo LLC, Oregon, USA
GraphPad Prism 8	GraphPad Software, San Diego, USA
Illumina GenomeStudio	Illumina, San Diego, USA
Image J	National Institutes of Health, Bethesda, USA
PyroMark Assay Design 2.0	Qiagen, Dusseldorf, Germany
PyroMark Q24	Qiagen, Dusseldorf, Germany
SPECTROstar Nano-Data Analysis	BMG Labtech, Ortenberg, Germany
StepOne™	Thermo Fisher Scientific, Waltham, USA

2.2 Methods

2.2.1 Cell culture

2.2.1.1 Culture of human glioblastoma cell lines

Details of all glioblastoma cell lines that we used are shown in **Table 6**. The glioblastoma cell lines T98G and LN18 were cultured in Dulbecco's Modified Eagle's medium (DMEM) Glutamax supplemented with 10 % heat-inactivated fetal bovine serum (FBS) and 1 % penicillin/streptomycin. The glioblastoma cell line U138MG was cultured in Ham's F-10 supplemented with 10 % heat-inactivated FBS and 1 % penicillin/streptomycin. All cell lines were cultured in a humidified incubator containing 5 % CO_2 at 37 °C. For subculturing, when the cultured cell reached about 80 % confluence, discarded the growth medium and washed the cells once time with DPBS, then the cells were detached using 1 % trypsin EDTA with incubation for 5-10 min at 37 °C. 9 volumes of the complete

growth medium was added to neutralize trypsin and resuspended the cells. The cells were subcultured at a ratio of 1:5-1:10 depending on the different cell lines two or three times a week.

2.2.1.2 Thawing and freezing of cells

For the thawing of cells, the cryovials with frozen cells were removed from -80 °C and quickly immersed by gently swirling in the water bath at 37 °C until only a small amount of ice remained in the tube. The cells were transferred to a T25 tissue culture flask containing the complete growth medium and cultured in a humidified incubator containing 5 % CO_2 at 37 °C for 24 h. Afterward, the medium was replaced with a fresh one to remove the DMSO.

When the cells reached about 80-90 % confluence, they were trypsinized, suspended in the complete growth medium, and transferred to a 15 ml falcon tube. Afterward, the cell suspension was centrifuged at 1500 rpm for 5 min, resuspended in the freezing medium, and 1 ml containing about 1-2 million cells was dispensed into cryovials. The cryovials were rapidly transferred to a cryo container and put in a -80 °C freezer for long-term storage.

2.2.1.3 Cell counting by cell counter

The cells were trypsinized and completely resuspended in the complete growth medium. 10 µl of the cell suspension was transferred to a 1.5 ml epi containing the same volume of 0.4 % trypan blue stain and piped up and down. 10 ul stained cell suspension was loaded in a cell counting slides and the cell numbers were calculated using an automatic cell counter. The cell counting was performed at least twice every time.

2.2.1.4 Cell pellet preparation

The cells were detached by trypsin, suspended in the complete growth medium, and transferred to 1.5 ml epi. The cell suspension was centrifuged at 1500 rpm for 5 min. Afterward, the cell pellet was washed once with PBS and centrifuged again at the same

condition, aspirated the supernatant, and stored the epi with the cell pellet in a -80 °C freezer for the DNA, RNA, or protein extraction. In addition, the cell pellet for RNA extraction was stored in the RNA lysis buffer to prevent RNA degradation.

2.2.2 Plasmid construction

2.2.2.1 Commercial plasmid preparation

The CRISPRoff plasmid and sgRNA cloning plasmid were purchased from Addgene. The map of the above plasmids is shown in **Figure 6**. After we received the bacterial stab culture containing plasmid, took some bacteria from the stab culture by a sterile pipette tip, and drew some streaks in an order in a LB agar plate with 100 μg/mL ampicillin. The agar plate was incubated in an incubator at 37 °C overnight. The next day, bacterial single colonies were picked up from the LB agar plate, transferred to culture tubes containing 5 ml sterile LB media with 100 μg/mL ampicillin, and incubated in an orbital shaker-incubator at 37 °C overnight. The glycerol stock (300ul sterile glycerol + 700ul bacteria suspension) was prepared and put in a -80 °C freezer for long-term storage. The plasmid DNA was isolated using a plasmid miniprep kit according to the manufacturer's instructions. The Sanger sequencing was performed by Eurofins Genomics and the plasmid sequence was analyzed by ApE software.

According to the sequencing result, the bacterial colony containing CRISPRoff or sgRNA cloning plasmid was chosen for a large amount of plasmid preparation. The appropriate amount of glycerol stock was added in 200 ml LB medium with 100 μg/mL ampicillin in a conical flask, and incubated in an orbital shaker-incubator at 37 °C for 14-16 h. The plasmid DNA was isolated using a plasmid maxiprep kit according to the manufacturer's instructions, eluted in 1 ml nuclease-free water, and the DNA concentration was measured by the Nanodrop spectrophotometer.

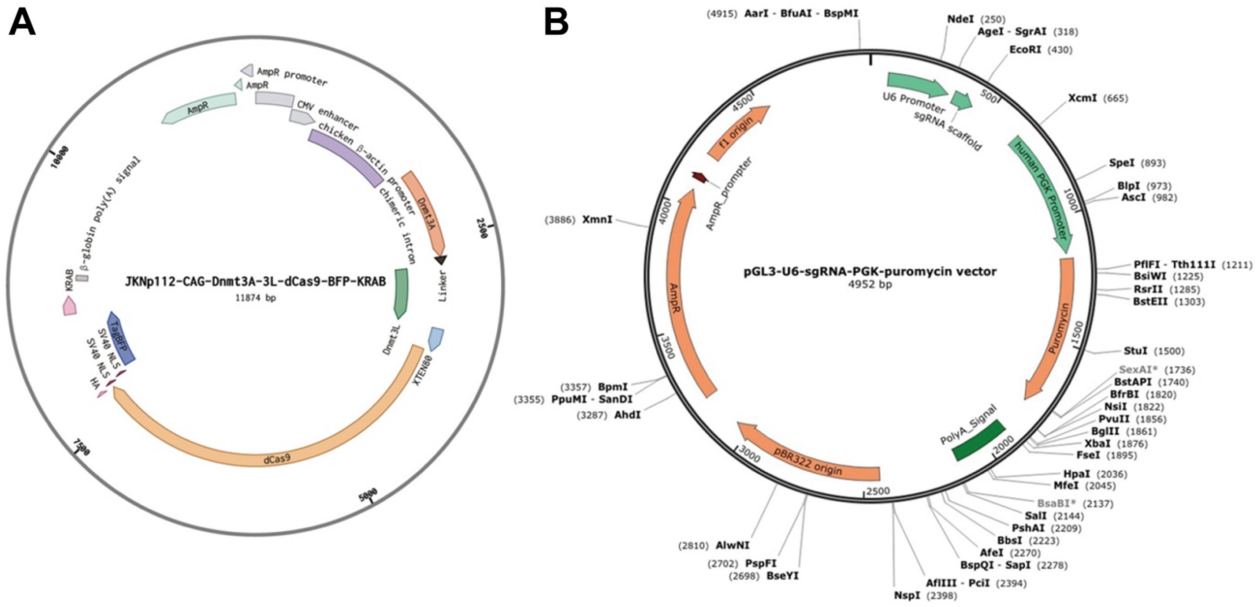

Figure 6: Map of different commercial plasmids. (A) The map of CRISPRoff plasmid contains a methyltransferase Dnmt3A/3L gene except the dCas9. **(B)** The map of empty sgRNA cloning plasmid containing a sgRNA insertion position downstream of a U6 promoter and a puromycin resistance gene.

2.2.2.2 Different recombinant sgRNA plasmid construction

We designed the sgRNAs targeting CGI in the MGMT promoter region by the UCSC genome browser (https://genome.ucsc.edu/) and the integrated CRISPOR tool (http://crispor.tefor.net). Based on the position, efficiency, and off-target effect of different sgRNAs, three sgRNAs were selected, named gRNA2, gRNA4, and gRNA10. The primers for different sgRNAs are shown in **Table 8**. We need to clone the sequence of different sgRNAs to the empty sgRNA cloning plasmid respectively.

Double-stranded DNA oligos generation

The primers of different sgRNAs were dissolved in nuclease-free water, and the concentration was 200 μM. The required reagents were added to a sterile 0.2 ml epi at room temperature as shown in **Table 30**. Diluted the 50 μM double-strand DNA oligos stock using nuclease-free water with a ratio of 1:100, then the 5 nM working solution was prepared according to **Table 31**.

Table 30: 50 µM double-strand DNA oligos stock

Reagent	Volume (µl)
Forward strand oligo (200 µM)	5
Reverse strand oligo (200 µM)	5
10x oligo annealing buffer	2
Nuclease free water	8
Total volume	20
Incubated at 95 ℃ for 4 min, cooled it down to room temperature for 5-10 min, stored in -20 °C	

Table 31: 5 nM double-strand DNA oligos working solution

Reagent	Volume (µl)
500 nM double-strand DNA oligos	1
10x oligo annealing buffer	10
Nuclease free water	89
Total volume	100

Empty sgRNA cloning plasmid linearization

The empty sgRNA cloning plasmid was linearized using restriction enzyme BsaI, and the reaction system was set up as shown in **Table 32**.

Table 32: Plasmid linearization by restriction enzyme reaction

Reagent	Amount or volume	Final conc. or amount
Plasmid DNA	1 µg	
10X NEB buffer	5 µl	1X
Restriction enzyme--BsaI	1µl	10 units
Nuclease-free water	To 50	

Restriction enzyme was added last, incubated at 37 °C for 30 min, and heat inactivated at 80 °C for 20 min

Agarose gel electrophoresis was performed to verify the plasmid linearization, 1.0 % agarose gel was prepared by dissolving 1 g agarose in 100 ml Tris-borate-EDTA (TBE) buffer in the microwave, and 2.5 µl GelRed® Nucleic Acid Gel Stain was added before polymerization of agarose solution. Afterward, the linearized plasmid solution containing an appropriate volume of 6X DNA loading buffer was loaded into the agarose gel. The electrophoresis was performed at 150 V for 50 min. Finally, the bands were visualized under ultraviolet – light and photographed by the Intas GDS system. A small volume of origin and linearized plasmid DNA was also loaded as the negative and positive control respectively as shown in **Figure 7A**. The bands of linearized plasmid DNA were cut and recovered using a gel DNA recovery kit according to the manufacturer's instructions, the recovered DNA was measured by nanodrop and verified again by agarose gel electrophoresis as shown in **Figure 7B**.

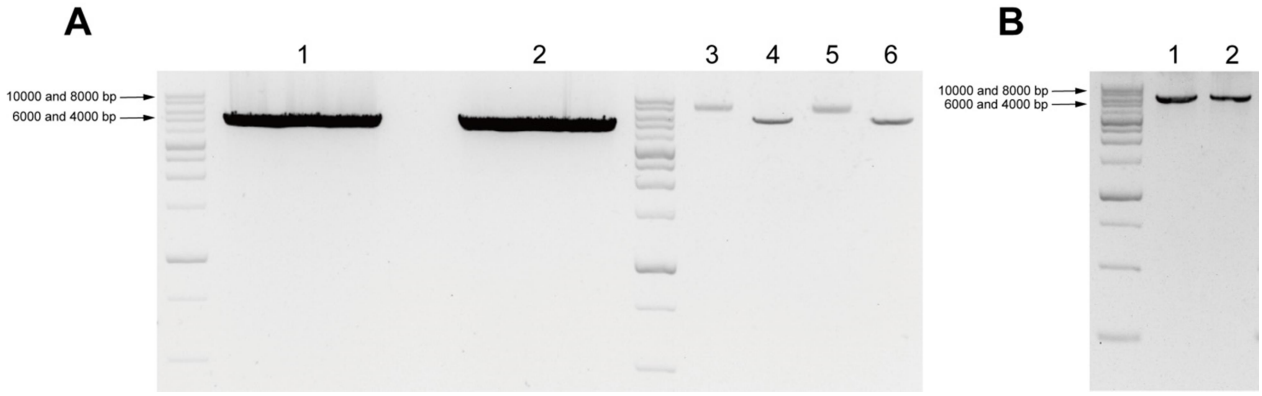

Figure 7: Verification of Empty sgRNA cloning plasmid linearization. (A) The agarose gel showed the two independent samples of linearized empty sgRNA cloning plasmid (lane 1,2), the corresponding original plasmid control (lane 3,5), and linearized plasmid control (lane 4,6). **(B)** The agarose gel showed the two independent samples of the gel-recovered linearized plasmid.

Ligation reaction

The ligation reaction system for different sgRNA plasmids was set up with a molar ratio of 7:1 (insert: vector), and the required reagents were added in the order as shown in **Table 33**.

Table 33: sgRNAs plasmid ligation reaction

Reagent	Volume (µl)
10X ligation buffer	2
Linearized sgRNA cloning vector (13.6 ng/ul)	2.2
double-strand DNA oligos (5 nM)	13.8
Nuclease free water	1.5
T4 DNA ligase	0.5
Total volume	20
Ligation mixture Incubated at 14 °C overnight	

Bacterial transformation with ligation mixture

4 ul of different sgRNAs ligation mixture were added to 1.5 ml tubes containing 50 µl thawed Top10 *E.coli*, mixed up gently, and incubated on ice for 30 min. A heat shock was given to transformation tubes at a 42 °C water bath for 35 s, then put tubes back on ice for 40 s. 250 µl of Soci medium was added to each tube and bacteria was incubated in an orbital shaker-incubator at 37 °C for 45 min. 50 µl and 250 µl bacterial suspension were added to two LB agar plates with 100 µg/mL ampicillin respectively, and sterile glass beads were also added to dispend the bacterial suspension by gently shaking. The plates were incubated in a 37 °C incubator overnight.

Afterward, at least 10 colonies were picked up from each sgRNA agar plate, transferred to a 96-well tissue culture plate containing 100 µl LB medium with 100 µg/mL ampicillin, and the plate was incubated in an orbital shaker-incubator at 37 °C for 30 min. During the

30 min of incubation, the reaction system of colony PCR was set up on ice according to **Table 34**.

Table 34: Colony PCR reaction system

Reagent	Volume (µl)
HotStarTaq master mix	12.5
10 pM Forward primer (hU6 promoter)	0.5
10 pM Reverse primer (sgRNAs U6 bottom strand)	0.5
Template	2
Nuclease free water	7
10X Coraload	2.5
Total volume	25
Cycling conditions:	
95 °C 5 min; 25 x cycles (94 °C 30 s, 51 °C 45 s, 72 °C 1 min); 72 °C	
10 min; 8 °C ∞	

Agarose gel electrophoresis was performed to check the colony PCR product, and the different sgRNAs ligation mixture was used as the positive control. 4 µl PCR product was loaded into the prepared 1.5 % agarose gel, the electrophoresis was performed at 150 V for 30 min, and the bands were visualized under ultraviolet – light as shown in **Figure 8**.

50 µl bacterial suspension from at least three colonies of each sgRNA was transferred to bacterial culture tubes containing 5 ml LB medium with 100 µg/mL ampicillin and incubated in an orbital shaker-incubator at 37 °C overnight. The recombinant sgRNA plasmid DNA miniprep, maxiprep, and Sanger sequencing were described in section 2.2.2.1 commercial plasmid preparation.

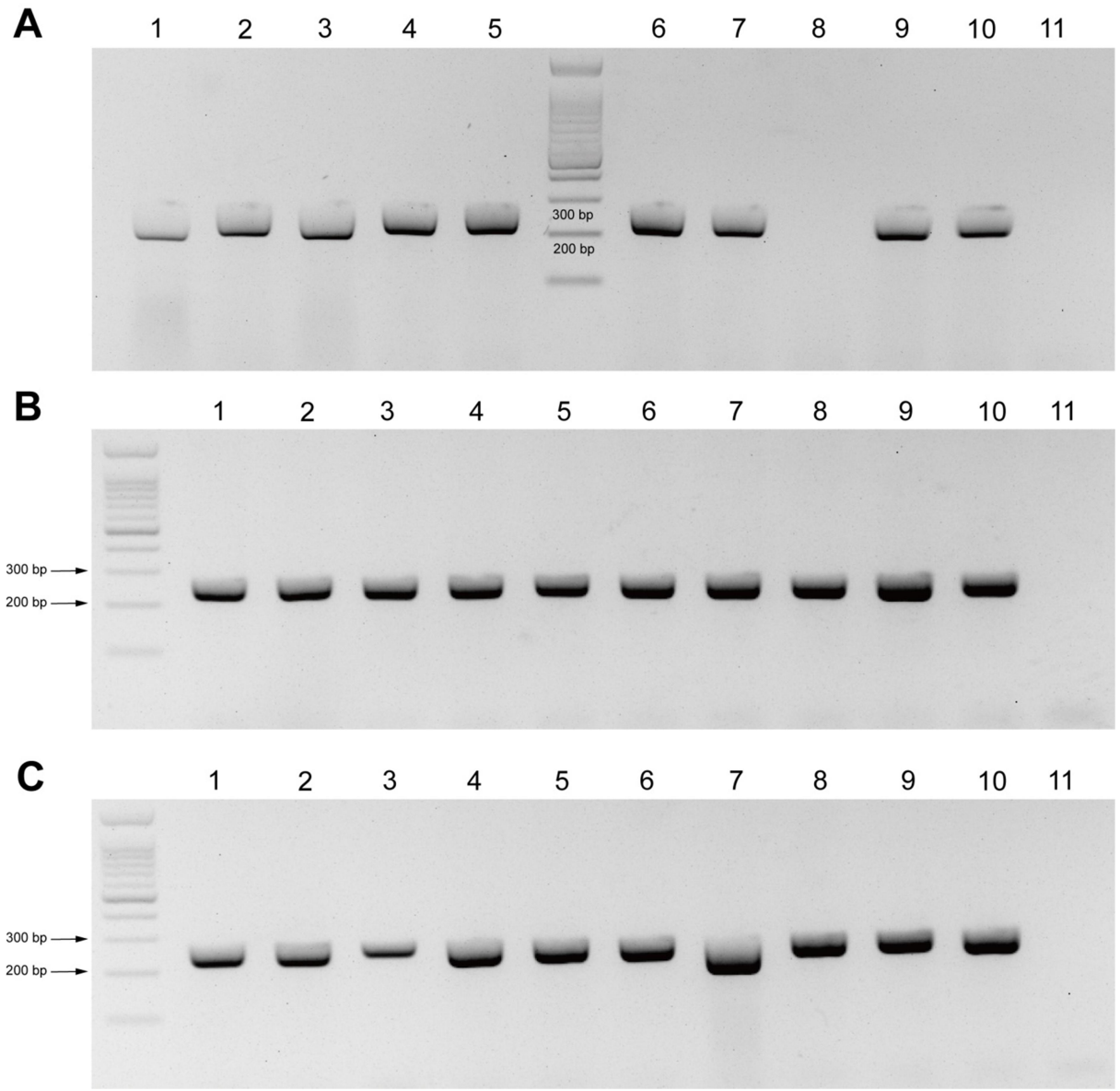

Figure 8: Colony PCR of different MGMT-targeted sgRNAs. The agarose gels showed the PCR amplicons from 10 independent bacterial colonies (lanes 1-10) and the corresponding negative control (lane 11) of gRNA2 **(A)**, gRNA4 **(B)**, and gRNA10 **(C)**.

2.2.3 Different sgRNA stably expressing glioblastoma cell lines construction

2.2.3.1 Co-transfection of CRISPRoff and different sgRNAs in glioblastoma cell lines

To construct different sgRNA stably expressing glioblastoma cell lines, 1.5 x 10^6 cells of T98G or LN18 were seeded on four 10 cm tissue culture dishes 24-48 h before the cell transfection. When the cells reached a density of about 80 %, cells were co-transfected with the CRISPRoff plasmid and one of each of the sgRNA or the empty sgRNA plasmid

with a molar ratio of 10:1. Transfection reagents and plasmid DNA were prepared in sterile 1.5 ml epi as shown in **Table 35**.

Table 35: Cell transfection by ROTI ® Fect PLUS

	Reagent	Volume per 10 cm dish (µl)
Solution A	Opti-MEM	600
	CRISPRoff plasmid (1 µg/ul)	19.2
	sgRNA plasmid (1 µg/ul)	0.8
Solution B	Opti-MEM	600
	ROTI ® Fect PLUS	60
Mixed of solutions A and B within 5 min, incubated at room temperature for 20 min		

During the incubation of the transfection solution, the old growth medium was aspirated in the 10 cm dishes, cells were washed once with DPBS, and 4 ml Opti-MEM was added to the dishes. After 20 min, the mixed transfection solutions were added dropwise to the dishes and shaken well gently. The dishes were incubated in a humidified incubator under appropriate conditions (5 % CO_2 at 37 °C) for 6 h. Afterward, 5 ml of complete growth medium was added to each dish and continued incubation until 24 h.

2.2.3.2 Different sgRNAs stably expressing clonal cell lines selection

After 24 h of co-transfection, 1 µg/ml puromycin was added to the transfected cells for the selection of single colonies. Single puromycin-resistant colonies were picked using cloning cylinders after approximately 3-4 weeks of cultivation and transferred into single wells of 24-well tissue culture plates. When picked colonies were confluent in 24-well plates (approximately 5–7 days), colonies were split into two separate 12-well tissue culture plates. One 12-well plate was used for further expansion and the another for analysis of MGMT expression by Western blot. The different sgRNA clonal cell lines carrying the desired MGMT expression were transferred to T25 flasks, and the cell stocks were prepared and stored at -80 °C for further analysis.

2.2.4 Protein extraction, quantification, and Western blot analysis

2.2.4.1 Protein extraction and quantification

The frozen cell pellet was thawed and lysed in 1x RIPA lysis buffer supplemented with 10 µl/ml Halt protease Inhibitor-cocktail and 0.5 µl/ml Benzonase on ice for 30 min. The cell lysate was centrifuged at 13200 rpm, 4 °C for 10 min, and the supernatant was transferred to a new 1.5 ml epi for subsequent analysis. The protein concentrations were determined using Bicinchoninic Acid (BCA) Protein Assay. Briefly, the Bovine Serum Albumin (BSA) standard proteins with different concentrations were plated in triplicates, the protein samples were also plated in duplicates with a water dilution at a ratio of 1:10 in a 96-well tissue culture plate. Afterward, 200 µl BCA working solution was added to each well and incubated at 37 °C for 30 min. The intensity of the color in each well was measured by a SPECTROstar Nano Absorbance Reader, and protein concentration was calculated by SPECTROstar Nano-Data Analysis software. An appropriate volume of 4X Laemmli loading buffer was added to cell lysates to a final concentration of 1X and boiled at 95 °C for 5 min.

2.2.4.2 Western blot analysis

40 µg protein samples with loading dye and 3 µl of protein ladder were loaded on the 10 % SDS-PAGE gels that were prepared according to **Table 36**.

Table 36: 10 % SDS-PAGE gel

10 % Separating gel (for 2 gels)		7.5 % Stacking gel (for 2 gels)	
Solution	Volume	Solution	Volume
ddH_2O	8.3 ml	ddH_2O	5 ml
Separating gel buffer	5 ml	Stacking gel buffer	2.5 ml
30 % Acrylamide	6.7 ml	30 % Acrylamide	2.5 ml
TEMED	10 µl	TEMED	5 µl
10 % APS	100 µl	10 % APS	50 µl

The electrophoresis was performed at 80 V for 20 min, and 120 V until the loading dye moved to the bottom of the separating gel. Afterward, the separated proteins were transferred from the gel to 0.45 µm nitrocellulose membranes. The membranes were incubated in the blocking buffer at room temperature for 1 h, and incubated with anti-MGMT (1:1000) or anti-beta-actin (1:10000) antibodies at 4 °C overnight. Subsequently, the membranes were washed three times with TBST for 15 min, and incubated with a secondary, horseradish peroxidase (HRP)-conjugated anti-mouse antibody (1:5000) at room temperature for 1 h. After washing three times again with TBST for 15 min, the membranes were developed with ECL solution using the ChemoCam imager, photographed by the ChemoStar Imager system. Densitometric quantification was performed using Image J software and normalized to the corresponding beta-actin levels.

2.2.5 RNA isolation and quantitative reverse transcription polymerase chain reaction (qRT-PCR)

2.2.5.1 RNA isolation

In order to investigate *MGMT* mRNA expression, the total RNA was isolated from the cell pellet using a Quick-RNA MiniPrep kit according to the manufacturer‘s instructions. The concentration and quality of RNA samples were measured by a nanodrop spectrophotometer. An $A_{260/280}$ ratio ranging from 1.8 to 2.0, along with an $A_{260/230}$ ratio between 2.0 and 2.2, serve as reliable benchmarks for assessing excellent RNA quality. Reduced ratios suggest the potential presence of protein, phenol, or other contaminants within isolated RNA samples.

2.2.5.2 qRT-PCR analysis

qRT-PCR stands as an efficient method for real-time monitoring of the entire PCR process. This technique integrates fluorescent dyes like SYBR Green into the PCR reaction system, enabling observation of fluorescence during the exponential growth phase. Notably, an inverse correlation exists between the cycle threshold (Ct) value and

the initial template quantity (Taylor et al., 2010). Consequently, this method facilitates the comparative analysis of gene expression across diverse samples. In this study, qRT-PCR was performed using the QuantiTect SYBR Green RT-PCR Kit in a 96-well format on StepOnePlus™ Real-time PCR system. The reaction system and conditions of qRT-PCR were set up as shown in **Tables 37 and 38**.

Table 37: qRT-PCR reaction system

Reagent	Volume (µl)
2x QuantiTect SYBR Green RT PCR Master Mix	10
10 µM Forward primer	2
10 µM Reverse primer	2
Template	2
QuantiTect RT Mix	0.2
5x Qsolution	1
Nuclease free water	2.8
Total volume	20

Table 38: qRT-PCR cycler conditions

Number of cycles	Step	Time	temperature
1	Reverse transcription	30 min	50 °C
1	PCR initial activation	15 min	95 °C
	Denaturation	15 s	94 °C
35	Annealing	30 s	60 °C
	Extension	30 s	72 °C
Melt curve	Dissociation	5 s	65-95 °C

Ubiquitin C (UBC) and hypoxanthine phosphoribosyl-transferase 1 (HPRT1) were used as endogenous normalization controls. The sequences of primers are shown in **Table 9**. All samples were performed as triplicates. The mRNA relative expression was determined by the 2−ΔΔCt method (Livak and Schmittgen, 2001). ΔCt = Ct (a target gene)

– Ct (a housekeeping gene). ΔΔCt = ΔCt (a target sample) – ΔCt (a control sample). The relative gene expression was standardized to 1 for the control sample.

2.2.6 Cell cytotoxicity analysis by Alamar blue assay

Different glioblastoma cells were collected by trypsin and the cell number was estimated as previously described. Cells were seeded at a density of 2,500 cells/well in triplicates in 96-well tissue culture plates and cultured for 24 h. Subsequently, the medium was replaced by fresh growth medium with TMZ at the indicated concentrations, and continued culturing for 144 h; DMSO was used as the control. The cell viability was determined by adding Alamar blue reagent (1:10) into each well and incubation for 2 h at 37 °C. After 2 h, the fluorescence was measured at 560 nm excitation and 590 nm emission wavelengths using a fluorescence spectrophotometer.

2.2.7 Flow cytometry

To evaluate cell death after treatment with TMZ at different time points, DNA-fragmentation of propidium iodide (PI)-stained nuclei was measured by flow cytometric analysis on a FACSCanto II in the Core Facility, University of Bonn, Germany. Apoptotic cells are characterized by DNA fragmentation and loss of nuclear DNA content among other typical signs (Riccardi and Nicoletti, 2006). As a result, dead cells subjected to Triton-X treatment and PI staining showcase a hypodiploid (sub-G1) peak, distinctly discernible from the narrow peak observed in cells possessing typical (diploid) DNA content. Briefly, cells were collected by trypsin and the cell number was estimated as previously described. Cells were seeded at a density of 20,000 cells per well in triplicates in 24-well tissue culture plates and cultured for 24 h. Then, the medium was replaced with the growth medium containing DMSO or TMZ at the indicated concentrations and the cells were cultured for an additional 72 or 144 h. Afterward, the cells were harvested by trypsin and centrifuged at 1300 rpm 4 °C for 5 min, resuspended in PI staining buffer, and incubated at 4 °C for 1 h. The data were analyzed using FlowJo V10 Software. The rates of specific DNA fragmentation were calculated by the following equation: 100 ×

(experimental DNA fragmentation (%) - spontaneous DNA fragmentation (%))/(100 % - spontaneous DNA fragmentation (%)).

2.2.8 Genomic DNA extraction, Bisulfite conversion, and pyrosequencing

2.2.8.1 Genomic DNA extraction

Genomic DNA was extracted from a frozen cell pellet of different sgRNAs stably expressing glioblastoma cell lines using DNA lysis buffer supplemented with Proteinase K (20 mg/ml). Briefly, the cell pellet was incubated with 500 µl DNA lysis buffer and 12.5 µl Proteinase K at 55 °C overnight. The next day, 210 µl saturated NaCl solution (5 M) was added and centrifuged for 30 min. The supernatant was transferred into a new sterile 1.5 ml epi, mixed with 700 µl isopropanol, and incubated for 10 min at room temperature. Afterward, samples were centrifuged for another 30 min, the supernatant was discarded and the pellet was washed with 70 % fresh ethanol followed by another centrifugation step for 30 min. The supernatant was discarded and dried the left ethanol at 37 °C. After this step, the DNA pellet was dissolved in 200 µl TE buffer, and stored at 4 °C. The concentration and quality of DNA samples were measured by a nanodrop spectrophotometer.

2.2.8.2 Bisulfite conversion and pyrosequencing

The bisulfite conversion is a landmark technology for the study of DNA methylation, The sodium bisulfite treatment can convert unmethylated cytosine (C) into uracil (U), and preserve methylated cytosine in DNA samples. In the subsequent PCR process, uracil (U) is further converted back to thymidine (T). The pyrosequencing can measure the methylation levels of individual CpG sites in the PCR product amplified using primers shared by methylated and unmethylated sequences following bisulfite conversion. In pyrosequencing, the amount of C and T at specific CpG sites are converted to the amount of released pyrophosphates by sequencing primers, so that the quantitative DNA methylation level can be detected by the Pyrosequencer System (Hattori and Ushijima, 2017).

Briefly, 500 ng genomic DNA was used for the bisulfite conversion that was performed using a DNA Methylation-Gold kit according to the manufacturer's protocol. The bisulfite-converted DNA was eluted in 25 µl elution buffer and stored at -20 °C. The PCR production was amplified with biotinylated primers using a PyroMark PCR kit, and the different reaction systems for MGMT DMR1 and DMR2 regions were set up according to **Table 39**.

Table 39: bisulfite-converted DNA PCR reaction systems

Reagent	DMR1 Volume (µl)	DMR2 Volume (µl)
PyroMark PCR Master Mix, 2x	12.5	6.25
CoralLoad Concentrate, 10x	2.5	1.25
25 mM $MgCl_2$	0.5	0.25
Forward primer	0.5	0.75
Reverse primer	0.5	0.75
Template	2	1.5
Nuclease free water	6.5	1.75
Total volume	25	12.5
Cycling conditions: 95 °C 15 min; 50 x cycles (94 °C 30 s, 49.5 or 55 °C 30 s, 72 °C 30 s); 72 °C 10 min; 8 °C ∞		

Note: The annealing temperature for DMR1 and DMR2 regions is 55 and 49.5 °C respectively.

10 µl of PCR product was used for the pyrosequencing using PyroMark Gold Q96 Reagents on the PyroMark Q24 Sequencer System according to the manufacturer's instructions. The data of pyrosequencing were analyzed by PyroMark Q24 Software. The sequence of PCR primers and sequencing primers are shown in **Table 10**.

2.2.9 Global DNA methylation assay

In order to evaluate the off-target effect of the CRISPRoff system in the edited cell lines, the global DNA methylation status of the WT and edited cell lines was detected through specifically measuring the levels of 5-methylcytosine (5-mC) by the MethylFlash Global DNA methylation (5-mC) ELISA kit according to the instructions of the manufacturer. The optical density in each well was measured at 450 nm using a SPECTROstar Nano absorbance reader. The percentage of methylated DNA is proportional to the OD intensity measured. To calculate the fraction of methylated cytosines, the ODs are referenced to a standard curve set in parallel. The samples were measured in duplicate in three independent experiments.

2.2.10 DNA methylation profiling by 850K array

The Illumina 850K array is a technique that detects the methylation status of approximately 853,307 CpG sites in the human genome. The 850K chip comprehensively covers gene promoter regions, gene coding regions, CpG islands, and enhancer regions, which is widely used in complex disease methylation research. In this study, we performed the 850K array to evaluate the off-target effect of the CRISPRoff system, especially the predicted potential off-target sites of gRNA10 obtained from CRISPROR software.

Briefly, Genomic DNA samples of three EgRNA control and three gRNA10 edited T98G cell lines were transferred to the Core Facility, University of Bonn, Germany. Each sample was isolated according to the methods described previously, purified using spin columns, and the DNA quantity and quality were assessed. Bisulfite-conversion was carried out using the Epitect 96 bisulfite kit according to the manufacturer‘s instructions, and 300 ng of converted DNA were hybridized to Illumina Infinium MethylationEPIC 850K BeadChips, following the manufacturer’s instructions. Methylation profiles were exported from Illumina GenomeStudio as IDAT files. The Sesame Bioconductor package v 1.18.3 was utilized for quality control, differential methylation analysis, and visualization.

2.2.11 Gene expression profiling by RNA sequencing

2.2.11.1 Library preparation and RNA sequencing

Total RNA isolation and quantification as described above. The library construction was performed using the QuantSeq FWD 3' -mRNA-Seq Kit (Lexogen, Vienna, Austria) according to the manufacturer's instructions (procedure executed by the NGS core facility, University Hospital Bonn). Each sample was diluted in 14 ul TE buffer with the same concentration of 100 ng/ul. An oligo-dT primer containing an Illumina-compatible sequence at its 5′ end was hybridized to the RNA and reverse transcription was performed. After degradation of the RNA template, second-strand synthesis was initiated by a random primer containing an Illumina-compatible linker sequence at its 5′ end. The double-stranded library was purified by using magnetic beads to remove all reaction components. The library was amplified to add the complete adapter sequences required for cluster generation. The finished library was purified from PCR components. High-throughput sequencing was performed as single-end 100 bp sequencing using NovaSeq 6000 (Illumina, Inc., San Diego, CA, USA).

2.2.11.2 RNA sequencing data analysis

For RNA sequencing analysis and visualization, the R/Bioconductor computing platform was used. Initial raw read counts, in a FASTQ file format, were aligned to the Hg38 human reference genome using the RSubread aligner package (Liao et al., 2019). As suggested by Lexogen, the Rsubread align function was executed without trimming but allowing for mismatches in the initial cycles. For the final analysis, only those reads, spanning a maximum length of 45 bases were included. The gene-level summary was generated with unique mapping using the featureCounts function. The aligned sequencing reads were then assigned to genomic features specified by an ENTREZ Gene ID (NCBI Gene database) (Maglott et al., 2010). Quality control steps such as variance stabilizing transformation (VST) and principal component analysis (PCA) have been applied. The differential gene expression analysis for EgRNA or gRNA10 stably

expressing cell line was performed using the DESeq2 package (Anders and Huber, 2010). Following filtering steps based on a p-adjusted value of less than 0.05 and a log2 fold change greater than 2.5 or less than -2.5 and displayed in a Volcano Plot (EnhancedVolcano). To investigate the genes of gRNA10 potential off-target sites, we generated boxplots using the Limma package. Subsequently, we conducted pairwise t-tests to assess significant differences in mRNA expression levels among the various groups.

2.2.12 Statistical analysis

The GraphPad Prism 8 software was used to perform all statistical analysis. Student's t-test or multiple t-test was conducted to analyze the comparisons between two groups, while one-way ANOVA was performed to analyze the differences among three groups. P values less than 0.05 were considered statistically significant. All data are expressed as mean ± standard deviation (SD) from at least three independent experiments.

3. Results

3.1 Characterization of CGI in the *MGMT* promoter region and design of different sgRNAs

The promoter of the *MGMT* gene contains a CGI encompassing 98 CpG sites that spans 760bp (chr10: 131264949-131265710), which contains promoter, exon 1, enhancer, and intron 1 regions **(Fig9. A-C)**. Notably, 2 distinct differentially methylated regions (DMR1 and DMR2) were previously defined **(Fig19. A)**. To achieve efficient epigenetic editing of CpG sites within the CGI, three individual sgRNAs (gRNA2, gRNA4, and gRNA10) targeting three specific regions distributed across the CGI of the *MGMT* promoter were selected from UCSC based on the on-target capacity and off-target risk of sgRNA **(Fig. 9C)**.

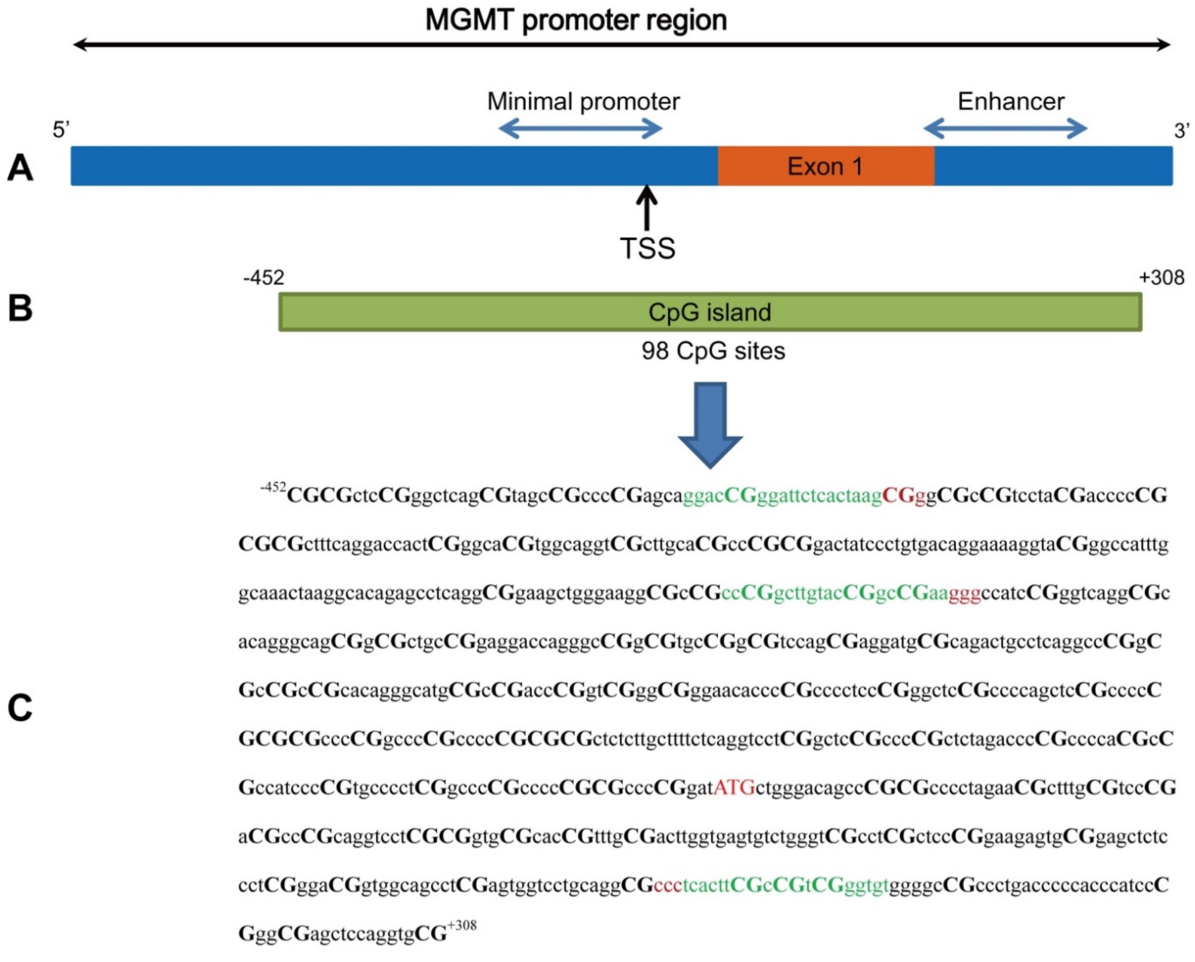

Figure 9: Schematic representation of the epigenetically targeted region of the *MGMT* gene promoter. (A) Structure of the *MGMT* promoter region and location of the minimal promoter (-69 to +19) and enhancer (+143 to +202) (blue arrows), as well as the transcriptional start site (TSS +1, black arrow) and exon 1 (orange box). **(B)** Location of the CGI with 98 CpG sites in the *MGMT* promoter region. **(C)** The DNA sequence of the CGI (-452 to +308) in the *MGMT* promoter region; CpG sites are shown in capital letters, the sequences and location of the sgRNAs used are marked in green and the PAM motifs are in red. MGMT, O^6-methylguanine DNA methyltransferase; CGI, CpG island.

3.2 The expression of MGMT and TMZ cytotoxicity in different TMZ-resistant human glioblastoma cell lines

In order to identify the suitable glioblastoma cell lines for the subsequent experiments, the expression of endogenous MGMT was characterized in three human glioblastoma wild-type (WT) cell lines (LN18, T98G, and U138MG), known for their resistance to TMZ. Western blot analysis showed a high expression of MGMT in the T98G and LN18 cell lines, but only slight MGMT expression in the U138MG cell line **(Fig. 10A)**. Subsequently, to investigate the sensitivity of T98G and LN18 cells to TMZ, different cells were treated with increasing concentrations of TMZ (50, 100, 200, 400, 800 and 1000 µM) for 144 h and the cell viability was measured by Alamar blue assay. Our results revealed a dose-dependent decrease of cell viability in both cell lines **(Fig. 10B)**. The 50 % growth-inhibitory concentrations (IC50) after TMZ treatment for 144 h were 475.6uM in T98G cells, 424.7uM in LN18 cell lines **(Fig. 10C).**

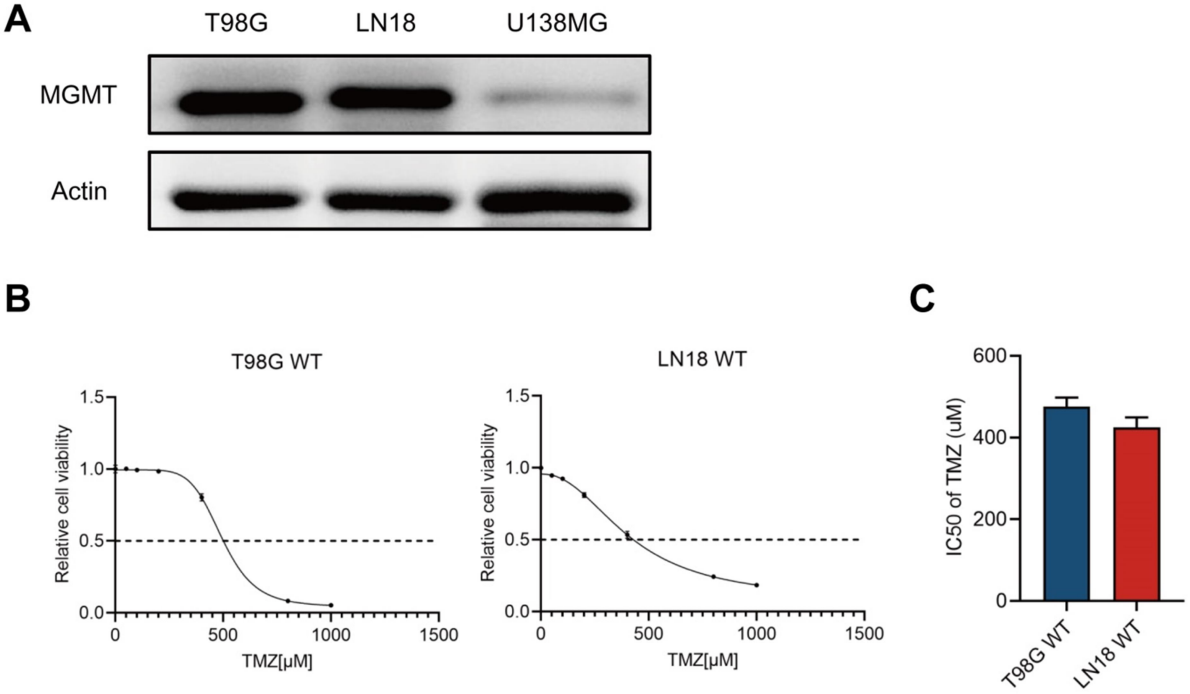

Figure 10: Characterization of different glioblastoma wild-type cell lines. (A) Western blot analysis of endogenous MGMT and actin expression in whole cell lysates prepared from T98G, LN18, and U138MG WT cells. **(B)** Cell viability of T98G (left) and LN18 (right) WT cells treated with increasing concentrations of TMZ (0, 50, 100, 200, 400, 800, and 1000 μM) for 144 h using the Alamar blue assay. **(C)** Calculated IC50 values for TMZ of T98G (blue) and LN18 (red) WT cells treated with increasing concentrations of TMZ. Results are averaged from triplicates and are expressed as the mean ± SD. Data are representative of three independent experiments.

3.3 Construction of different glioblastoma cell lines containing increased DNA methylation in the *MGMT* promoter region through the CRISPRoff system

3.3.1 Different sgRNA stably expressing T98G clonal cell lines

T98G cells were first co-transfected with the CRISPRoff plasmid containing dCas9-DNMT3A/3L and one of the selected *MGMT* promoter region targeting sgRNA; simultaneously, an empty sgRNA (EgRNA) cloning plasmid was also co-transfected with CRISPRoff as the negative control. Several T98G clonal cell lines stably expressing different sgRNAs were constructed under the treatment of 1 μg/mL puromycin and analyzed for MGMT protein expression by Western blot analysis. The expression of

MGMT was reduced to varying degrees in different T98G clonal cell lines stably expressing gRNA2 or gRNA10 compared with the corresponding EgRNA control cell lines **(Fig. 11A-C)**; whereas, no gRNA4 stably expressing clonal cell line with decreased MGMT expression was isolated **(Fig. 11B)**.

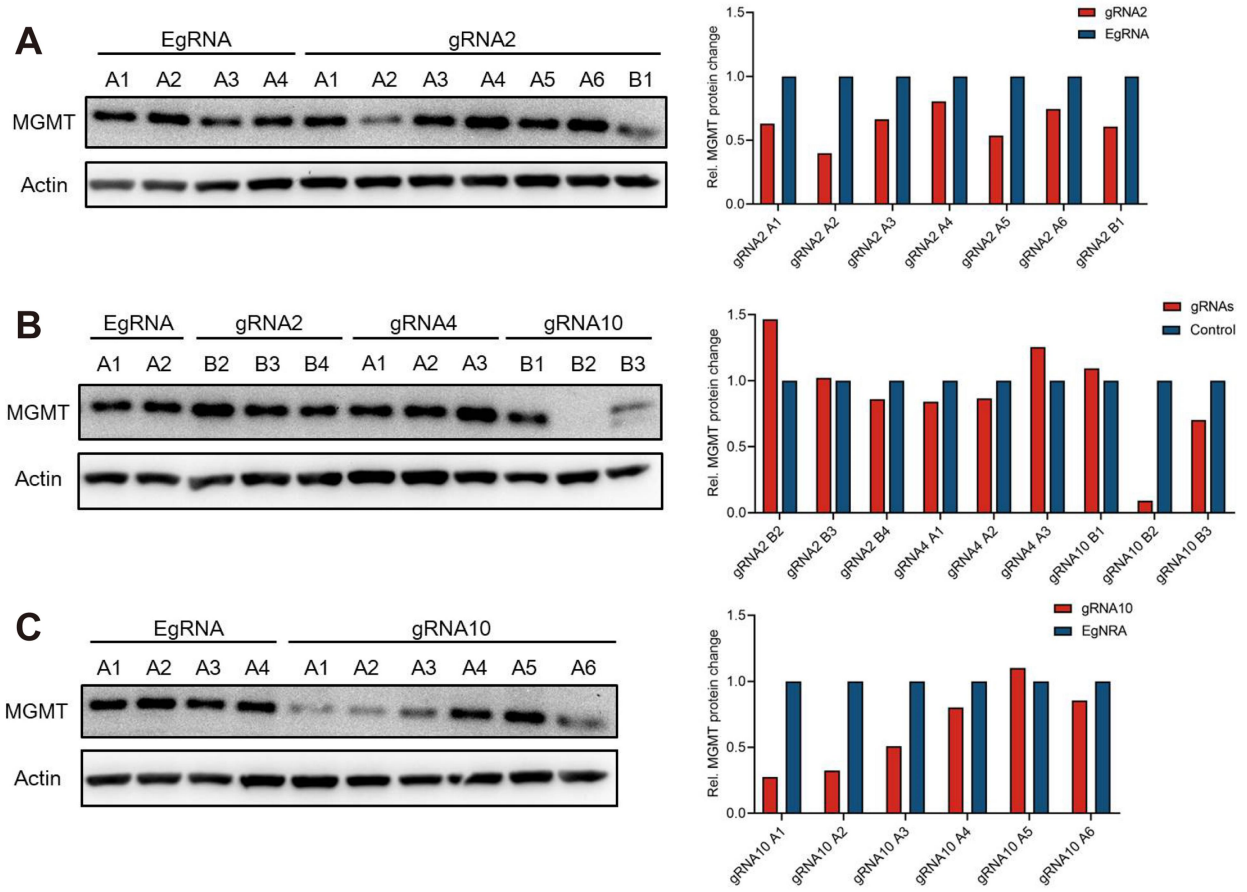

Figure 11: The screening of T98G clonal cell lines stably expressing different sgRNAs. (A-C) (left) Representative western blot analysis showed MGMT and actin protein expression in different T98G clonal cell lines stably expressing gRNA2 **(A and B)**, gRNA4 **(B)**, or gRNA10 **(B and C)**. **(A-C) (right)** Semi-quantitative analysis revealed the degree of reduction in MGMT protein expression levels in different T98G clonal cell lines stably expressing gRNA2 **(A and B)**, gRNA4 **(B)**, or gRNA10 **(B and C)** compared with the T98G clonal cell lines stably expressing EgRNA. EgRNA, empty sgRNA.

3.3.2 gRNA10 stably expressing LN18 clonal cell lines

To further verify the inhibitory effect of gRNA10 on MGMT expression, LN18 cell lines were stably transfected with CRISPRoff and gRNA10. According to the western blot analysis, reductions of MGMT expression were also detected in different LN18 clonal cell

lines stably expressing gRNA10 in comparison with the EgRNA control cell lines **(Fig. 12A-C)**.

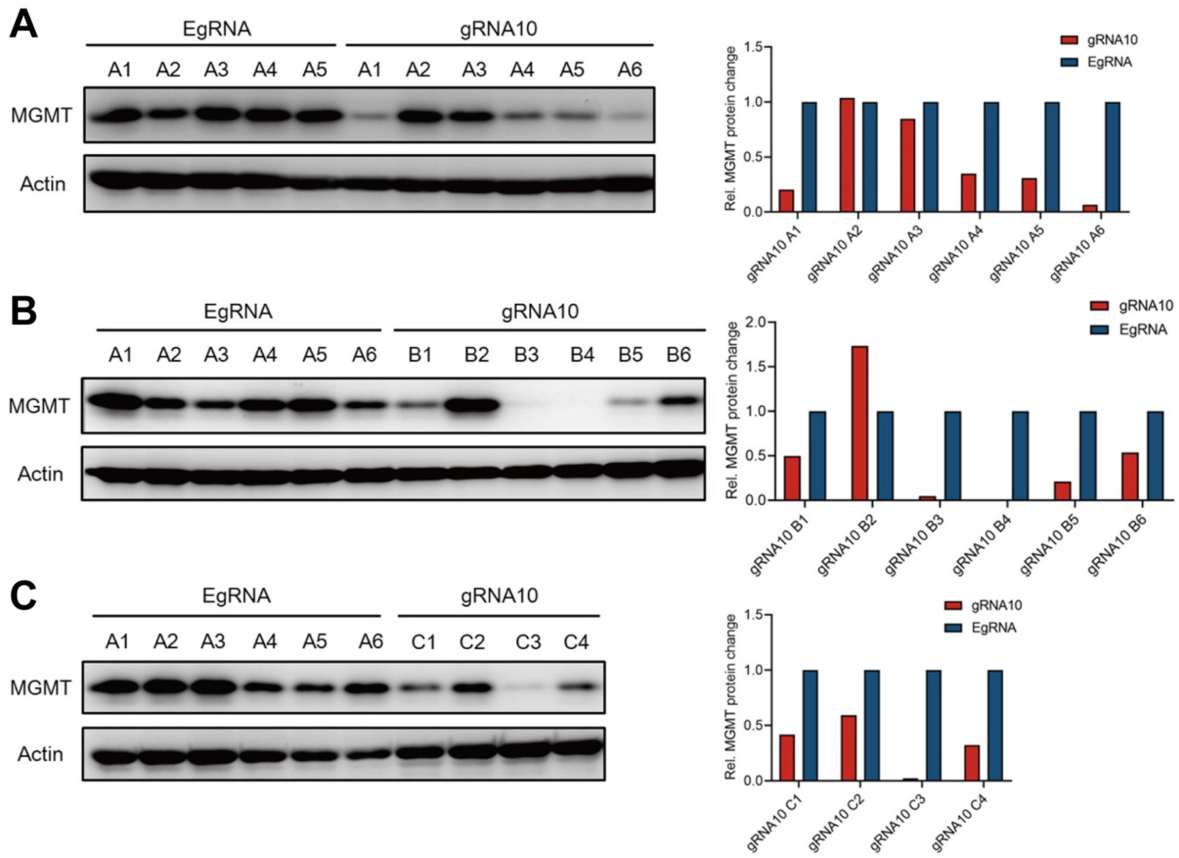

Figure 12: The screening of LN18 clonal cell lines stably expressing gRNA10. (A-C) (left) Representative western blot analysis of MGMT and actin protein expression in different LN18 clonal cell lines stably expressing gRNA10. **(A-C) (right)** Semi-quantitative analysis revealed the degree of reduction in MGMT protein expression levels in different LN18 clonal cell lines stably expressing gRNA10 compared with the LN18 clonal cell lines stably expressing EgRNA. EgRNA, empty sgRNA.

3.4 Downregulation of MGMT mRNA and protein expression levels in different sgRNA-edited cell lines

Representative clonal cell lines were selected, one each from T98G stably expressing gRNA2 or gRNA10, and LN18 stably expressing gRNA10. To test whether the reduction of MGMT is stably transmitted, we analyzed the MGMT mRNA and protein expression

levels in at least three consecutive cell generations from different representative clonal cell lines. The results of quantitative RT-PCR and western blot analysis revealed a significant decrease in MGMT mRNA and protein expression levels by approximately 50 % in T98G cell line stably expressing gRNA2 in comparison with the T98G EgRNA control cell line **(Fig. 13A and Fig. 14A)**; a stronger reduction of MGMT mRNA and protein expression levels was observed in T98G cell line stably expressing gRNA10 which decreased more than 60 % compared with the T98G EgRNA control cell line **(Fig. 13B and Fig. 14B)**. In comparison with edited T98G cell line, the strongest repression of the MGMT expression was achieved in LN18 cell lines stably expressing gRNA10. Our results showed that MGMT mRNA and protein expression were almost silenced in LN18 cell line stably expressing gRNA10 compared with the LN18 EgRNA control cell line **(Fig. 13C and Fig. 14C)**.

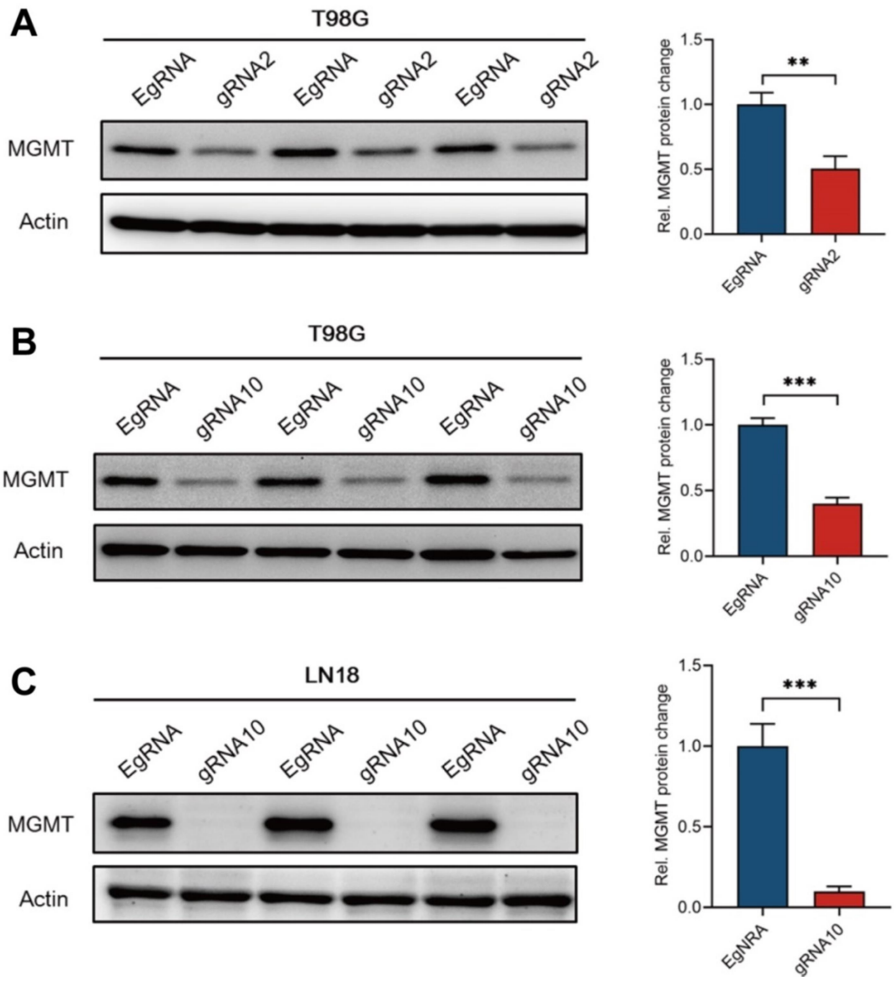

Figure 13: MGMT protein expression level of edited glioblastoma cell lines in different cell generations. (A-C) (left) Representative western blot analysis of MGMT and actin expression in whole cell lysates of T98G clonal cell lines stably expressing gRNA2 **(A)** or gRNA10 **(B)**, and LN18 clonal cell lines stably expressing gRNA10 **(C)** compared with the corresponding cell lines stably expressing EgRNA. **(A-C) (right)** The relative protein amounts of MGMT were detected by Western blots and quantitated by densitometry. The MGMT levels were normalized to the corresponding actin levels. Results are averaged from triplicates and are expressed as the mean ± SD. Data are representative of three independent experiments. ***P<0.001, **P<0.01. EgRNA, empty sgRNA.

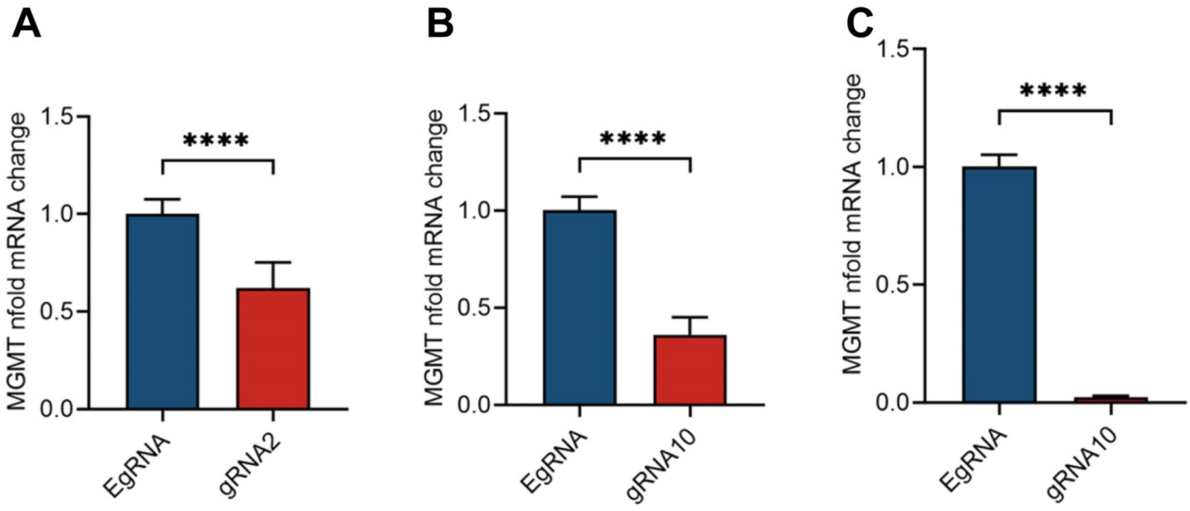

Figure 14: *MGMT* mRNA expression level of edited glioblastoma cell lines in different cell generations. (A-C) Quantitative RT PCR of *MGMT* mRNA expression levels in T98G clonal cell lines stably expressing gRNA2 **(A)** or gRNA10 **(B)**, and LN18 clonal cell lines stably expressing gRNA10 **(C)** compared with the corresponding cell lines stably expressing EgRNA. The data were normalized to the housekeeping genes ubiquitin C and hypoxanthine phosphoribosyl-transferase 1 (see Materials & Methods). Results are averaged from triplicates and are expressed as the mean ± SD. Data are representative of three independent experiments. ****P<0.0001. EgRNA, empty sgRNA.

3.5 Reduction of MGMT expression enhances the effect of TMZ in different sgRNA-edited cell lines

To detect whether edited human glioblastoma cells show enhanced cytotoxicity to TMZ treatment, different cell lines stably expressing gRNA2 or gRNA10 were treated with increasing concentrations of TMZ for 144 h and the cell viability was measured by the

Alamar blue assay. In the different cell lines stably expressing gRNA10, the cytotoxicity of TMZ increased significantly resulting in dramatically reduced TMZ IC50 values compared with the corresponding EgRNA control cell lines (TMZ IC50: 110.9 µM vs 498.9 µM in T98G cells, 8.5 µM vs 386.5 µM in LN18 cells) **(Fig. 15B-C)**. In addition, we also observed a significant reduction of TMZ IC50 values in the T98G cell line stably expressing gRNA2 in comparison with the EgRNA control cell line albeit to a much lower extent (TMZ IC50: 437.2 µM vs 619.0 µM) **(Fig. 15A).** The obtained results from the T98G and LN18 cell lines stably expressing the different sgRNAs clearly confirmed the relationship between MGMT expression level and TMZ resistance in glioblastoma.

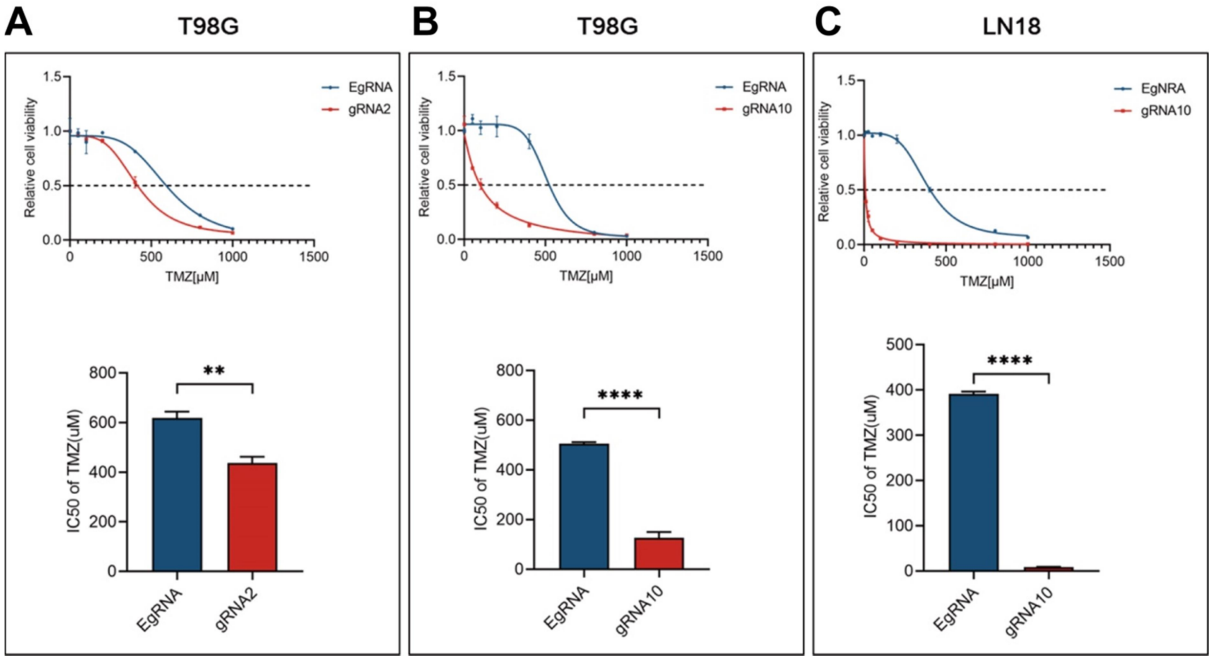

Figure 15: Targeted editing of the CGI in the *MGMT* promoter increases the cytotoxicity of TMZ and reduces the IC50 values for TMZ in edited glioblastoma cell lines. (A, B) (upper) T98G cells stably expressing gRNA2 **(A)** or gRNA10 **(B),** and the corresponding EgRNA were treated with increasing concentrations of TMZ (50, 100, 200, 400, 800, and 1000 µM) for 144 h, and cell viability was measured using Alamar blue assay. **(A, B) (lower)** Calculated IC50 values of TMZ for T98G clonal cell lines expressing gRNA2 **(A)** or gRNA10 **(B)** compared with the corresponding EgRNA control cell lines. **(C)** LN18 cells stably expressing EgRNA or gRNA10 were treated with increasing concentrations of TMZ (10, 25, 50, 100, 200, 400, 800, and 1000 µM) for 144 h, and cell viability was measured using Alamar blue **(upper)**. Calculated IC50 values of TMZ for EgRNA and gRNA10 expressing LN18 clonal cell lines **(lower)**. Data are shown as mean ± SD of values from three independent experiments with each of three replicates.

****P<0.0001, **P<0.01. TMZ, temozolomide; EgRNA, empty sgRNA.

3.6 Downregulation of MGMT expression restores the ability of TMZ to induce apoptosis in different sgRNA-edited cell lines

The significant reduction of the IC50 values for TMZ in the modified glioblastoma cell lines indicated that targeted DNA methylation of the MGMT promoter can restore the capability of TMZ to induce cell death in normally TMZ-resistant glioblastoma cell lines. To study the TMZ-induced cell death in more detail, T98G and LN18 stably expressing gRNA 10 cell lines were treated for 72 h and 144 h with increasing concentrations of TMZ (100, 200, and 400 µM for T98G; 25, 50, and 100 µM for LN18), and DNA fragmentation was measured as readout reflecting cell death induction by flow cytometry after PI staining of the cell nuclei **(Fig. 17)**. As expected, TMZ increased the percentage of cell death in a dose- and time-dependent manner in both cell lines stably expressing gRNA10. For T98G cells stably expressing gRNA10, the percentage of DNA fragmentation increased up to almost threefold at the highest TMZ concentration (400 µM) after 72 h and displayed the highest increase in the proportion of sub-G1/dead cells after 144 h each compared with the respective T98G EgRNA control cell line **(Fig. 17A-C)**. Interestingly, LN18 cells stably expressing gRNA10 showed a significantly increased cytotoxicity already at 100 µM TMZ with 20 % cell death after 72 h and 55 % cell death after 144 h each compared with the respective LN18 EgRNA control cell line; at the TMZ concentrations tested, virtually no induction of cytotoxicity or change in cell viability was detectable in LN18 EgRNA control cell line **(Fig. 17D-F)**. Furthermore, in T98G cell line stably expressing gRNA2, a significantly increased percentage of cell death was observed in comparison with the EgRNA control cell line after treating the cells with 400 µM TMZ for 72 h and 144 h **(Fig. 16A-D)**. Thus, targeted DNA methylation of the MGMT promoter is sufficient to overcome the TMZ resistance of established glioblastoma cell lines and induce cell death by TMZ.

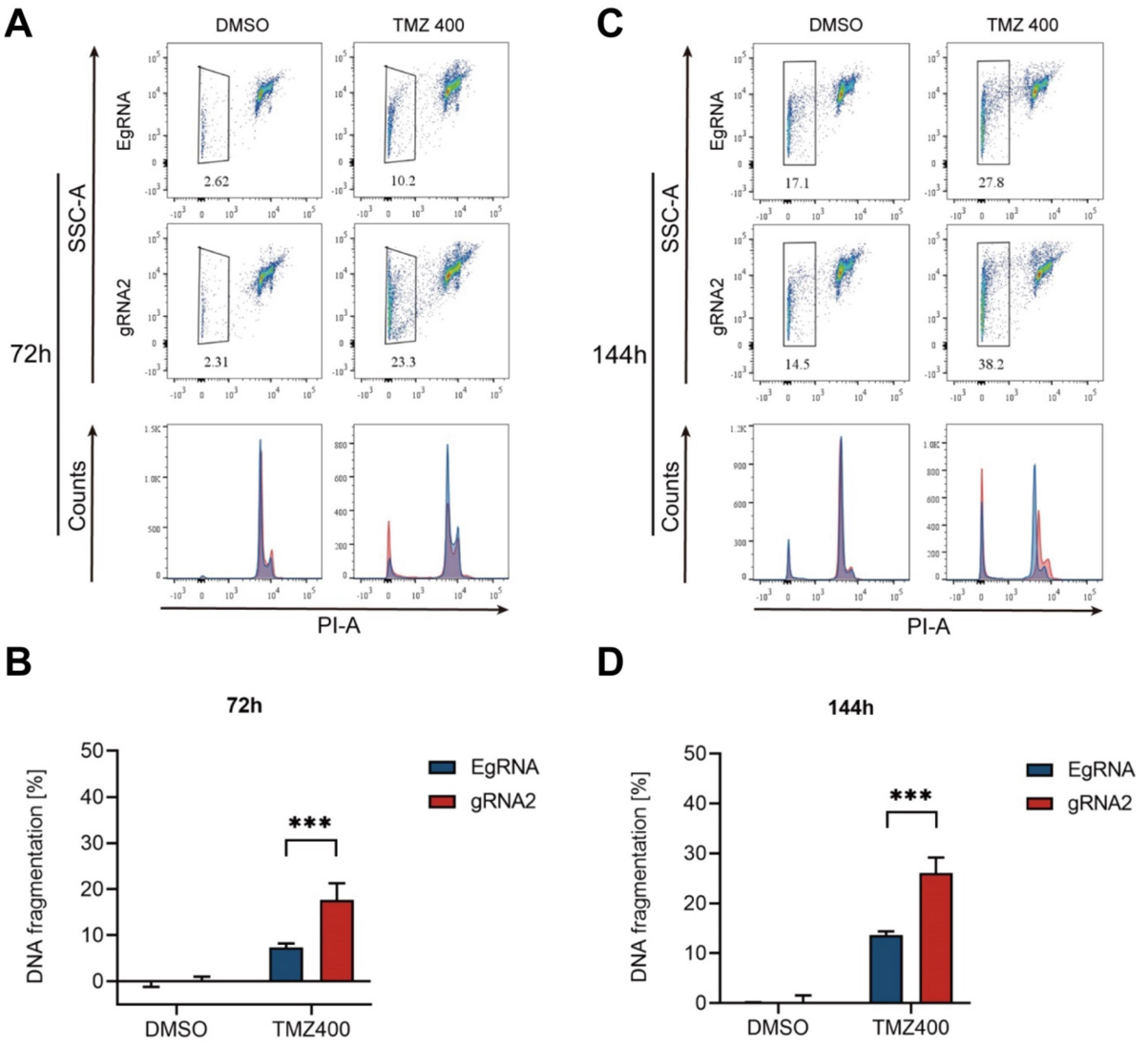

Figure 16: Targeted methylation of the *MGMT* promoter enhances TMZ-induced apoptotic cell death in gRNA2 stably expressing T98G clonal cell line. (A, C) Representative density plots **(upper)** and histograms **(lower)** from flow cytometric analysis of T98G cells stably expressing EgRNA or gRNA2 treated with 400 µM TMZ or vehicle control (DMSO) for 72 h **(A)** or 144 h **(C)**. The percentage of DNA fragmentation of PI-stained nuclei under the different concentrations of TMZ for 72 h **(A)** or 144 h **(C)** is indicated in the plots, respectively. In the overlays of the histograms, gRNA2 stably expressing T98G cells is shown in red, and EgRNA stably expressing T98G cells in blue. **(B, D)** The specific DNA fragmentation rates in T98G cell lines stably expressing EgRNA or gRNA2 in response to treatment with 400 µM TMZ for 72 h **(B)** or 144 h **(D)**, respectively. Data are shown as mean ± SD of values from three independent experiments with each of three replicates. ****P*<0.001. DMSO, Dimethyl sulfoxide; TMZ, temozolomide; PI, propidium iodide; SSC-A, side scatter area, EgRNA, empty sgRNA.

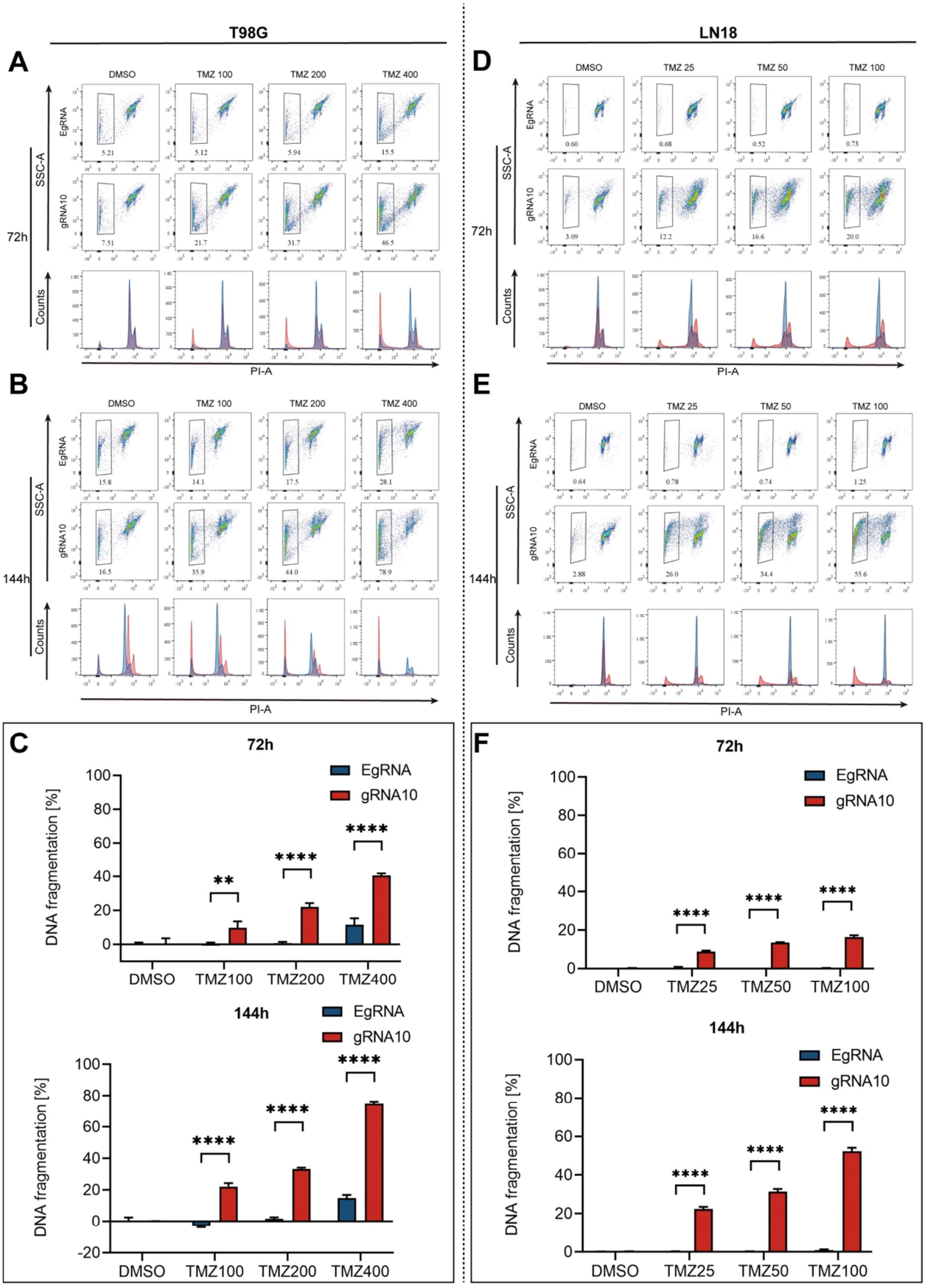
T98G
LN18
A
B
C
D
E
F
DMSO
TMZ 100
TMZ 200
TMZ 400
TMZ 25
TMZ 50
EgRNA
gRNA10
SSC-A
Counts
PI-A
72h
144h
DNA fragmentation [%]
DMSO
TMZ100
TMZ200
TMZ400
TMZ25
TMZ50
TMZ100
****
**

Figure 17: Targeted methylation of the *MGMT* promoter enhances TMZ-induced apoptotic cell death in different gRNA10 stably expressing clonal cell lines. (A and B) Representative density plots **(upper)** and histograms **(lower)** from flow cytometric analysis of T98G cells stably expressing EgRNA or gRNA10 treated with increasing concentrations of TMZ (100, 200, and 400 µM) or vehicle control (DMSO) for 72 h **(A)** or 144 h **(B)**. The percentage of DNA fragmentation of PI-stained nuclei under the different concentrations of TMZ for 72 h **(A)** or 144 h **(B)** is indicated in the plots, respectively. In the overlays of the histograms, gRNA10 expressing T98G cells is shown in red, and EgRNA expressing T98G cells in blue. **(C)** The specific DNA fragmentation rates in T98G cell lines stably expressing EgRNA or gRNA10 in response to different concentrations of TMZ for 72 h **(upper)** or 144 h **(lower)**, respectively. **(D and E)** Representative density plots **(upper)** and histograms **(lower)** from flow cytometric analysis of LN18 cells stably expressing EgRNA or gRNA10 treated with increasing concentrations of TMZ (25, 50, and 100 µM) or vehicle control (DMSO) for 72 h **(D)** or 144 h **(E)**. The percentage of DNA fragmentation of PI-stained nuclei in response to different concentrations of TMZ for 72 h **(D)** or 144 h **(E)** is indicated in the plots, respectively. In the overlays of the histograms, gRNA10 stably expressing LN18 cells is shown in red, and EgRNA stably expressing LN18 cells in blue. **(F)** The specific DNA fragmentation rates of LN18 cell lines stably expressing EgRNA or gRNA10 in response to the treatment with TMZ for 72 h **(upper)** or 144 h **(lower)** are shown in the histograms. Data are shown as mean ± SD of values from three independent experiments with each of three replicates. ****P<0.0001, **P<0.01. DMSO, Dimethyl sulfoxide; TMZ, temozolomide; PI, propidium iodide; SSC-A, side scatter area, EgRNA, empty sgRNA.

3.7 CRISPRoff induced increased DNA methylation level of *MGMT* promoter CGI in different sgRNA-edited cell lines

CRISPRoff-mediated downregulation of MGMT expression reversed TMZ resistance in the different glioblastoma cell lines. Therefore, we next determined whether it was caused indeed by changes in the methylation pattern of *MGMT* promoter CGI in different sgRNA-edited cell lines. According to the findings of Malley et al, different regions of the *MGMT* promoter region were amplified from bisulfite-converted DNA by PCR **(Fig. 18A and B)**, subsequent pyrosequencing was performed to measure the methylation level of CpG sites 25-42 in DMR1 region and CpG sites 76-90 in DMR2 region in the different cell lines stably expressing gRNA2 or gRNA10 and compared with corresponding EgRNA control cell lines **(Fig. 19A)**.

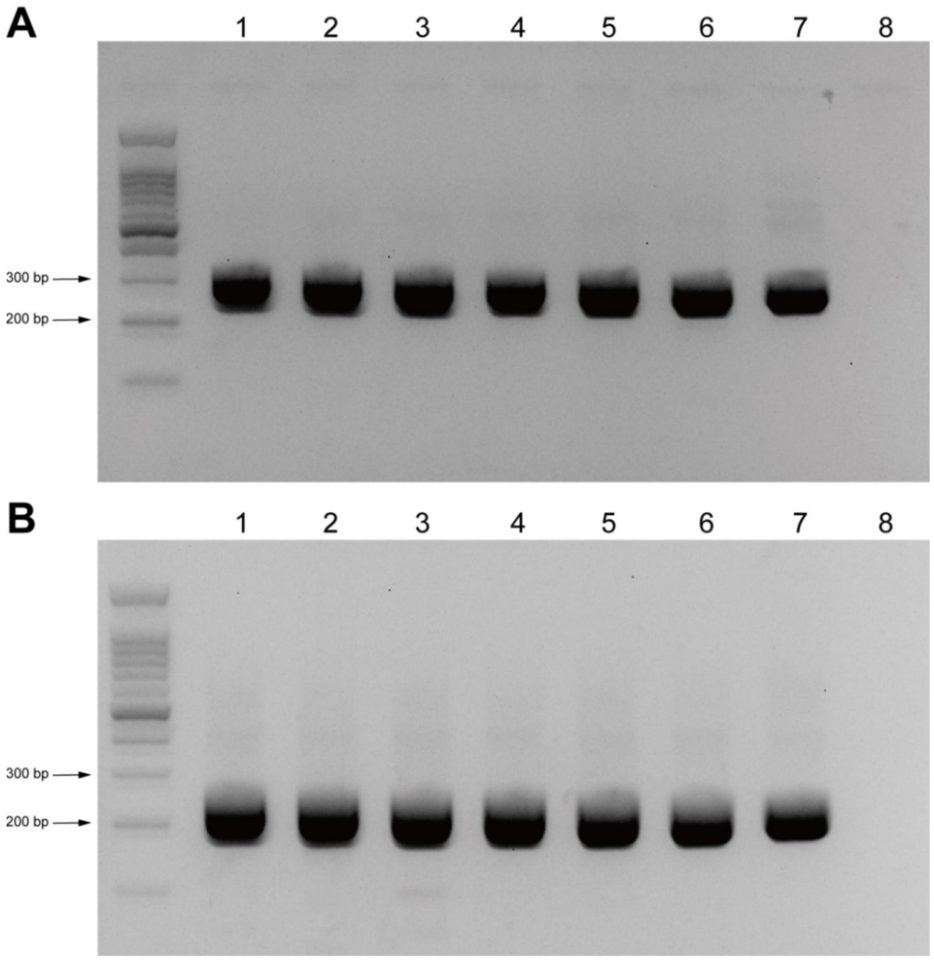

Figure 18: Bisulfite-converted DNA PCR in different sgRNA stably expressing cell lines for pyrosequencing. The representative agarose gels showed the PCR amplicons of MGMT promoter DMR1 **(329 bp, A)** and DMR2 **(266 bp, B)** regions in different sgRNA stably expressing cell lines. (lane 1-6: different sgRNA stably expressing cell lines, lane 7: positive control, lane 8: negative control).

According to the results of pyrosequencing, the methylation levels in the DMR2 region particularly of CpG sites 84-90 were significantly increased in T98G and LN18 cell lines stably expressing gRNA10 in comparison with the corresponding EgRNA control cell lines **(Fig. 19C) (Fig. 20D and F)**. Interestingly, a significantly increased methylation of CpG sites 25-38 in the DMR1 region was found only in the gRNA10 edited T98G cell line while in gRNA10 edited LN18 cell line only a few CpG sites in DMR1 showed increased methylation levels **(Fig. 19C) (Fig. 20C and E)**. On the contrary, in the gRNA2 edited T98G cell line, only a significantly increased methylation of CpG sites in the DMR1 region was observed but no significant methylation level changes in the DMR2 region compared

with the T98G EgRNA control cell line **(Fig. 19B) (Fig. 20A and B)**. Thus, the most significant changes in MGMT expression and mean methylation were achieved by gRNA10-mediated methylation of the DMR2 region in both T98G and LN18 edited cell lines.

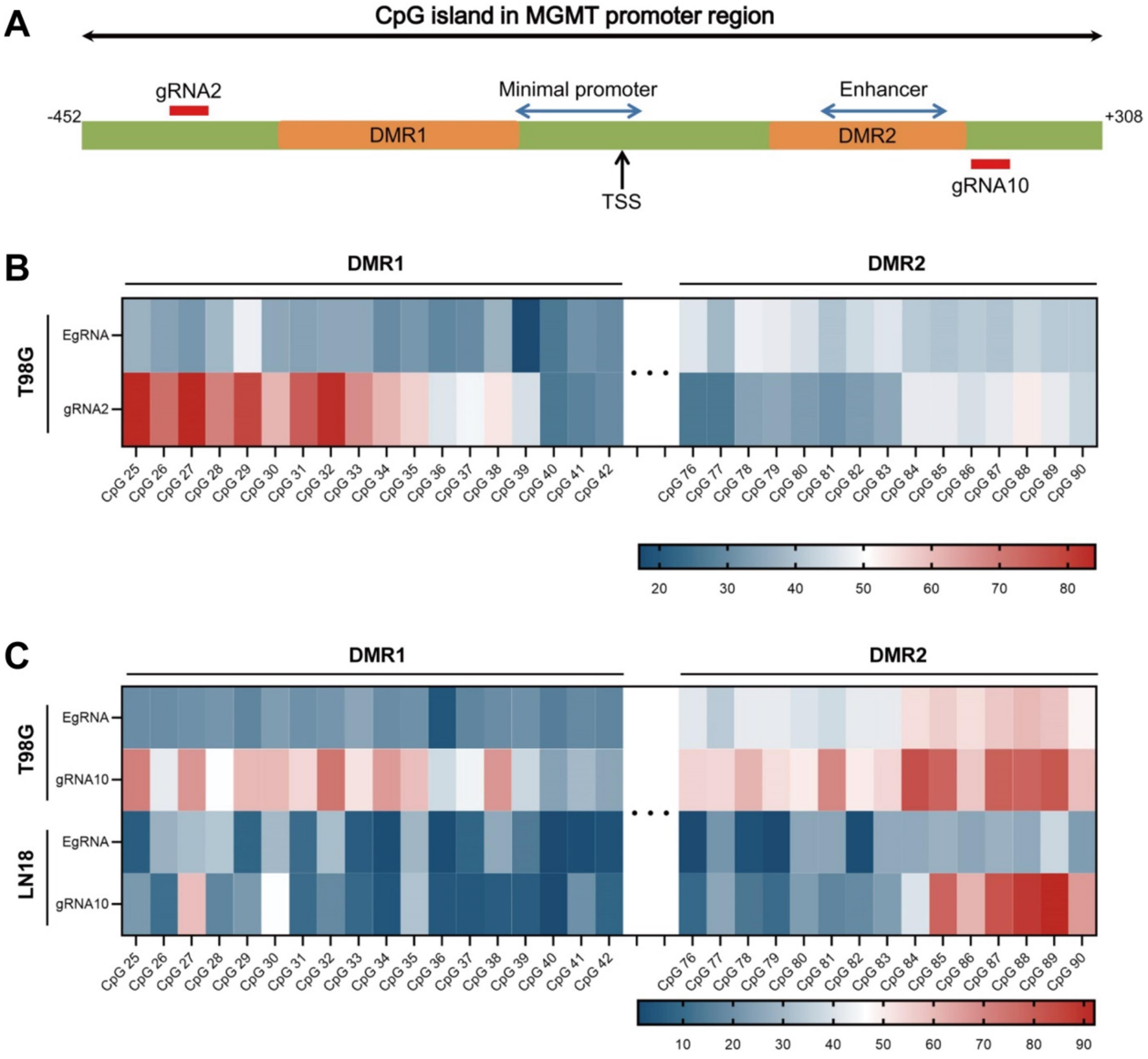

Figure 19: Differential DNA methylation pattern of the CGI in the *MGMT* promoter of the established edited glioblastoma cell lines. (A) Schematic showing the location of DMR1 and DMR2 (orange rectangle) and target site of gRNA2, gRNA10 (red rectangle) within the CGI of MGMT promoter. The location of the minimal promoter and enhancer (blue arrows) and the position of the transcription start site (TSS, black arrow) are indicated. **(B)** Heatmap showed the methylation level of single CpG sites in T98G cell

lines stably expressing EgRNA or gRNA2 determined by pyrosequencing. **(C)** Heatmap showed the methylation level of single CpG sites in different T98G and LN18 cell lines stably expressing EgRNA or gRNA10 determined by pyrosequencing. Each column represents one CpG site, CpG25-42 in the DMR1 region and CpG76-90 in the DMR2 region; each row represents one edited clonal cell line. Higher and lower rates of methylation are shown in red and blue, respectively. Data are shown as mean ± SD of values from two independent experiments with each of three replicates. DMR1, differentially methylated region 1; DMR2, differentially methylated region 2: EgRNA, empty sgRNA.

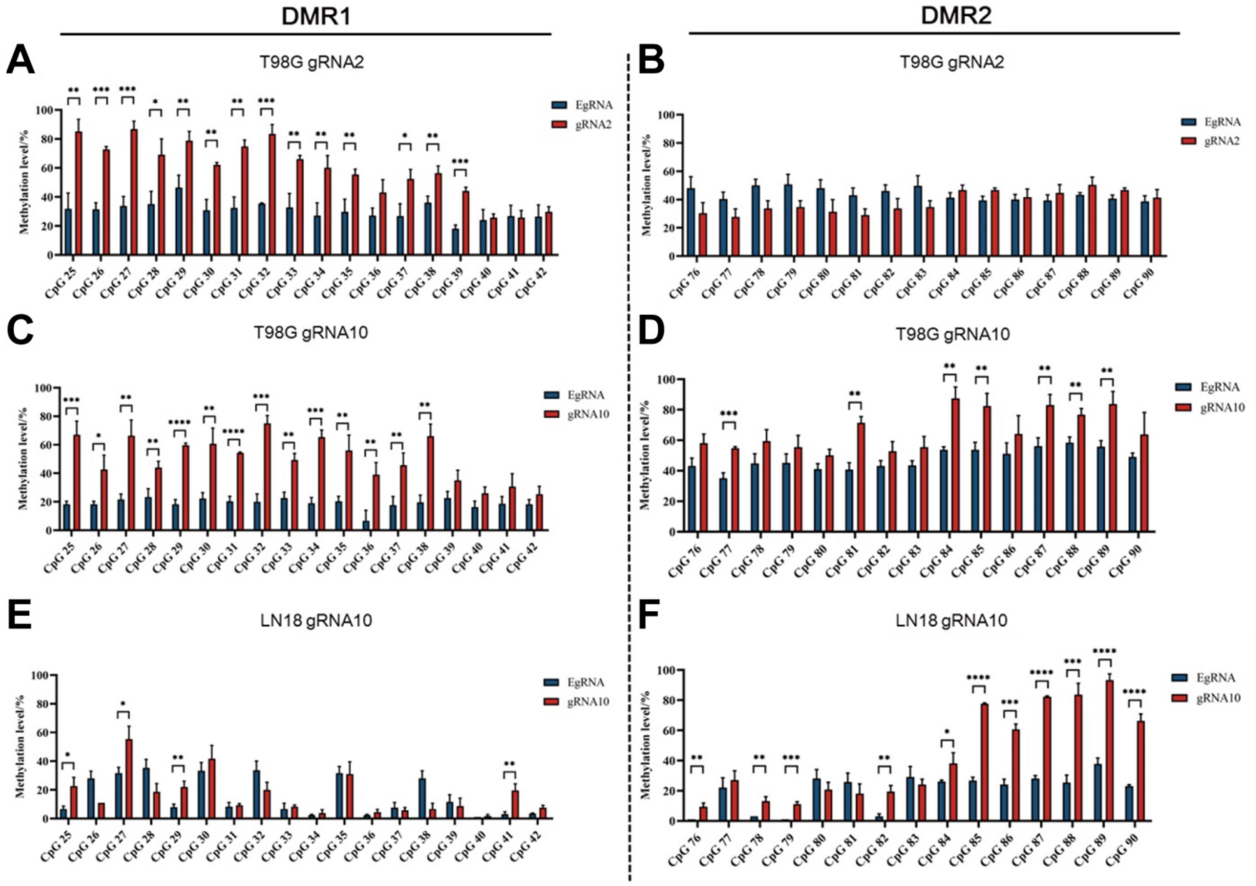

Figure 20: Methylation levels of individual CpG sites located in the CGI of the *MGMT* promoter of established edited T98G and LN18 cell lines. Methylation levels of single CpG sites in different T98G and LN18 cell lines stably expressing gRNA2 or gRNA10 in comparison with the corresponding EgRNA control cell lines. **(A-D)** Histograms showed the methylation level of CpG 25-42 in DMR1 **(A)** and CpG 76-90 in DMR2 **(B)** of T98G cell lines stably expressing EgRNA or gRNA2; the methylation level of CpG 25-42 in DMR1 **(C)** and CpG 76-90 in DMR2 **(D)** of T98G cell lines stably expressing EgRNA or gRNA10. **(E, F)** Histograms show the methylation level of CpG 25-42 in DMR1 **(E)** and CpG 76-90 in DMR2 **(F)** of LN18 cell lines stably expressing EgRNA or gRNA10.

The percentage of methylation was determined by pyrosequencing. Data are shown as mean ± SD of values from two independent experiments with each of three replicates. ****P<0.0001, ***P<0.001, **P<0.01, *P<0.05. DMR1, differentially methylated region 1; DMR2, differentially methylated region 2; EgRNA, empty sgRNA.

3.8 No obvious off-target effects of the CRISPRoff system were observed in different gRNA10 stably expressing cell lines

The above findings demonstrated that the CRISPRoff-mediated epigenetic editing with gRNA10 efficiently methylated CpG dinucleotides flanking the *MGMT* promoter target site, and was associated with transcriptional repression of *MGMT* expression. However, the off-target effects mediated by sgRNAs are an unavoidable problem for the CRISPR/Cas9 system, which holds true also for the CRISPRoff that can cause off-target methylation on untargeted genomic sites. Considering that optimal MGMT repression was mediated by gRNA10, we evaluated the off-target effect of gRNA10 in T98G and LN18 cell lines from different aspects. The off-target sites of gRNA10 predicted by the tool CRISPOR included in the UCSC genome browser are shown in **Table 40**.

3.8.1 Determination of global methylation level

To verify the target specificity of the RNA-guided methylation, we performed an immunoassay quantifying the global DNA methylation by measuring the percentage of 5'-methylcytosine using DNA samples of the respective parental cell lines, the corresponding EgRNA control cell lines and the gRNA10 stably expressing cell lines of T98G and LN18, respectively **(Fig. 21)**. The results for WT, EgRNA control, and the gRNA10 cell lines did not reveal significantly altered global methylation in either the T98G (0.15 % vs 0.16 % vs 0.18 %, respectively) or LN18 cell lines (0.35 % vs 0.34 % vs 0.32 %, respectively).

Table 40: The list of potential off-targets for gRNA10

Off-target ID	Locus	Position	CpG sites covered by 850k array probes
Off-target 1	Intergenic RP5-1071N3.1/ECE-ECE1	Chr1: 21334529 (-)	2
Off-target 2	Intergenic AC062017.1-AC079612.1	Chr2: 239554941 (+)	0
Off-target 3	Exon UBXN7-AS1/UBXN7	Chr3: 196432453 (-)	11
Off-target 4	Intron ACOX3	Chr4: 8370901 (-)	5
Off-target 5	Exon ARSJ	Chr4: 113979451 (+)	12
Off-target 6	Intergenic MIR1202-SNORD28	Chr6: 156155681 (-)	0
Off-target 7	Exon C9orf9/AK8	Chr9: 132878102 (+)	13
Off-target 8	Intergenic RP11-260M19.2-RP11-260M19.1	Chr14: 104315879 (+)	2
Off-target 9	IntergenicRP11-37/J13.1/snoZ278-FAM189A1	Chr15: 29239951 (-)	0
Off-target 10	Intergenic RP11-20G13.4-RPL7P5	Chr15: 99511316 (+)	1
Off-target 11	Intergenic RP11-420N3.3-RBFOX1	Chr16: 5922921 (+)	0
Off-target 12	Intergenic CTA-481E9.4-CTA-481E9.3	Chr16: 17989338 (-)	0
Off-target 13	Intron RP11-118F19.1	Chr16: 85582314 (-)	2
Off-target 14	Intergenic Rp11-542M13.3-RP11-542M13.2	Chr16: 85953646 (+)	1
Off-target 15	Intergenic RP11-316M20.1-AC104981.1	Chr17: 77755142 (+)	0
Off-target 16	Intron ENPP7	Chr17: 79736419 (-)	4
Off-target 17	Intron COL4A5	ChrX: 108440528 (-)	4

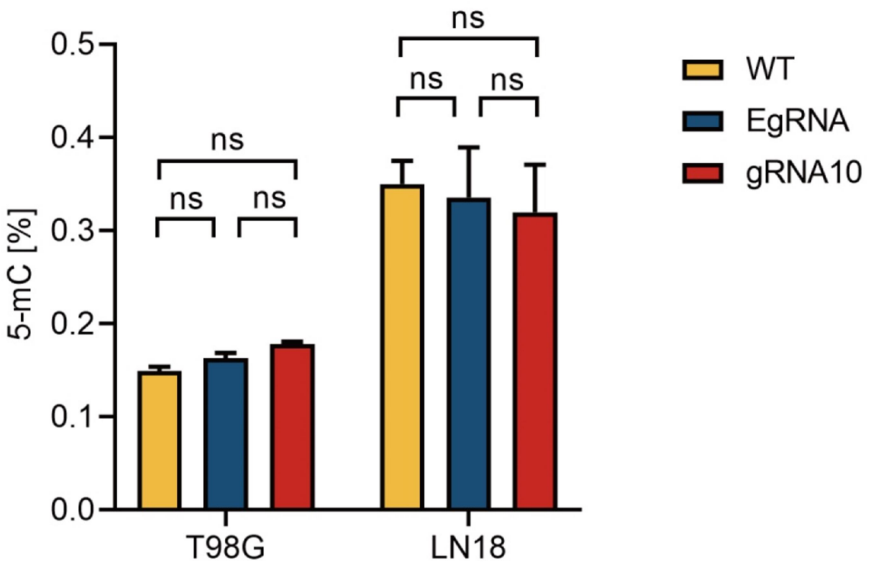

Figure 21: Global DNA methylation of WT, and edited T98G and LN18 cell lines. The analysis of the global DNA methylation (5-mC %) among the WT cell lines of T98G and LN18 and the cell lines established from them expressing EgRNA or gRNA10. Data are shown as mean ± SD of values from three independent experiments. WT, wild type; EgRNA, empty sgRNA.

3.8.2 Gene expression profiling by RNA sequencing

To detect the potential changes in mRNA expression due to the epigenetic modification of the CRISPRoff system, we performed RNA sequencing in gRNA10 stably expressing T98G and LN18 cell lines compared with the different EgRNA control cell lines respectively. Using differential gene expression (DGE) analysis (in addition to the reduced mRNA expression of *MGMT*), we found a relatively small number of 91 genes in the whole genome with a slight increase or decrease in mRNA expression in gRNA10 edited LN18 cell lines in comparison with the EgRNA control cell line **(Fig. 22A-B)**. Simultaneously, the mRNA expression of genes related to different potential off-target sites was also analyzed; and only a decrease in *COL4A5* mRNA expression was detected **(Fig. 22C-M)**, which was identified as an off-target site **(Table 40)**. Similar trends of changes in mRNA expression were also detected in gRNA10-edited T98G cell lines in comparison with its control cell line (data not shown).

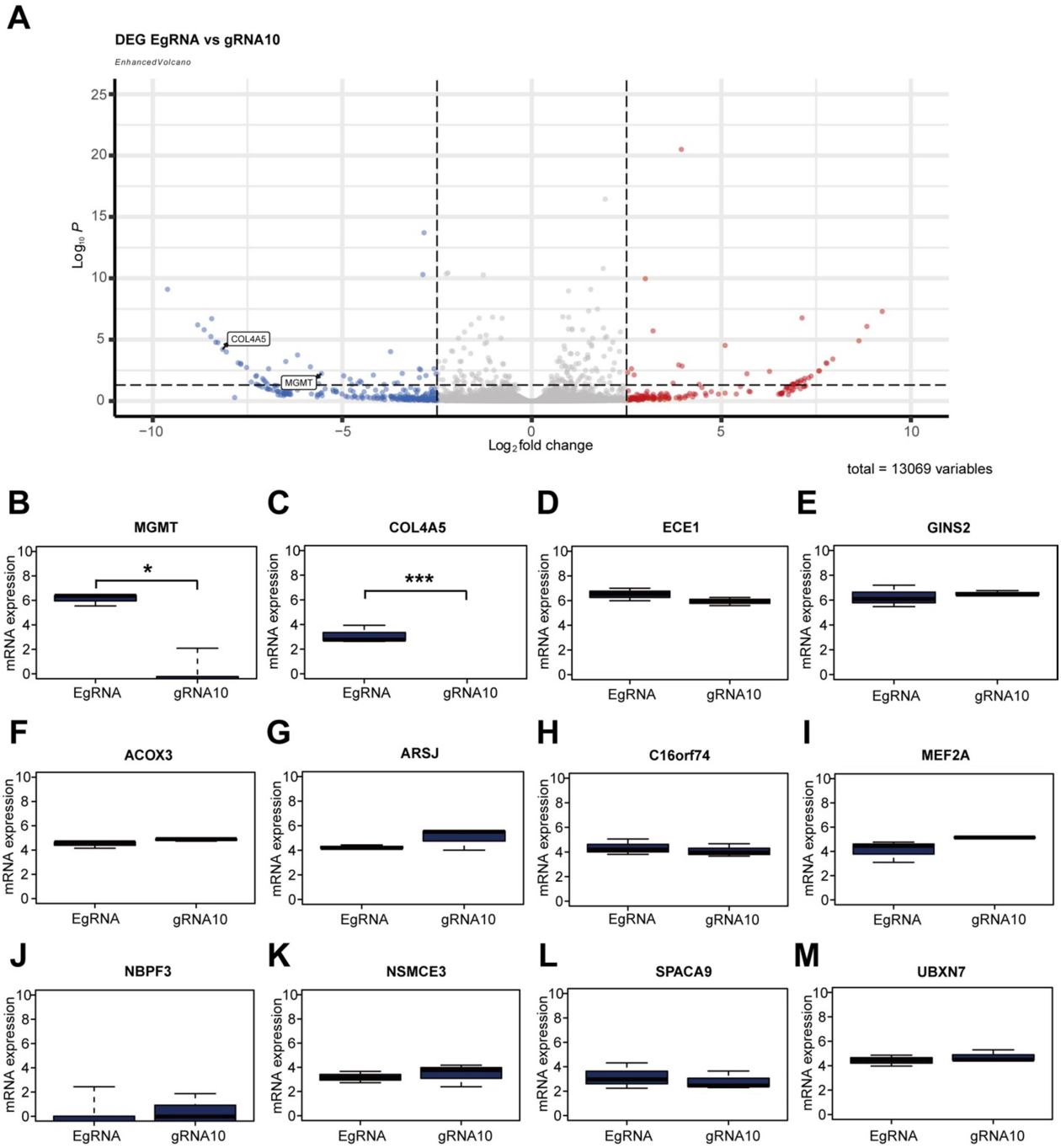

Figure 22: Gene expression profiling in gRNA10 stably expressing LN18 cell lines and its corresponding EgRNA control cell line. (A) The volcano plot showed all expressed transcripts in gRNA10 and EgRNA edited LN18 cell lines: of 13069 expressed transcripts, 91 statistically significant differentially expressed genes were identified in gRNA10 stably expressing LN18 cell line compared with its EgRNA control cell line (p-value < 0.05, FC cutoff 2.5); including 56 down- (blue dots) and 35 up-regulated (red dots) genes. **(B)** The box plot showed the *MGMT* mRNA expression level. **(C-M)** Different box plots represented the mRNA expression level of predicted off-target site-related genes. ***P<0.001, *P<0.05.

3.8.3 Genomic DNA methylation profiling by 850K array

To further evaluate the potential genome-wide off-target methylation status of the gRNA10-CRISPRoff transgene, we analyzed the gRNA10 stably expressing T98G cell line and its corresponding EgRNA control cell line using the Illumina EPIC (850K) bead array. Out of seventeen predicted off-target regions **(Table 40)**, only ten regions were covered by the Illumina EPIC array probes. All ten regions showed no signs of differential methylation between control and gRNA10-edited T98G cell lines **(Fig. 23A-J)**. Although seven regions were not covered by methylation probes, the overall results suggested the likelihood of off-target methylation occurring in the gRNA10-edited T98G cell line is quite low.

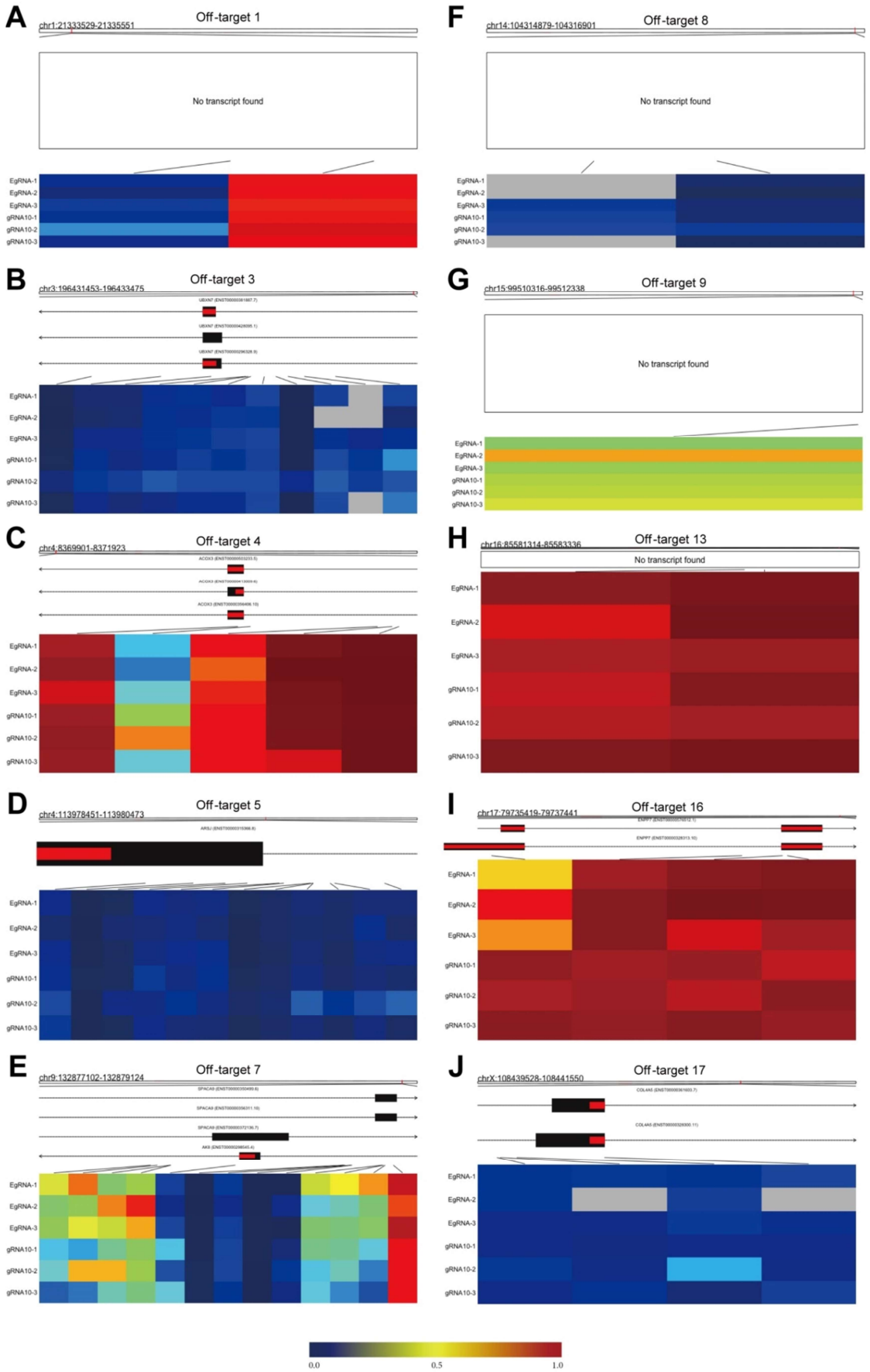
A
Off-target 1
chr1:21333529-21335551
No transcript found
EgRNA-1
EgRNA-2
EgRNA-3
gRNA10-1
gRNA10-2
gRNA10-3
B
Off-target 3
chr3:196431453-196433475
C
Off-target 4
chr4:8369901-8371923
D
Off-target 5
chr4:113978451-113980473
E
Off-target 7
chr9:132877102-132879124
F
Off-target 8
chr14:104314879-104316901
G
Off-target 9
chr15:99510316-99512338
H
Off-target 13
chr16:85581314-85583336
I
Off-target 16
chr17:79735419-79737441
J
Off-target 17
chrX:108439528-108441550
0.0
0.5
1.0

Figure 22: Genomic DNA methylation profiling in EgRNA and gRNA10 stably expressing T98G clonal cell lines. (A-J) Different heat maps represented the methylation levels of specific CpGs within predicted genomic off-target sites of gRNA10 in gRNA10 or EgRNA stably expressing T98G clonal cell lines (arrayed using IlluminaEPIC 850k bead array). Each row is representative for the analysis of one DNA sample from each EgRNA or gRNA10 edited cells, each column represents one probe present on the 850K array for the analysis of specific CpG sites. Higher and lower rates of methylation are shown in red and blue, respectively; gray indicates that the probe did not detect the target in the sample. The list of predicted gRNA10 off-targets is shown in **Table 40**. EgRNA, empty sgRNA.

4. Discussion

TMZ is the current standard therapy for glioblastoma, but TMZ chemotherapy is compromised by the development of resistance in nearly 40 % of all patients with glioblastoma (Stupp et al., 2005). The endogenous expression level of MGMT is an important factor associated with TMZ resistance in glioblastoma; approximately 60 % of glioblastoma patients harbor an unmethylated *MGMT* promoter, leading to a poor prognosis as they experience limited benefit from TMZ treatment. Overall, this study shows that the CRISPR/dCas9-based epigenetic editing system can induce targeted DNA methylation with remarkable density and frequency at CpG sites within the CGI in the MGMT promoter region. Subsequently, this induced DNA methylation was sufficient to downregulate the MGMT expression and reversed the TMZ resistance of known TMZ-resistant glioblastoma cell lines. Furthermore, no obvious off-target effects of CRISPRoff were identified by analyzing gene expression profiling and genomic DNA methylation patterns.

4.1 Downregulation of MGMT expression in edited glioblastoma cell lines

As a cellular DNA repair protein, MGMT is regulated by multiple factors including transcription factors, microRNAs, histone modifications such as acetylation, and especially methylation of the MGMT promoter region (Nie et al., 2021). Previous studies have already linked high levels of MGMT activity to resistance to alkylating agents such as TMZ in tumor tissue, and are used to predict its therapeutic effect in glioblastoma (Baer et al., 1993; Friedman et al., 2000). Given the enormous importance of MGMT in TMZ resistance, a variety of approaches have already been used to improve the sensitivity of TMZ.

Except for the pseudosubstrate for MGMT that we mentioned above, a common approach for the treatment of TMZ-resistant glioblastoma cells consists of a combination of different compounds that inhibit MGMT or suppress its expression. For example, NCT503 a highly selective inhibitor of the rate-limiting enzyme of serine biosynthesis was shown to inhibit the expression of MGMT and synergistically enhance the efficiency of TMZ in glioblastoma (Jin et al., 2022). Interestingly, treatment with NCT503 did not result in any change of methylation levels in the MGMT promoter, and other pathways such as the Wnt/ß-catenin pathways are likely involved in the regulation of MGMT expression (Jin et al., 2022). In addition, a small molecule compound, EPIC-0412, was discovered which enhanced the TMZ sensitivity in glioblastoma by acting on the p21-E2F1 DNA damage repair axis and ATF3-p-p65-MGMT axis (Zhao et al., 2023). In combination with TMZ, EPIC-0412 synergistically reduced the viability of glioblastoma cells and reversed TMZ resistance.

Toward this goal, small interfering RNAs (siRNAs) are considered to be another promising tool. siRNAs targeting transcription of *MGMT* succeeded in suppressing the expression of MGMT and increased the cytotoxicity of TMZ in T98G glioblastoma cells (Kato et al., 2010). In addition, some microRNAs have also been reported to be involved in the downregulation of MGMT expression. For instance, miR-181d effectively downregulates MGMT by directly interacting with the 3'UTR of *MGMT*, thereby enhancing the efficacy of TMZ as a sensitizing agent in MGMT-targeted therapy (Zhang et al., 2012). MiR-198 inhibited the translation of *MGMT* mRNA in glioblastoma cells by directly binding to the *MGMT* 3'UTR, which can reverse the TMZ resistance in glioblastoma with MGMT overexpression. However, the effectiveness of siRNAs may be limited by the poor specificity, causing potential safety issues and sometimes reducing therapeutic efficacy (Nie et al., 2017).

The CRISPR/Cas9 system has become an important technology for human genome editing. Originally discovered as an adaptive immune system in prokaryotes consisting of

a DNA endonuclease and a sgRNA, it has been widely used in glioblastoma to uncover the function of genes involved in tumor cell growth, suppression of apoptosis, induction of autophagy, deregulation of the immune response, cell migration, and metastasis (Al-Sammarraie and Ray, 2021). In recent years, modifications of the CRISPR/Cas9 system have been developed using dCas9 for epigenetic editing in glioblastoma. For instance, Jameson et al. identified two enhancers within the first intron of the epidermal growth factor receptor (EGFR) gene which is frequently overexpressed in a variety of cancer types including glioblastoma (Jameson et al., 2019; Salomon et al., 1995). Using a dCas9 protein fused to the Krüppel-associated box (dCas9-KRAB), the authors were able to target the enhancer elements and repress EGFR transcription by histone deacetylation (Jameson et al., 2019). In addition, glioblastoma progression was also successfully suppressed with an RNA-guided CRISPR/dCas9 synergistic activation mediator system overexpressing full-length HECT domain-containing E3 ubiquitin ligase (HUWE1) (Yuan et al., 2022). HUWE1 is widely known to regulate the complex interactions between proliferation, differentiation, and DNA damage response (Hao et al., 2012; Inoue et al., 2013; Kurokawa et al., 2013; Zhang et al., 2011).

Here, we used a CRISPR/dCas9 (CRISPRoff) system in different glioblastoma cell lines to achieve targeted methylation of CpG sites in the *MGMT* promoter region by a methyltransferase (DNMT3A/3L) fused to dCas9. Three individual sgRNAs targeting different regions of the *MGMT* promoter were studied for their capability to repress the endogenous MGMT expression. Using the CRISPRoff system we isolated several clonal cell lines of LN18 and T98G showing a strong reduction in their endogenous MGMT expression at both the mRNA and protein levels, which is almost silenced in gRNA10 stably expressing T98G and LN18 cell lines. Moreover, expression of MGMT was stably repressed over multiple generations in the epigenetically silenced clonal cell lines of T98G and LN18 for at least 10-15 passages.

In comparison with other MGMT silencing techniques described above, the approach of CRISPRoff has several advantages: 1. A high efficiency of MGMT repression by specific epigenetic modification without changing in DNA sequence. 2. The downregulation of MGMT is heritable during cell division. 3. If some side effects due to silencing of MGMT expression are observed, the CRISPRoff-induced DNA methylation can be reversed by another epigenetic editing system called CRISPRon.

4.2 Enhancement of TMZ sensitivity in different TMZ-resistant glioblastoma cell lines

The CRISPRoff-based hypermethylation of the *MGMT* promoter enhanced the sensitivity for TMZ in resistant glioblastoma cell lines. The IC50 values for TMZ which were initially measured in the parental cell lines of T98G (476 µM) and LN18 (425 µM) were comparable to those reported previously for T98G (502 µM) and LN18 (511 µM) (Hermisson et al., 2006; Lee, 2016).

Using CRISPRoff-mediated methylation of MGMT promoter CGI in the TMZ-resistant glioblastoma cell lines decreased the IC50 values of TMZ by 78 % and 98 % in gRNA10 stably expressing T98G and LN18 cell lines, respectively. In addition, the increased sensitivity to TMZ of the gRNA10 edited cell lines was confirmed by DNA fragmentation analysis using PI staining and flow cytometry. The epigenetically silenced different gRNA10 clonal cell lines showed significantly higher levels of DNA fragmentation upon treatment with a lower concentration of TMZ compared with the respective control cell lines indicating an enhanced induction of apoptotic cell death by TMZ treatment.

Interestingly, the cytotoxic effect of TMZ in gRNA2 stably expressing T98G cell line was less pronounced, and no increased cell death induced by a lower concentration of TMZ was observed; which can be explained most likely by an insufficient reduction of the MGMT expression and still too high residual expression of MGMT. During the DNA repair

process, one MGMT molecule irreversibly removes only one alkyl group from the O^6 position of guanine to its cysteine residue; hence, the capacity of the DNA repair depends on the amount of MGMT (Malley et al., 2011).

4.3 Remodeling of methylation patterns of *MGMT* promoter CGI in glioblastoma cell lines edited by different sgRNAs

Given the impact of MGMT expression levels on TMZ resistance, the methylation status of *MGMT* promoter is routinely assessed by diverse technologies to stratify patients with glioblastoma. In the past two decades, several studies identified distinct regions across *MGMT* promoter CGI, whose methylation level may play a critical role in the regulation of *MGMT* expression (Everhard et al., 2009; Malley et al., 2011; Nakagawachi et al., 2003; Watts et al., 1997). Particularly, the DMR1 (contains CpG25-50) and DMR2 (contains CpG73-90) regions, which were defined previously (Malley et al., 2011). Except for the demonstration of the methylation status of these two regions that strongly correlates with *MGMT* mRNA expression, the authors also confirmed the important role of several specific CpG sites within the DMR2 region in controlling *MGMT* expression by selective site-directed mutagenesis (Malley et al., 2011). In addition, Bady et al. revealed that methylation of the DMR1 and DMR2 regions in the *MGMT* promoter CGI is associated with improved overall survival of glioblastoma patients treated with alkylating agents (Bady et al., 2012).

Here, we tested individual sgRNAs targeting three different regions of the CGI in the *MGMT* promoter and evaluated their capability to repress endogenous MGMT expression. While one sgRNA (gRNA4) showed no repressive effect at all, two sgRNAs (gRNA2, 10) targeting both ends of the CGI, showed a different degree of reduction of their endogenous MGMT expression. In this regard, the location of the sgRNA-targeted

sequence appears to play an important role in regulating MGMT expression. We further assessed the modified methylation pattern in the *MGMT* promoter CGI.

The gRNA2 binds to a DNA sequence on the sense strand close to the DMR1 region in the *MGMT* promoter CGI and causes increased methylation level of multiple CpG sites in the DMR1 region decreasing endogenous MGMT expression by 50 %, especially the CpG25-32 sites. For gRNA10, which targets a DNA sequence at the end of MGMT promoter CGI on the antisense strand, mediated strong increased methylation level of the DMR2 region resulting in a strong to almost complete reduction of endogenous MGMT expression in both T98G and LN18 glioblastoma cell lines stably expressing gRNA10. In particular, we found hypermethylation of CpG84-89 sites in the DMR2 region of gRNA10 stably expressing glioblastoma cell lines. These CpG sites are located within the enhancer region of the *MGMT* promoter and 5'upstream of the gene region targeted by gRNA10. These findings show that by using CRISPRoff and one specific sgRNA, efficient methylation of CpG sites in the DMR2 region and silencing of the MGMT expression can be achieved in formerly TMZ-resistant glioblastoma cell lines. Consistent with our results, Malley et al. reported that CpG sites 83, 86, 87, and 89 closely correlate with the transcriptional control of *MGMT* expression by luciferase assay; in particular, the mutation of CpG site 89 alone almost entirely extinguished the promoter activity (Malley et al., 2011).

The critical role of the methylation status within the DMR2 region in promoting *MGMT* gene transcription may be explained by nucleosome positioning, which is an important mechanism for gene expression regulation because linker DNA is more approachable for regulatory proteins like transcription factors (TFs) than nucleosome-bound DNA (Segal and Widom, 2009). It is possible that CpG83-89 located within the DMR2 region is less affected by nucleosome binding and methylation. Therefore, when aberrant methylation occurs in this region, it may prevent regulatory proteins from binding to this region, either by direct blockade or by remodeling chromatin via methyl CpG-binding proteins like

methyl CpG binding protein 2 (MeCP2). It has been reported that the binding sites of some TFs are located in this region, such as the Signal transducer and activator of transcription 3 (STAT3), which is associated with gliomagenesis (la Iglesia et al., 2009). Furthermore, nuclease accessibility analysis revealed that the open chromosomal structure is lost in cells with *MGMT* methylation; subsequently, the TSS becomes unapproachable, even though the TSS region itself is unmethylated (Patel et al., 1997; Watts et al., 1997). This indicates that the hypermethylation of regions outside of the TSS like DMR2 region, may block the TSS through chromatin remodeling, resulting in silencing of gene transcription.

4.4 Evaluation of CRISPRoff potential off-target effect in different gRNA10 stably expressing cell lines

While the CRISPR/Cas9 gene editing system has been extensive utilization and ongoing advancements, demonstrating promising potential for clinical transformation, the persistence of off-target effects remains a major issue that urgently needs to be addressed (Fu et al., 2013; Hsu et al., 2013; Pacesa et al., 2022). Generally, off-target effects refer to the adverse consequences caused by the sgRNA binding at non-targeted genomic locations (1-5 base pairs mismatch) and resulting from Cas9 cleavage, which has been widely reported in CRISPR/Cas9-edited human cell lines (Guo et al., 2023; Han et al., 2020). The specificity of the CRISPR/Cas9 system is thought to be closely governed by the 20bp nucleotide sequence of the crRNA within the sgRNA, along with the PAM sequence. Notably, the “seed sequence”, 10–12 base pairs of the crRNA adjacent to the PAM sequence, was defined and confirmed to be more important in determining Cas9 specificity than the rest of the crRNA sequence (Cong et al., 2013; Jinek et al., 2012). The subsequent studies further showed that the 1-5 base pairs within the seed sequence proximal to the PAM sequence are the most crucial ones (Wu et al.,

2014). Moreover, mismatches spanning 1-5 base pairs at the 5' end of the crRNA are more readily tolerated compared with those occurring at the 3' end (Zhang et al., 2015).

In our research, off-target effects manifest as the CRISPRoff-induced hypermethylation at non-target sites of sgRNA in the genome. First of all, the global methylation levels of the silenced, parental, and control cell lines of T98G and LN18 did not exhibit significant changes in the genome-wide methylation status. Subsequently, combined with the RNA sequencing analysis and 850k genomic methylation profiling, no off-target effects were identified at the predicted gRNA10 off-target sites, except for the *COL4A5* gene.

The *COL4A5* gene is located on the X chromosome and encodes one of the six subunits of type IV collagen, mutations in this gene are associated with X-linked Alport syndrome, also known as hereditary nephritis (Pierides et al., 2013). According to the previous study, the hypermethylation of the *COL4A5* promoter region is related to the suppression of its expression (Ikeda et al., 2006). Interestingly, the *COL4A5* promoter hypermethylation was reported to be responsible for the development of colorectal cancer; on the contrary, it is also associated with improved survival in gastric cancer (Peng et al., 2020; Xu et al., 2019). In this study, we observed a decrease in *COL4A5* mRNA expression by RNA sequencing in gRNA10 edited cell lines compared with EgRNA control cell lines; on the other hand, no changes of methylation were found in the probes of 850k located in the *COL4A5* gene. Furthermore, the predicted off-target site in the *COL4A5* gene is located in the intron 1 region rather than the promoter region. Therefore, it is possible that changes in *COL4A5* gene expression levels are not due to off-target effects of the CRISPRoff system, however, future investigations are needed.

In order to reduce the off-target effects of the CRISPR/Cas9 system at unintended sites in the genome, various strategies are currently being considered, such as sgRNA alteration, Cas9 protein modification, and delivery modality improvement (Han et al., 2020). First, the alteration of sgRNA includes two possibilities: truncation of base pairs at the 5' end of the crRNA, resulting in 17-18 bp complementary sequence within sgRNA,

and adjunction of 2 guanine nucleotides to the 5' end of the crRNA; both ways are confirmed to effectively decrease the off-target effects (Cho et al., 2014; Fu et al., 2014; Pattanayak et al., 2013). second, it has been reported that the use of recombinant Cas9 protein results in much lower off-target editing than expression-based approaches (Vakulskas and Behlke, 2019). In addition, the frequency of off-target effects can be minimized by ribonucleoprotein (RNP)-based methods to limit the exposure of the genome to active Cas9 complexes. Recently, Yan et al. developed a noninvasive CRISPR/Cas9 brain nano-delivery system that could be used in combination with RNPs to limit off-target effects and provide excellent gene editing efficiencies (Zou et al., 2022).

4.5 Limitations and outlook of the study

The study proved the feasibility of reversing TMZ resistance caused by high expression of MGMT in glioblastoma through the CRISPR/dCas9-based epigenetic editing system. While no apparent off-target effects were observed at the cellular level through RNA sequencing and 850K analysis, it is imperative to acknowledge that this does not preclude the possibility of side effects arising from potential off-target effects in animal models and within the organism. For example, the *COL4A5* gene, although changes in its methylation level were not detected with the currently available methods, investigations to determine the *COL4A5* mRNA level and its potential consequences in patient-derived glioblastoma organoids and vivo xenograft studies are pending. This will also determine whether we need to make subtle adjustments to the DNA sequence binding position of the sgRNA in the DMR2 region to eliminate potentially serious off-target effects.

In this study, indirect effects of MGMT gene silencing through the CRISPRoff system were not excluded. MGMT is an important DNA repair enzyme in cells, so silencing its activity could potentially lead to some indirect negative effects. For instance, in the

absence of MGMT protein expression, DNA demethylase cannot be effectively repaired, which will lead to the failure of downstream target gene demethylation.

In summary, CRISPRoff-based epigenetic modifications in patient-derived glioblastoma organoids and animal models will be the remaining steps on the road towards a new therapy. In addition, it is also needed to determine the minimum amount of sgRNA required to achieve the current effective methylation pattern in subsequent preclinical translation studies.

5. Summary

Glioblastoma is the most common and aggressive primary tumor of the central nervous system with poor outcomes. The current gold standard treatment is surgical resection followed by a combination of radio- and chemotherapy. The efficacy of temozolomide (TMZ), the primary chemotherapeutic agent, depends on the DNA methylation status of the O6-methylguanine DNA methyltransferase (MGMT), which has been identified as a prognostic biomarker in glioblastoma patients. Clinical studies revealed that glioblastoma patients with hypermethylated MGMT promoter have a better response to TMZ treatment and a significantly improved overall survival.

In this study, we thus used the CRISPRoff genome editing tool to mediate targeted DNA methylation within the *MGMT* promoter region. The system carrying a CRISPR-dCas9 fused with a methyltransferase (Dnmt3A/3L) domain downregulated MGMT expression in TMZ-resistant human glioblastoma cell lines through targeted DNA methylation. The reduction of MGMT expression levels reversed TMZ resistance in TMZ-resistant glioblastoma cell lines resulting in TMZ-induced dose-dependent cell death rates. In addition, no obvious off-target effects of the CRISPRoff system are detected at the cellular level.

In conclusion, we demonstrate that targeted RNA-guided methylation of the MGMT promoter emerged as a promising tool to overcome chemoresistance and improve the cytotoxic effect of TMZ in glioblastoma.

6. List of Figures

7. List of tables

8. References

Akhtar-Zaidi, B., Cowper-Sal· lari, R., Corradin, O., Saiakhova, A., Bartels, C.F., Balasubramanian, D., Myeroff, L., Lutterbaugh, J., Jarrar, A., and Kalady, M.F. Epigenomic enhancer profiling defines a signature of colon cancer. Science, 2012; 336: 736-739

Al-Sammarraie, N., and Ray, S.K. Applications of CRISPR-Cas9 technology to genome editing in glioblastoma multiforme. Cells, 2021; 10: 2342

Alexander, B.M., and Cloughesy, T.F. Adult glioblastoma. J Clin Oncol, 2017; 35: 2402-2409

Amirian, E.S., Zhou, R., Wrensch, M.R., Olson, S.H., Scheurer, M.E., Il'Yasova, D., Lachance, D., Armstrong, G.N., McCoy, L.S., and Lau, C.C. Approaching a scientific consensus on the association between allergies and glioma risk: a report from the glioma international case-control study. Cancer Epidemiology, Biomarkers & Prevention, 2016; 25: 282-290

Anders, S., and Huber, W. Differential expression analysis for sequence count data. Nature Precedings, 2010: 1-1

Ansari, I., Chaturvedi, A., Chitkara, D., and Singh, S. CRISPR/Cas mediated epigenome editing for cancer therapy. Semin Cancer Biol, 2022; 83: 570-583

Aran, D., Sabato, S., and Hellman, A. DNA methylation of distal regulatory sites characterizes dysregulation of cancer genes. Genome Biol, 2013; 14: 1-14

Bady, P., Sciuscio, D., Diserens, A.-C., Bloch, J., Van Den Bent, M.J., Marosi, C., Dietrich, P.-Y., Weller, M., Mariani, L., and Heppner, F.L. MGMT methylation analysis of glioblastoma on the Infinium methylation BeadChip identifies two distinct CpG regions associated with gene silencing and outcome, yielding a prediction model for comparisons

across datasets, tumor grades, and CIMP-status. Acta Neuropathol, 2012; 124: 547-560

Baer, J., Freeman, A., Newlands, E., Watson, A., Rafferty, J., and Margison, G. Depletion of O6-alkylguanine-DNA alkyltransferase correlates with potentiation of temozolomide and CCNU toxicity in human tumour cells. Br J Cancer, 1993; 67: 1299-1302

Baylin, S.B., and Jones, P.A. A decade of exploring the cancer epigenome—biological and translational implications. Nature Reviews Cancer, 2011; 11: 726-734

Berger, S.L. The complex language of chromatin regulation during transcription. Nature, 2007; 447: 407-412

Bier, E. Drosophila, the golden bug, emerges as a tool for human genetics. Nature Reviews Genetics, 2005; 6: 9-23

Bird, A. CpG-rich islands and the function of DNA methylation. Nature, 1986; 321: 209-213

Bird, A. DNA methylation patterns and epigenetic memory. Genes Dev, 2002; 16: 6-21

Brandes, A.A., Tosoni, A., Franceschi, E., Sotti, G., Frezza, G., Amistà, P., Morandi, L., Spagnolli, F., and Ermani, M. Recurrence pattern after temozolomide concomitant with and adjuvant to radiotherapy in newly diagnosed patients with glioblastoma: correlation with MGMT promoter methylation status. J Clin Oncol, 2009; 27: 1275-1279

Brennan, C.W., Verhaak, R.G., McKenna, A., Campos, B., Noushmehr, H., Salama, S.R., Zheng, S., Chakravarty, D., Sanborn, J.Z., and Berman, S.H. The somatic genomic landscape of glioblastoma. Cell, 2013; 155: 462-477

Brocken, D.J.W., Tark-Dame, M., and Dame, R.T. dCas9: A Versatile Tool for Epigenome Editing. Curr Issues Mol Biol, 2018; 26: 15-32

Brodbelt, A., Greenberg, D., Winters, T., Williams, M., Vernon, S., and Collins, V.P.

Glioblastoma in england: 2007–2011. Eur J Cancer, 2015; 51: 533-542

Brown, T.J., Brennan, M.C., Li, M., Church, E.W., Brandmeir, N.J., Rakszawski, K.L., Patel, A.S., Rizk, E.B., Suki, D., and Sawaya, R. Association of the extent of resection with survival in glioblastoma: a systematic review and meta-analysis. JAMA oncology, 2016; 2: 1460-1469

Cai, R., Lv, R., Shi, X.e., Yang, G., and Jin, J. CRISPR/dCas9 tools: Epigenetic mechanism and application in gene transcriptional regulation. Int J Mol Sci, 2023; 24: 14865

Canoll, P., and Goldman, J.E. The interface between glial progenitors and gliomas. Acta Neuropathol, 2008; 116: 465-477

Capecchi, M.R. Generating mice with targeted mutations. Nat Med, 2001; 7: 1086-1090

Ceccarelli, M., Barthel, F.P., Malta, T.M., Sabedot, T.S., Salama, S.R., Murray, B.A., Morozova, O., Newton, Y., Radenbaugh, A., and Pagnotta, S.M. Molecular profiling reveals biologically discrete subsets and pathways of progression in diffuse glioma. Cell, 2016; 164: 550-563

Chaichana, K.L., Jusue-Torres, I., Navarro-Ramirez, R., Raza, S.M., Pascual-Gallego, M., Ibrahim, A., Hernandez-Hermann, M., Gomez, L., Ye, X., and Weingart, J.D. Establishing percent resection and residual volume thresholds affecting survival and recurrence for patients with newly diagnosed intracranial glioblastoma. Neuro Oncol, 2014; 16: 113-122

Chaichana, K.L., Parker, S.L., Olivi, A., and Quiñones-Hinojosa, A. Long-term seizure outcomes in adult patients undergoing primary resection of malignant brain astrocytomas. J Neurosurg, 2009; 111: 282-292

Chedin, F., Lieber, M., and Hsieh, C. The DNA methyltransferase-like protein DNMT3L stimulates de novo methylation by Dnmt3a. Proc Natl Acad Sci U S A, 2002; 99:

16916-16921

Chekani-Azar, S., GHARIB MOMBENI, E., BIRHAN, M., and YOUSEFI, M. CRISPR/Cas9 gene editing technology and its application to the coronavirus disease (COVID-19), a review. Journal of Life Science and Biomedicine, 2020; 10: 01-09

Chen, C., Shi, Y., Li, Y., He, Z.-C., Zhou, K., Zhang, X.-N., Yang, K.-D., Wu, J.-R., Kung, H.-F., and Ping, Y.-F. A glycolysis-based ten-gene signature correlates with the clinical outcome, molecular subtype and IDH1 mutation in glioblastoma. Journal of Genetics and Genomics, 2017; 44: 519-530

Cho, S.W., Kim, S., Kim, Y., Kweon, J., Kim, H.S., Bae, S., and Kim, J.-S. Analysis of off-target effects of CRISPR/Cas-derived RNA-guided endonucleases and nickases. Genome Res, 2014; 24: 132-141

Christmann, M., Nagel, G., Horn, S., Krahn, U., Wiewrodt, D., Sommer, C., and Kaina, B. MGMT activity, promoter methylation and immunohistochemistry of pretreatment and recurrent malignant gliomas: a comparative study on astrocytoma and glioblastoma. Int J Cancer, 2010; 127: 2106-2118

Clarke, J.L., Ennis, M.M., Yung, W.A., Chang, S.M., Wen, P.Y., Cloughesy, T.F., DeAngelis, L.M., Robins, H.I., Lieberman, F.S., and Fine, H.A. Is surgery at progression a prognostic marker for improved 6-month progression-free survival or overall survival for patients with recurrent glioblastoma? Neuro Oncol, 2011; 13: 1118-1124

Cong, L., Ran, F.A., Cox, D., Lin, S., Barretto, R., Habib, N., Hsu, P.D., Wu, X., Jiang, W., and Marraffini, L.A. Multiplex genome engineering using CRISPR/Cas systems. Science, 2013; 339: 819-823

Costello, J.F., Futscher, B.W., Tano, K., Graunke, D.M., and Pieper, R.O. Graded methylation in the promoter and body of the O6-methylguanine DNA methyltransferase (MGMT) gene correlates with MGMT expression in human glioma cells. J Biol Chem,

1994; 269: 17228-17237

Couturier, C.P., Ayyadhury, S., Le, P.U., Nadaf, J., Monlong, J., Riva, G., Allache, R., Baig, S., Yan, X., and Bourgey, M. Single-cell RNA-seq reveals that glioblastoma recapitulates a normal neurodevelopmental hierarchy. Nature communications, 2020; 11: 3406

Cox, D.B.T., Platt, R.J., and Zhang, F. Therapeutic genome editing: prospects and challenges. Nat Med, 2015; 21: 121-131

Cullot, G., Boutin, J., Toutain, J., Prat, F., Pennamen, P., Rooryck, C., Teichmann, M., Rousseau, E., Lamrissi-Garcia, I., and Guyonnet-Duperat, V. CRISPR-Cas9 genome editing induces megabase-scale chromosomal truncations. Nature communications, 2019; 10: 1136

Dawson, M., and Kouzarides, T. Cancer epigenetics: from mechanism to therapy. Cell, 2012; 150: 12-27

de Souza, C.F., Sabedot, T.S., Malta, T.M., Stetson, L., Morozova, O., Sokolov, A., Laird, P.W., Wiznerowicz, M., Iavarone, A., and Snyder, J. A distinct DNA methylation shift in a subset of glioma CpG island methylator phenotypes during tumor recurrence. Cell reports, 2018; 23: 637-651

Delgado‐Martín, B., and Medina, M.Á. Advances in the knowledge of the molecular biology of glioblastoma and its impact in patient diagnosis, stratification, and treatment. Advanced Science, 2020; 7: 1902971

Della Monica, R., Cuomo, M., Buonaiuto, M., Costabile, D., Franca, R.A., Del Basso De Caro, M., Catapano, G., Chiariotti, L., and Visconti, R. MGMT and Whole-Genome DNA Methylation Impacts on Diagnosis, Prognosis and Therapy of Glioblastoma Multiforme. Int J Mol Sci, 2022; 23: 7148

Deplus, R., Brenner, C., Burgers, W.A., Putmans, P., Kouzarides, T., Launoit, Y.d., and

Fuks, F. Dnmt3L is a transcriptional repressor that recruits histone deacetylase. Nucleic Acids Res, 2002; 30: 3831-3838

Desai, S., Ding, M., Wang, B., Lu, Z., Zhao, Q., Shaw, K., Yung, W.A., Weinstein, J.N., Tan, M., and Yao, J. Tissue-specific isoform switch and DNA hypomethylation of the pyruvate kinase PKM gene in human cancers. Oncotarget, 2014; 5: 8202

Dewdney, B., Jenkins, M.R., Best, S.A., Freytag, S., Prasad, K., Holst, J., Endersby, R., and Johns, T.G. From signalling pathways to targeted therapies: unravelling glioblastoma's secrets and harnessing two decades of progress. Signal Transduction and Targeted Therapy, 2023; 8: 400

Dobes, M., Khurana, V.G., Shadbolt, B., Jain, S., Smith, S.F., Smee, R., Dexter, M., and Cook, R. Increasing incidence of glioblastoma multiforme and meningioma, and decreasing incidence of Schwannoma (2000–2008): findings of a multicenter Australian study. Surgical neurology international, 2011; 2:

Dong, Z., and Cui, H. Epigenetic modulation of metabolism in glioblastoma. Semin Cancer Biol, 2019; 57: 45-51

Egli, D., Zuccaro, M.V., Kosicki, M., Church, G.M., Bradley, A., and Jasin, M. Inter-homologue repair in fertilized human eggs? Nature, 2018; 560: E5-E7

Ehrlich, M., and Lacey, M. DNA hypomethylation and hemimethylation in cancer. Epigenetic alterations in oncogenesis, 2012: 31-56

Esteller, M., Corn, P.G., Baylin, S.B., and Herman, J.G. A gene hypermethylation profile of human cancer. Cancer Res, 2001; 61: 3225-3229

Esteller, M., Hamilton, S.R., Burger, P.C., Baylin, S.B., and Herman, J.G. Inactivation of the DNA repair gene O6-methylguanine-DNA methyltransferase by promoter hypermethylation is a common event in primary human neoplasia. Cancer Res, 1999; 59:

793-797

Everhard, S., Tost, J.r., El Abdalaoui, H., Crinière, E., Busato, F., Marie, Y., Gut, I.G., Sanson, M., Mokhtari, K., and Laigle-Donadey, F. Identification of regions correlating MGMT promoter methylation and gene expression in glioblastomas. Neuro Oncol, 2009; 11: 348-356

Felsenfeld, G. A brief history of epigenetics. Cold Spring Harb Perspect Biol, 2014; 6:

Fisher, J.L., Schwartzbaum, J.A., Wrensch, M., and Wiemels, J.L. Epidemiology of brain tumors. Neurol Clin, 2007; 25: 867-890

Friedman, H.S., Kerby, T., and Calvert, H. Temozolomide and treatment of malignant glioma. Clin Cancer Res, 2000; 6: 2585-2597

Fu, Y., Foden, J.A., Khayter, C., Maeder, M.L., Reyon, D., Joung, J.K., and Sander, J.D. High-frequency off-target mutagenesis induced by CRISPR-Cas nucleases in human cells. Nat Biotechnol, 2013; 31: 822-826

Fu, Y., Sander, J.D., Reyon, D., Cascio, V.M., and Joung, J.K. Improving CRISPR-Cas nuclease specificity using truncated guide RNAs. Nat Biotechnol, 2014; 32: 279-284

Gardiner-Garden, M., and Frommer, M. CpG islands in vertebrate genomes. J Mol Biol, 1987; 196: 261-282

Gartler, S., and Riggs, A. Mammalian X-chromosome inactivation. Annu Rev Genet, 1983; 17: 155-190

Genovese, P., Schiroli, G., Escobar, G., Di Tomaso, T., Firrito, C., Calabria, A., Moi, D., Mazzieri, R., Bonini, C., and Holmes, M.C. Targeted genome editing in human repopulating haematopoietic stem cells. Nature, 2014; 510: 235-240

Gerson, S.L., Trey, J.E., Miller, K., and Berger, N.A. Comparison of O 6

-alkylguanine-DNA alkyltransferase activity based on cellular DNA content in human, rat and mouse tissues. Carcinogenesis, 1986; 7: 745-749

Gilard, V., Tebani, A., Dabaj, I., Laquerrière, A., Fontanilles, M., Derrey, S., Marret, S., and Bekri, S. Diagnosis and management of glioblastoma: A comprehensive perspective. Journal of Personalized Medicine, 2021; 11: 258

Gilbert, L.A., Larson, M.H., Morsut, L., Liu, Z., Brar, G.A., Torres, S.E., Stern-Ginossar, N., Brandman, O., Whitehead, E.H., and Doudna, J.A. CRISPR-mediated modular RNA-guided regulation of transcription in eukaryotes. Cell, 2013; 154: 442-451

Godde, J.S., and Bickerton, A. The repetitive DNA elements called CRISPRs and their associated genes: evidence of horizontal transfer among prokaryotes. J Mol Evol, 2006; 62: 718-729

Grech, N., Dalli, T., Mizzi, S., Meilak, L., Calleja, N., and Zrinzo, A. Rising incidence of glioblastoma multiforme in a well-defined population. Cureus, 2020; 12:

Guo, A.C., Cummings, T.J., Dash, R.C., and Provenzale, J.M. Lymphomas and high-grade astrocytomas: comparison of water diffusibility and histologic characteristics. Radiology, 2002; 224: 177-183

Guo, C., Ma, X., Gao, F., and Guo, Y. Off-target effects in CRISPR/Cas9 gene editing. Frontiers in Bioengineering and Biotechnology, 2023; 11: 1143157

Han, H.A., Pang, J.K.S., and Soh, B.-S. Mitigating off-target effects in CRISPR/Cas9-mediated in vivo gene editing. Journal of Molecular Medicine, 2020; 98: 615-632

Hao, Z., Duncan, G.S., Su, Y.-W., Li, W.Y., Silvester, J., Hong, C., You, H., Brenner, D., Gorrini, C., and Haight, J. The E3 ubiquitin ligase Mule acts through the ATM–p53 axis to maintain B lymphocyte homeostasis. J Exp Med, 2012; 209: 173-186

Hattori, N., and Ushijima, T. Analysis of gene-specific DNA methylation. Handbook of epigenetics, 2017: 113-123

Hayashida, Y., Hirai, T., Morishita, S., Kitajima, M., Murakami, R., Korogi, Y., Makino, K., Nakamura, H., Ikushima, I., and Yamura, M. Diffusion-weighted imaging of metastatic brain tumors: comparison with histologic type and tumor cellularity. Am J Neuroradiol, 2006; 27: 1419-1425

Hegi, M., Diserens, A., Gorlia, T., Hamou, M., de Tribolet, N., Weller, M., Kros, J., Hainfellner, J., Mason, W., Mariani, L., Bromberg, J., Hau, P., Mirimanoff, R., Cairncross, J., Janzer, R., and Stupp, R. MGMT gene silencing and benefit from temozolomide in glioblastoma. The New England journal of medicine, 2005; 352: 997-1003

Hegi, M., Liu, L., Herman, J., Stupp, R., Wick, W., Weller, M., Mehta, M., and Gilbert, M. Correlation of O6-methylguanine methyltransferase (MGMT) promoter methylation with clinical outcomes in glioblastoma and clinical strategies to modulate MGMT activity. Journal of clinical oncology : official journal of the American Society of Clinical Oncology, 2008; 26: 4189-4199

Hermisson, M., Klumpp, A., Wick, W., Wischhusen, J., Nagel, G., Roos, W., Kaina, B., and Weller, M. O6‐methylguanine DNA methyltransferase and p53 status predict temozolomide sensitivity in human malignant glioma cells. J Neurochem, 2006; 96: 766-776

Higano, S., Yun, X., Kumabe, T., Watanabe, M., Mugikura, S., Umetsu, A., Sato, A., Yamada, T., and Takahashi, S. Malignant astrocytic tumors: clinical importance of apparent diffusion coefficient in prediction of grade and prognosis. Radiology, 2006; 241: 839-846

Hilton, I.B., D'Ippolito, A.M., Vockley, C.M., Thakore, P.I., Crawford, G.E., Reddy, T.E., and Gersbach, C.A. Epigenome editing by a CRISPR-Cas9-based acetyltransferase

activates genes from promoters and enhancers. Nat Biotechnol, 2015; 33: 510-517

Holliday, R. Epigenetics: A Historical Overview. Epigenetics, 2006; 1: 76-80

Horvath, P., Romero, D.A., Coûté-Monvoisin, A.-C., Richards, M., Deveau, H., Moineau, S., Boyaval, P., Fremaux, C., and Barrangou, R. Diversity, activity, and evolution of CRISPR loci in Streptococcus thermophilus. J Bacteriol, 2008; 190: 1401-1412

House, S. Epigenetics in adaptive evolution and development: the interplay between evolving species and epigenetic mechanisms: extract from Trygve Tollefsbol (ed.) (2011) Handbook of epigenetics--the new molecular and medical genetics. Chapter 26. Amsterdam, USA: Elsevier, pp. 423-446. Nutrition and health, 2013; 22: 105-131

Hsu, P.D., Lander, E.S., and Zhang, F. Development and applications of CRISPR-Cas9 for genome engineering. Cell, 2014; 157: 1262-1278

Hsu, P.D., Scott, D.A., Weinstein, J.A., Ran, F.A., Konermann, S., Agarwala, V., Li, Y., Fine, E.J., Wu, X., and Shalem, O. DNA targeting specificity of RNA-guided Cas9 nucleases. Nat Biotechnol, 2013; 31: 827-832

Ikeda, K., Iyama, K.-i., Ishikawa, N., Egami, H., Nakao, M., Sado, Y., Ninomiya, Y., and Baba, H. Loss of expression of type IV collagen α5 and α6 chains in colorectal cancer associated with the hypermethylation of their promoter region. The American journal of pathology, 2006; 168: 856-865

Inoue, S., Hao, Z., Elia, A.J., Cescon, D., Zhou, L., Silvester, J., Snow, B., Harris, I.S., Sasaki, M., and Li, W.Y. Mule/Huwe1/Arf-BP1 suppresses Ras-driven tumorigenesis by preventing c-Myc/Miz1-mediated down-regulation of p21 and p15. Genes Dev, 2013; 27: 1101-1114

Jameson, N.M., Ma, J., Benitez, J., Izurieta, A., Han, J.Y., Mendez, R., Parisian, A., and Furnari, F. Intron 1–Mediated Regulation of EGFR Expression in EGFR-Dependent

Malignancies Is Mediated by AP-1 and BET Proteins. Mol Cancer Res, 2019; 17: 2208-2220

Jasin, M., and Rothstein, R. Repair of strand breaks by homologous recombination. Cold Spring Harb Perspect Biol, 2013; 5: a012740

Jin, L., Kiang, K.M.-Y., Cheng, S.Y., and Leung, G.K.-K. Pharmacological inhibition of serine synthesis enhances temozolomide efficacy by decreasing O6-methylguanine DNA methyltransferase (MGMT) expression and reactive oxygen species (ROS)-mediated DNA damage in glioblastoma. Lab Invest, 2022; 102: 194-203

Jinek, M., Chylinski, K., Fonfara, I., Hauer, M., Doudna, J.A., and Charpentier, E. A programmable dual-RNA–guided DNA endonuclease in adaptive bacterial immunity. Science, 2012; 337: 816-821

Johnson, C., Warmoes, M., Shen, X., and Locasale, J. Epigenetics and cancer metabolism. Cancer Lett, 2015; 356: 309-314

Jones, P. Functions of DNA methylation: islands, start sites, gene bodies and beyond. Nature reviews Genetics, 2012; 13: 484-492

Jones, P.A., and Baylin, S.B. The fundamental role of epigenetic events in cancer. Nature reviews genetics, 2002; 3: 415-428

Jones, P.A., and Baylin, S.B. The epigenomics of cancer. Cell, 2007; 128: 683-692

Kalpathy-Cramer, J., Gerstner, E.R., Emblem, K.E., Andronesi, O.C., and Rosen, B. Advanced magnetic resonance imaging of the physical processes in human glioblastoma. Cancer Res, 2014; 74: 4622-4637

Kampmann, M. CRISPRi and CRISPRa Screens in Mammalian Cells for Precision Biology and Medicine. ACS Chem Biol, 2018; 13: 406-416

Kato, T., Natsume, A., Toda, H., Iwamizu, H., Sugita, T., Hachisu, R., Watanabe, R., Yuki, K., Motomura, K., and Bankiewicz, K. Efficient delivery of liposome-mediated MGMT-siRNA reinforces the cytotoxity of temozolomide in GBM-initiating cells. Gene Ther, 2010; 17: 1363-1371

Kelly, A.D., and Issa, J.-P.J. The promise of epigenetic therapy: reprogramming the cancer epigenome. Curr Opin Genet Dev, 2017; 42: 68-77

Kelly, P.J., Daumas-Duport, C., Kispert, D.B., Kall, B.A., Scheithauer, B.W., and Illig, J.J. Imaging-based stereotaxic serial biopsies in untreated intracranial glial neoplasms. J Neurosurg, 1987; 66: 865-874

Kent, W. BLAT--the BLAST-like alignment tool. Genome Res, 2002; 12: 656-664

Khalil, A.M. The genome editing revolution. Journal of genetic engineering and biotechnology, 2020; 18: 1-16

Kickingereder, P., Wiestler, B., Sahm, F., Heiland, S., Roethke, M., Schlemmer, H.-P., Wick, W., Bendszus, M., and Radbruch, A. Primary central nervous system lymphoma and atypical glioblastoma: multiparametric differentiation by using diffusion-, perfusion-, and susceptibility-weighted MR imaging. Radiology, 2014; 272: 843-850

Kloosterhof, N.K., de Rooi, J.J., Kros, M., Eilers, P.H., Smitt, P.A.S., van den Bent, M.J., and French, P.J. Molecular subtypes of glioma identified by genome‐wide methylation profiling. Genes, Chromosomes and Cancer, 2013; 52: 665-674

Kulis, M., and Esteller, M. DNA methylation and cancer. Adv Genet, 2010; 70: 27-56

Kurokawa, M., Kim, J., Geradts, J., Matsuura, K., Liu, L., Ran, X., Xia, W., Ribar, T.J., Henao, R., and Dewhirst, M.W. A network of substrates of the E3 ubiquitin ligases MDM2 and HUWE1 control apoptosis independently of p53. Science signaling, 2013; 6: ra32-ra32

la Iglesia, N.d., Puram, S.V., and Bonni, A. STAT3 regulation of glioblastoma pathogenesis. Curr Mol Med, 2009; 9: 580-590

Lacroix, M., and Toms, S.A. Maximum safe resection of glioblastoma multiforme. J Clin Oncol, 2014; 32: 727-728

Lamborn, K.R., Yung, W.A., Chang, S.M., Wen, P.Y., Cloughesy, T.F., DeAngelis, L.M., Robins, H.I., Lieberman, F.S., Fine, H.A., and Fink, K.L. Progression-free survival: an important end point in evaluating therapy for recurrent high-grade gliomas. Neuro Oncol, 2008; 10: 162-170

Law, M., Yang, S., Babb, J.S., Knopp, E.A., Golfinos, J.G., Zagzag, D., and Johnson, G. Comparison of cerebral blood volume and vascular permeability from dynamic susceptibility contrast-enhanced perfusion MR imaging with glioma grade. Am J Neuroradiol, 2004; 25: 746-755

Lee, B., Park, J., Bjørnerud, A., Kim, J., Lee, J., and Kim, H. Clinical value of vascular permeability estimates using dynamic susceptibility contrast MRI: improved diagnostic performance in distinguishing hypervascular primary CNS lymphoma from glioblastoma. Am J Neuroradiol, 2018; 39: 1415-1422

Lee, S.Y. Temozolomide resistance in glioblastoma multiforme. Genes & diseases, 2016; 3: 198-210

Leece, R., Xu, J., Ostrom, Q.T., Chen, Y., Kruchko, C., and Barnholtz-Sloan, J.S. Global incidence of malignant brain and other central nervous system tumors by histology, 2003–2007. Neuro Oncol, 2017; 19: 1553-1564

Li, H., Haurigot, V., Doyon, Y., Li, T., Wong, S.Y., Bhagwat, A.S., Malani, N., Anguela, X.M., Sharma, R., and Ivanciu, L. In vivo genome editing restores haemostasis in a mouse model of haemophilia. Nature, 2011; 475: 217-221

Liao, P., Ostrom, Q.T., Stetson, L., and Barnholtz-Sloan, J.S. Models of epigenetic age capture patterns of DNA methylation in glioma associated with molecular subtype, survival, and recurrence. Neuro Oncol, 2018; 20: 942-953

Liao, Y., Smyth, G.K., and Shi, W. The R package Rsubread is easier, faster, cheaper and better for alignment and quantification of RNA sequencing reads. Nucleic Acids Res, 2019; 47: e47-e47

Linos, E., Raine, T., Alonso, A., and Michaud, D. Atopy and risk of brain tumors: a meta-analysis. Journal of the National Cancer Institute, 2007; 99: 1544-1550

Livak, K.J., and Schmittgen, T.D. Analysis of relative gene expression data using real-time quantitative PCR and the 2− ΔΔCT method. Methods, 2001; 25: 402-408

Lövkvist, C., Dodd, I., Sneppen, K., and Haerter, J. DNA methylation in human epigenomes depends on local topology of CpG sites. Nucleic Acids Res, 2016; 44: 5123-5132

Lu, X., Xu, W., Wei, Y., Li, T., Gao, L., Fu, X., Yao, Y., and Wang, L. Diagnostic performance of DWI for differentiating primary central nervous system lymphoma from glioblastoma: a systematic review and meta-analysis. Neurol Sci, 2019; 40: 947-956

Lu, Y., Chan, Y.-T., Tan, H.-Y., Li, S., Wang, N., and Feng, Y. Epigenetic regulation in human cancer: the potential role of epi-drug in cancer therapy. Mol Cancer, 2020; 19: 1-16

Mack, S.C., Witt, H., Piro, R., Gu, L., Zuyderduyn, S., Stütz, A., Wang, X., Gallo, M., Garzia, L., and Zayne, K. Epigenomic alterations define lethal CIMP-positive ependymomas of infancy. Nature, 2014; 506: 445-450

Maglott, D., Ostell, J., Pruitt, K.D., and Tatusova, T. Entrez Gene: gene-centered information at NCBI. Nucleic Acids Res, 2010; 39: D52-D57

Mali, P., Yang, L., Esvelt, K.M., Aach, J., Guell, M., DiCarlo, J.E., Norville, J.E., and Church, G.M. RNA-guided human genome engineering via Cas9. Science, 2013; 339: 823-826

Malley, D.S., Hamoudi, R.A., Kocialkowski, S., Pearson, D.M., Collins, V.P., and Ichimura, K. A distinct region of the MGMT CpG island critical for transcriptional regulation is preferentially methylated in glioblastoma cells and xenografts. Acta Neuropathol, 2011; 121: 651-661

Malta, T.M., de Souza, C.F., Sabedot, T.S., Silva, T.C., Mosella, M.S., Kalkanis, S.N., Snyder, J., Castro, A.V.B., and Noushmehr, H. Glioma CpG island methylator phenotype (G-CIMP): biological and clinical implications. Neuro Oncol, 2018; 20: 608-620

Mansouri, A., Hachem, L.D., Mansouri, S., Nassiri, F., Laperriere, N.J., Xia, D., Lindeman, N.I., Wen, P.Y., Chakravarti, A., and Mehta, M.P. MGMT promoter methylation status testing to guide therapy for glioblastoma: refining the approach based on emerging evidence and current challenges. Neuro Oncol, 2019; 21: 167-178

Marraffini, L.A., and Sontheimer, E.J. CRISPR interference: RNA-directed adaptive immunity in bacteria and archaea. Nature Reviews Genetics, 2010; 11: 181-190

Maxwell, A., McCudden, C.R., Wians, F., and Willis, M.S. Recent Advances in the Detection of Prostate Cancer Using Epigenetic Markers in Commonly Collected Laboratory Samples. Lab Med, 2009; 40: 171-178

McDonald, J.I., Celik, H., Rois, L.E., Fishberger, G., Fowler, T., Rees, R., Kramer, A., Martens, A., Edwards, J.R., and Challen, G.A. Reprogrammable CRISPR/Cas9-based system for inducing site-specific DNA methylation. Biology Open, 2016; 5: 866-874

Mohandas, T., Sparkes, R.S., and Shapiro, L.J. Reactivation of an Inactive Human X Chromosome: Evidence for X Inactivation by DNA Methylation. Science, 1981; 211: 393-396

Molinaro, A.M., Hervey-Jumper, S., Morshed, R.A., Young, J., Han, S.J., Chunduru, P., Zhang, Y., Phillips, J.J., Shai, A., and Lafontaine, M. Association of maximal extent of resection of contrast-enhanced and non–contrast-enhanced tumor with survival within molecular subgroups of patients with newly diagnosed glioblastoma. JAMA oncology, 2020; 6: 495-503

naidu gopal Hariprabu, K., Sathya, M., and Vimalraj, S. CRISPR/Cas9 in cancer therapy: A review with a special focus on tumor angiogenesis. Int J Biol Macromol, 2021; 192: 913-930

Nakagawachi, T., Soejima, H., Urano, T., Zhao, W., Higashimoto, K., Satoh, Y., Matsukura, S., Kudo, S., Kitajima, Y., and Harada, H. Silencing effect of CpG island hypermethylation and histone modifications on O6-methylguanine-DNA methyltransferase (MGMT) gene expression in human cancer. Oncogene, 2003; 22: 8835-8844

Neftel, C., Laffy, J., Filbin, M.G., Hara, T., Shore, M.E., Rahme, G.J., Richman, A.R., Silverbush, D., Shaw, M.L., and Hebert, C.M. An integrative model of cellular states, plasticity, and genetics for glioblastoma. Cell, 2019; 178: 835-849. e821

Nie, E., Jin, X., Miao, F., Yu, T., Zhi, T., Shi, Z., Wang, Y., Zhang, J., Xie, M., and You, Y. TGF-β1 modulates temozolomide resistance in glioblastoma via altered microRNA processing and elevated MGMT. Neuro Oncol, 2021; 23: 435-446

Nie, E., Jin, X., Wu, W., Yu, T., Zhou, X., Shi, Z., Zhang, J., Liu, N., and You, Y. MiR-198 enhances temozolomide sensitivity in glioblastoma by targeting MGMT. J Neurooncol, 2017; 133: 59-68

Nishimasu, H., Ran, F.A., Hsu, P.D., Konermann, S., Shehata, S.I., Dohmae, N., Ishitani, R., Zhang, F., and Nureki, O. Crystal structure of Cas9 in complex with guide RNA and target DNA. Cell, 2014; 156: 935-949

Noorbakhsh, A., Tang, J.A., Marcus, L.P., McCutcheon, B., Gonda, D.D., Schallhorn, C.S., Talamini, M.A., Chang, D.C., Carter, B.S., and Chen, C.C. Gross-total resection outcomes in an elderly population with glioblastoma: a SEER-based analysis. J Neurosurg, 2014; 120: 31-39

Nunez, J.K., Chen, J., Pommier, G.C., Cogan, J.Z., Replogle, J.M., Adriaens, C., Ramadoss, G.N., Shi, Q., Hung, K.L., Samelson, A.J., Pogson, A.N., Kim, J.Y.S., Chung, A., Leonetti, M.D., Chang, H.Y., Kampmann, M., Bernstein, B.E., Hovestadt, V., Gilbert, L.A., and Weissman, J.S. Genome-wide programmable transcriptional memory by CRISPR-based epigenome editing. Cell, 2021; 184: 2503-2519 e2517

Nüsslein-Volhard, C., and Wieschaus, E. Mutations affecting segment number and polarity in Drosophila. Nature, 1980; 287: 795-801

Ohgaki, H., and Kleihues, P. The definition of primary and secondary glioblastoma. Clin Cancer Res, 2013; 19: 764-772

Omuro, A., and DeAngelis, L.M. Glioblastoma and other malignant gliomas: a clinical review. Jama, 2013; 310: 1842-1850

Ostrom, Q.T., Gittleman, H., Truitt, G., Boscia, A., Kruchko, C., and Barnholtz-Sloan, J.S. CBTRUS statistical report: primary brain and other central nervous system tumors diagnosed in the United States in 2011–2015. Neuro Oncol, 2018; 20: iv1-iv86

Pacesa, M., Lin, C.-H., Cléry, A., Saha, A., Arantes, P.R., Bargsten, K., Irby, M.J., Allain, F.H.-T., Palermo, G., and Cameron, P. Structural basis for Cas9 off-target activity. Cell, 2022; 185: 4067-4081. e4021

Patel, A.P., Fisher, J.L., Nichols, E., Abd-Allah, F., Abdela, J., Abdelalim, A., Abraha, H.N., Agius, D., Alahdab, F., and Alam, T. Global, regional, and national burden of brain and other CNS cancer, 1990–2016: a systematic analysis for the Global Burden of Disease Study 2016. The Lancet Neurology, 2019; 18: 376-393

Patel, S.A., Graunke, D.M., and Pieper, R.O. Aberrant silencing of the CpG island-containing human O 6-methylguanine DNA methyltransferase gene is associated with the loss of nucleosome-like positioning. Mol Cell Biol, 1997; 17: 5813-5822

Pattanayak, V., Lin, S., Guilinger, J.P., Ma, E., Doudna, J.A., and Liu, D.R. High-throughput profiling of off-target DNA cleavage reveals RNA-programmed Cas9 nuclease specificity. Nat Biotechnol, 2013; 31: 839-843

Peng, Y., Wu, Q., Wang, L., Wang, H., and Yin, F. A DNA methylation signature to improve survival prediction of gastric cancer. Clin Epigenetics, 2020; 12: 1-16

Perry, J.R., Laperriere, N., O'Callaghan, C.J., Brandes, A.A., Menten, J., Phillips, C., Fay, M., Nishikawa, R., Cairncross, J.G., and Roa, W. Short-course radiation plus temozolomide in elderly patients with glioblastoma. New Engl J Med, 2017; 376: 1027-1037

Pierides, A., Voskarides, K., Kkolou, M., Hadjigavriel, M., and Deltas, C. X-linked, COL4A5 hypomorphic Alport mutations such as G624D and P628L may only exhibit thin basement membrane nephropathy with microhematuria and late onset kidney failure. Hippokratia, 2013; 17: 207

Pruitt, K., Tatusova, T., and Maglott, D. NCBI Reference Sequence (RefSeq): a curated non-redundant sequence database of genomes, transcripts and proteins. Nucleic Acids Res, 2005; 33: D501-504

Quinn, J.A., Jiang, S.X., Reardon, D.A., Desjardins, A., Vredenburgh, J.J., Rich, J.N., Gururangan, S., Friedman, A.H., Bigner, D.D., and Sampson, J.H. Phase II trial of temozolomide plus o6-benzylguanine in adults with recurrent, temozolomide-resistant malignant glioma. J Clin Oncol, 2009; 27: 1262

Ranger, A.M., Patel, Y.K., Chaudhary, N., and Anantha, R.V. Familial syndromes associated with intracranial tumours: a review. Child's Nervous System, 2014; 30: 47-64

Redman, M., King, A., Watson, C., and King, D. What is CRISPR/Cas9? Archives of Disease in Childhood-Education and Practice, 2016; 101: 213-215

Riccardi, C., and Nicoletti, I. Analysis of apoptosis by propidium iodide staining and flow cytometry. Nat Protoc, 2006; 1: 1458-1461

Rouet, P., Smih, F., and Jasin, M. Expression of a site-specific endonuclease stimulates homologous recombination in mammalian cells. Proceedings of the National Academy of Sciences, 1994; 91: 6064-6068

Salomon, D.S., Brandt, R., Ciardiello, F., and Normanno, N. Epidermal growth factor-related peptides and their receptors in human malignancies. Critical reviews in oncology/hematology, 1995; 19: 183-232

Sander, J.D., and Joung, J.K. CRISPR-Cas systems for editing, regulating and targeting genomes. Nat Biotechnol, 2014; 32: 347-355

Saxonov, S., Berg, P., and Brutlag, D. A genome-wide analysis of CpG dinucleotides in the human genome distinguishes two distinct classes of promoters. Proc Natl Acad Sci U S A, 2006; 103: 1412-1417

Schaff, L.R., and Mellinghoff, I.K. Glioblastoma and other primary brain malignancies in adults: a review. Jama, 2023; 329: 574-587

Scheurer, M.E., Etzel, C.J., Liu, M., Barnholtz-Sloan, J., Wiklund, F., Tavelin, B., Wrensch, M.R., Melin, B.S., Bondy, M.L., and Consortium, G. Familial aggregation of glioma: a pooled analysis. Am J Epidemiol, 2010; 172: 1099-1107

Segal, E., and Widom, J. What controls nucleosome positions? Trends Genet, 2009; 25: 335-343

Skvortsova, K., Stirzaker, C., and Taberlay, P. The DNA methylation landscape in cancer. Essays Biochem, 2019; 63: 797-811

Stepper, P., Kungulovski, G., Jurkowska, R.Z., Chandra, T., Krueger, F., Reinhardt, R., Reik, W., Jeltsch, A., and Jurkowski, T.P. Efficient targeted DNA methylation with chimeric dCas9–Dnmt3a–Dnmt3L methyltransferase. Nucleic Acids Res, 2016; 45: 1703-1713

Stummer, W., Pichlmeier, U., Meinel, T., Wiestler, O.D., Zanella, F., and Reulen, H.-J. Fluorescence-guided surgery with 5-aminolevulinic acid for resection of malignant glioma: a randomised controlled multicentre phase III trial. The lancet oncology, 2006; 7: 392-401

Stupp, R., Hegi, M., Mason, W., van den Bent, M., Taphoorn, M., Janzer, R., Ludwin, S., Allgeier, A., Fisher, B., Belanger, K., Hau, P., Brandes, A., Gijtenbeek, J., Marosi, C., Vecht, C., Mokhtari, K., Wesseling, P., Villa, S., Eisenhauer, E., Gorlia, T., Weller, M., Lacombe, D., Cairncross, J., and Mirimanoff, R. Effects of radiotherapy with concomitant and adjuvant temozolomide versus radiotherapy alone on survival in glioblastoma in a randomised phase III study: 5-year analysis of the EORTC-NCIC trial. The Lancet Oncology, 2009; 10: 459-466

Stupp, R., Mason, W.P., Van Den Bent, M.J., Weller, M., Fisher, B., Taphoorn, M.J., Belanger, K., Brandes, A.A., Marosi, C., and Bogdahn, U. Radiotherapy plus concomitant and adjuvant temozolomide for glioblastoma. New Engl J Med, 2005; 352: 987-996

Stupp, R., Taillibert, S., Kanner, A., Read, W., Steinberg, D.M., Lhermitte, B., Toms, S., Idbaih, A., Ahluwalia, M.S., and Fink, K. Effect of tumor-treating fields plus maintenance temozolomide vs maintenance temozolomide alone on survival in patients with glioblastoma: a randomized clinical trial. Jama, 2017; 318: 2306-2316

Sturm, D., Witt, H., Hovestadt, V., Khuong-Quang, D.-A., Jones, D.T., Konermann, C., Pfaff, E., Tönjes, M., Sill, M., and Bender, S. Hotspot mutations in H3F3A and IDH1 define distinct epigenetic and biological subgroups of glioblastoma. Cancer Cell, 2012; 22: 425-437

Sugahara, T., Korogi, Y., Kochi, M., Ikushima, I., Shigematu, Y., Hirai, T., Okuda, T., Liang,

L., Ge, Y., and Komohara, Y. Usefulness of diffusion‐weighted MRI with echo‐planar technique in the evaluation of cellularity in gliomas. Journal of Magnetic Resonance Imaging: An Official Journal of the International Society for Magnetic Resonance in Medicine, 1999; 9: 53-60

Suh, C.H., Kim, H.S., Jung, S.C., Park, J.E., Choi, C.G., and Kim, S.J. MRI as a diagnostic biomarker for differentiating primary central nervous system lymphoma from glioblastoma: A systematic review and meta‐analysis. J Magn Reson Imaging, 2019; 50: 560-572

Taberlay, P.C., Achinger-Kawecka, J., Lun, A.T., Buske, F.A., Sabir, K., Gould, C.M., Zotenko, E., Bert, S.A., Giles, K.A., and Bauer, D.C. Three-dimensional disorganization of the cancer genome occurs coincident with long-range genetic and epigenetic alterations. Genome Res, 2016; 26: 719-731

Takai, D., and Jones, P. Comprehensive analysis of CpG islands in human chromosomes 21 and 22. Proc Natl Acad Sci U S A, 2002; 99: 3740-3745

Tan, A.C., Ashley, D.M., López, G.Y., Malinzak, M., Friedman, H.S., and Khasraw, M. Management of glioblastoma: State of the art and future directions. CA: a cancer journal for clinicians, 2020; 70: 299-312

Taylor, S., Wakem, M., Dijkman, G., Alsarraj, M., and Nguyen, M. A practical approach to RT-qPCR—publishing data that conform to the MIQE guidelines. Methods, 2010; 50: S1-S5

Tebas, P., Stein, D., Tang, W.W., Frank, I., Wang, S.Q., Lee, G., Spratt, S.K., Surosky, R.T., Giedlin, M.A., and Nichol, G. Gene editing of CCR5 in autologous CD4 T cells of persons infected with HIV. New Engl J Med, 2014; 370: 901-910

Ting, A.H., Jair, K.W., Schuebel, K.E., and Baylin, S.B. Differential requirement for DNA methyltransferase 1 in maintaining human cancer cell gene promoter hypermethylation.

Cancer Res, 2006; 66: 729-735

Topkan, E., Selek, U., Ozdemir, Y., Yildirim, B.A., Guler, O.C., Ciner, F., Mertsoylu, H., and Tufan, K. Prognostic value of the Glasgow Prognostic Score for glioblastoma multiforme patients treated with radiotherapy and temozolomide. J Neurooncol, 2018; 139: 411-419

Topper, M.J., Vaz, M., Marrone, K.A., Brahmer, J.R., and Baylin, S.B. The emerging role of epigenetic therapeutics in immuno-oncology. Nature Reviews Clinical Oncology, 2020; 17: 75-90

Torp, S.H., Solheim, O., and Skjulsvik, A.J. The WHO 2021 Classification of Central Nervous System tumours: a practical update on what neurosurgeons need to know—a minireview. Acta Neurochir (Wien), 2022; 164: 2453-2464

Tost, J. DNA methylation: methods and protocols. Springer, 2009

Uddin, F., Rudin, C.M., and Sen, T. CRISPR gene therapy: applications, limitations, and implications for the future. Frontiers in oncology, 2020; 10: 1387

Uddin, M.S., Mamun, A.A., Alghamdi, B.S., Tewari, D., Jeandet, P., Sarwar, M.S., and Ashraf, G.M. Epigenetics of glioblastoma multiforme: From molecular mechanisms to therapeutic approaches. Semin Cancer Biol, 2022; 83: 100-120

Vakulskas, C.A., and Behlke, M.A. Evaluation and reduction of CRISPR off-target cleavage events. Nucleic Acid Ther, 2019; 29: 167-174

Vojta, A., Dobrinić, P., Tadić, V., Bočkor, L., Korać, P., Julg, B., Klasić, M., and Zoldoš, V. Repurposing the CRISPR-Cas9 system for targeted DNA methylation. Nucleic Acids Res, 2016; 44: 5615-5628

Wang, L., Jung, J., Babikir, H., Shamardani, K., Jain, S., Feng, X., Gupta, N., Rosi, S., Chang, S., and Raleigh, D. A single-cell atlas of glioblastoma evolution under therapy

reveals cell-intrinsic and cell-extrinsic therapeutic targets. Nature cancer, 2022a; 3: 1534-1552

Wang, Q., Hu, B., Hu, X., Kim, H., Squatrito, M., Scarpace, L., DeCarvalho, A.C., Lyu, S., Li, P., and Li, Y. Tumor evolution of glioma-intrinsic gene expression subtypes associates with immunological changes in the microenvironment. Cancer Cell, 2017; 32: 42-56. e46

Wang, S.-W., Gao, C., Zheng, Y.-M., Yi, L., Lu, J.-C., Huang, X.-Y., Cai, J.-B., Zhang, P.-F., Cui, Y.-H., and Ke, A.-W. Current applications and future perspective of CRISPR/Cas9 gene editing in cancer. Mol Cancer, 2022b; 21: 1-27

Wang, S., Shi, X., Wei, S., Ma, D., Oyinlade, O., Lv, S.-Q., Ying, M., Zhang, Y.A., Claypool, S.M., and Watkins, P. Krüppel-like factor 4 (KLF4) induces mitochondrial fusion and increases spare respiratory capacity of human glioblastoma cells. J Biol Chem, 2018; 293: 6544-6555

Warren, K.E., Gururangan, S., Geyer, J.R., McLendon, R.E., Poussaint, T.Y., Wallace, D., Balis, F.M., Berg, S.L., Packer, R.J., and Goldman, S. A phase II study of O6-benzylguanine and temozolomide in pediatric patients with recurrent or progressive high-grade gliomas and brainstem gliomas: a Pediatric Brain Tumor Consortium study. J Neurooncol, 2012; 106: 643-649

Watts, G., Pieper, R., Costello, J., Peng, Y., Dalton, W., and Futscher, B. Methylation of discrete regions of the O6-methylguanine DNA methyltransferase (MGMT) CpG island is associated with heterochromatinization of the MGMT transcription start site and silencing of the gene. Mol Cell Biol, 1997; 17: 5612-5619

Wen, P.Y., Weller, M., Lee, E.Q., Alexander, B.M., Barnholtz-Sloan, J.S., Barthel, F.P., Batchelor, T.T., Bindra, R.S., Chang, S.M., Chiocca, E.A., Cloughesy, T.F., DeGroot, J.F., Galanis, E., Gilbert, M.R., Hegi, M.E., Horbinski, C., Huang, R.Y., Lassman, A.B., Le Rhun, E., Lim, M., Mehta, M.P., Mellinghoff, I.K., Minniti, G., Nathanson, D., Platten, M.,

Preusser, M., Roth, P., Sanson, M., Schiff, D., Short, S.C., Taphoorn, M.J.B., Tonn, J.C., Tsang, J., Verhaak, R.G.W., von Deimling, A., Wick, W., Zadeh, G., Reardon, D.A., Aldape, K.D., and van den Bent, M.J. Glioblastoma in adults: a Society for Neuro-Oncology (SNO) and European Society of Neuro-Oncology (EANO) consensus review on current management and future directions. Neuro Oncol, 2020; 22: 1073-1113

Wesseling, P., van der Laak, J.A., de Leeuw, H., Ruiter, D.J., and Burger, P.C. Quantitative immunohistological analysis of the microvasculature in untreated human glioblastoma multiforme: computer-assisted image analysis of whole-tumor sections. J Neurosurg, 1994; 81: 902-909

Wu, W., Lamborn, K.R., Buckner, J.C., Novotny, P.J., Chang, S.M., O'Fallon, J.R., Jaeckle, K.A., and Prados, M.D. Joint NCCTG and NABTC prognostic factors analysis for high-grade recurrent glioma. Neuro Oncol, 2010; 12: 164-172

Wu, X., Scott, D.A., Kriz, A.J., Chiu, A.C., Hsu, P.D., Dadon, D.B., Cheng, A.W., Trevino, A.E., Konermann, S., and Chen, S. Genome-wide binding of the CRISPR endonuclease Cas9 in mammalian cells. Nat Biotechnol, 2014; 32: 670-676

Xu, N., Wu, Y.-P., Ke, Z.-B., Liang, Y.-C., Cai, H., Su, W.-T., Tao, X., Chen, S.-H., Zheng, Q.-S., and Wei, Y. Identification of key DNA methylation-driven genes in prostate adenocarcinoma: an integrative analysis of TCGA methylation data. J Transl Med, 2019; 17: 1-15

Xu, X., Hulshoff, M.S., Tan, X., Zeisberg, M., and Zeisberg, E.M. CRISPR/Cas derivatives as novel gene modulating tools: possibilities and in vivo applications. Int J Mol Sci, 2020; 21: 3038

Xu, X., Tao, Y., Gao, X., Zhang, L., Li, X., Zou, W., Ruan, K., Wang, F., Xu, G.-l., and Hu, R. A CRISPR-based approach for targeted DNA demethylation. Cell Discovery, 2016; 2: 16009

Xu, Y., and Li, Z. CRISPR-Cas systems: Overview, innovations and applications in human disease research and gene therapy. Computational and Structural Biotechnology Journal, 2020; 18: 2401-2415

Yamahara, T., Numa, Y., Oishi, T., Kawaguchi, T., Seno, T., Asai, A., and Kawamoto, K. Morphological and flow cytometric analysis of cell infiltration in glioblastoma: a comparison of autopsy brain and neuroimaging. Brain Tumor Pathol, 2010; 27: 81-87

Yang, K., Wu, Z., Zhang, H., Zhang, N., Wu, W., Wang, Z., Dai, Z., Zhang, X., Zhang, L., and Peng, Y. Glioma targeted therapy: insight into future of molecular approaches. Mol Cancer, 2022; 21: 1-32

Yin, H., Xue, W., Chen, S., Bogorad, R.L., Benedetti, E., Grompe, M., Koteliansky, V., Sharp, P.A., Jacks, T., and Anderson, D.G. Genome editing with Cas9 in adult mice corrects a disease mutation and phenotype. Nat Biotechnol, 2014; 32: 551-553

Yu, W., Zhang, L., Wei, Q., and Shao, A. O-Methylguanine-DNA Methyltransferase (MGMT): Challenges and New Opportunities in Glioma Chemotherapy. Frontiers in oncology, 2019; 9: 1547

Yuan, Y., Wang, L.H., Zhao, X.X., Wang, J., Zhang, M.S., Ma, Q.H., Wei, S., Yan, Z.X., Cheng, Y., and Chen, X.Q. The E3 ubiquitin ligase HUWE1 acts through the N‐Myc‐DLL1‐NOTCH1 signaling axis to suppress glioblastoma progression. Cancer Communications, 2022; 42: 868-886

Yuile, P., Dent, O., Cook, R., Biggs, M., and Little, N. Survival of glioblastoma patients related to presenting symptoms, brain site and treatment variables. J Clin Neurosci, 2006; 13: 747-751

Zhan, T., Rindtorff, N., Betge, J., Ebert, M.P., and Boutros, M. CRISPR/Cas9 for cancer research and therapy. Semin Cancer Biol, 2019; 55: 106-119

Zhang, J., Kan, S., Huang, B., Hao, Z., Mak, T.W., and Zhong, Q. Mule determines the apoptotic response to HDAC inhibitors by targeted ubiquitination and destruction of HDAC2. Genes Dev, 2011; 25: 2610-2618

Zhang, W., Zhang, J., Hoadley, K., Kushwaha, D., Ramakrishnan, V., Li, S., Kang, C., You, Y., Jiang, C., and Song, S.W. miR-181d: a predictive glioblastoma biomarker that downregulates MGMT expression. Neuro Oncol, 2012; 14: 712-719

Zhang, X.-H., Tee, L.Y., Wang, X.-G., Huang, Q.-S., and Yang, S.-H. Off-target effects in CRISPR/Cas9-mediated genome engineering. Molecular Therapy-Nucleic Acids, 2015; 4:

Zhao, J., Yang, S., Cui, X., Wang, Q., Yang, E., Tong, F., Hong, B., Xiao, M., Xin, L., and Xu, C. A novel compound EPIC-0412 reverses temozolomide resistance via inhibiting DNA repair/MGMT in glioblastoma. Neuro Oncol, 2023; 25: 857-870

Zhu, Y. Advances in CRISPR/Cas9. BioMed Research International, 2022; 2022:

Zou, Y., Sun, X., Yang, Q., Zheng, M., Shimoni, O., Ruan, W., Wang, Y., Zhang, D., Yin, J., and Huang, X. Blood-brain barrier–penetrating single CRISPR-Cas9 nanocapsules for effective and safe glioblastoma gene therapy. Science advances, 2022; 8: eabm8011

9. Acknowledgments

Since 2011, from bachelor to master to doctor, from China to Germany, I have been studying medicine for more than 10 years……And postdoc? Perhaps not. Thanks, I am full.

First and most importantly, I would like to thank my supervisor Prof. Ullrich Wüllner for the opportunity to do my doctorate in this laboratory and the continuous support for my doctoral thesis. I would also like to thank the entire Ph.D. committee for all their work on this process.

I would like to thank Dr.Bernd Evert and Dr. Peter Breuer. I want to thank Peter for the paper that you gave me about CRISPRoff, which brought the inspiration of my thesis to me. I would like to sincerely thank Bernd for his help throughout almost the entire process; without your help, I would not have been able to publish the paper and complete my thesis. Thanks a lot for your communication with other departments for my experiments! Thanks a lot for your revision of my published paper! I appreciate it!!

I would like to thank Hassan Khazneh for his excellent technical support, thank Sabine Proske-Schmitz for everything you have done for everyone in our lab. You are the solid backing for us! (FC Bayern München will be back, maybe next season; but the champion of the Bundesliga will belong to Leverkusen this year!)

I would like to thank my dear colleagues and friends Fabian Stahl and Yousuf Bakhit from the deepest in my heart. Firstly, I learned so much from both of you about research, thank you so much for your experience and suggestions! Secondly, I really appreciate your encouragement and the nice time that we spend together in Tuscolo every week! In addition, I really need to thank Fabian for his patience, especially in my first year. I owe you and I'm sorry that I almost exhausted your patience.

I would like to thank the support from Dr. Matthias Schneider’s lab, thanks for the supply of some necessary reagents for my study; thank Meng-Chun Hsieh for her help in flow cytometry, and Barbara Pregler for her help in the statistic analysis. At the same time, I would also like to thank the Department of Neuropathology, especially Prof. Andreas Waha and Verena Dreschmann, for their help with pyrosequencing. In addition, I need to thank Mohammed Abdallah for the help in the 850k array.

I would like to thank the support from Prof. Jochen Walter’s lab, especially Sandra Theil, and Dr. Florian Riffel. I want to thank my friends Yanxia Liu and Lin Peng for their encouragement when I was frustrated in my experiments, which helped me regain my confidence. At the same time, I also wish they could finish the thesis and get the doctoral degree as soon as possible!

I would like to thank my wife Dingding Ai for her concern and companionship. Except for the encouragement during my doctoral study, she also helped me gain extraordinary cooking skills. And I also want to thank my parents; I really appreciate your support in all my decisions!

Finally, I would like to quote two lines of poetry from the Tang Dynasty poet Li Bai to end my doctoral studies and start the next stage of my life:

两岸猿声啼不住，轻舟已过万重山.

The gibbons cry unending from the two riverbanks; the fragile craft has already passed the countless mountains.

乘风破浪会有时，直挂云帆济沧海！

A time will come to ride the wind and cleave the waves; I'll set my cloud-white sail and cross the sea which raves.

10. Publications list

[1] **Han, X.**; Abdallah, M. O. E.; Breuer, P.; et al. Downregulation of MGMT expression by targeted editing of DNA methylation enhances temozolomide sensitivity in glioblastoma. Neoplasia, 2023, 44, 100929. doi: 10.1016/j.neo.2023.100929.

[2] **Han, X.**; Bedarf J R.; Proske-Schmitz, S; et al. Increased diversity of Malassezia species on the skin of Parkinson‘s disease patients. Front Aging Neurosci, 2023, 15,1268751. doi: 10.3389/fnagi.2023.1268751.

[3] Chen, Z †; **Han, X.†**; Fan, G.; et al. Preliminary Application of Three-Dimensional Printing Technique in Preoperative Localization of Meningioma in Primary Hospitals. J Craniofac Surg, 2021, 32 (5), 1796-1799. doi: 10.1097/SCS.0000000000007509.

[4] Stahl F, Evert B O, **Han, X.**, et al. Spinocerebellar Ataxia Type 3 Pathophysiology—Implications for Translational Research and Clinical Studies. International Journal of Molecular Sciences, 2024, 25 (7) : 3984. doi: 10.3390/ijms25073984.

[5] Breuer, P.; Rasche, T.; **Han, X.**; Faber, J.; Haustein, K.; Klockgether, T.; Wullner, U., The Ratio of Expanded to Normal Ataxin 3 in Peripheral Blood Mononuclear Cells Correlates with the Age at Onset in Spinocerebellar Ataxia Type 3. Mov Disord, 2022, 37 (5), 1098-1099. doi: 10.1002/mds.28962.